

# **Rapid and epileptogenic astrocyte morphology changes in the hippocampus**

Doctoral thesis

to obtain a doctorate

from the Faculty of Medicine

of the University of Bonn

**Charlotte Ruth Wilma Behringer**

from Freiburg im Breisgau

2025

Written with authorization of  
the Faculty of Medicine of the University of Bonn

First reviewer: Prof. Dr. Christian Henneberger

Second reviewer: Prof. Dr. Sandra Blaess

Day of oral examination: 10.03.2025

From the Institute of Cellular Neurosciences

## Table of contents

### List of abbreviations

<b>1.</b>	<b>Introduction .....</b>	<b>8</b>
1.1	Hippocampus .....	8
1.2	Epilepsy.....	10
1.2.1.1	Mesial temporal lobe epilepsy .....	11
1.3	Astrocytes .....	12
1.3.1	Morphological plasticity of astrocytes.....	15
1.3.2	Alterations of astrocyte morphology in epilepsy .....	16
1.3.2.1	Molecular Basis of rapid astrocytic morphology changes induced by epileptiform activity .....	18
1.4	Inflammation in the central nervous system.....	21
1.4.1	Inflammation in the epileptic brain.....	23
1.4.1.1	Tumor necrosis factor alpha.....	24
1.4.1.2	Interleukin 1b.....	26
1.4.1.3	Brain derived neurotrophic factor .....	27
1.4.2	The role of norepinephrine in the epileptic brain .....	28
1.5	Aim of the study .....	29
<b>2.</b>	<b>Materials and methods .....</b>	<b>32</b>
2.1	Animal models.....	32
2.1.1	hGFAP-EGFP mice .....	32
2.1.2	EGFP-TNFR1 <sup>-/-</sup> mice .....	32
2.2	Materials.....	33
2.2.1	Chemicals .....	33
2.2.2	Solutions .....	33
2.3	Electrophysiology .....	35

2.3.1	Preparation of acute hippocampal slices .....	35
2.3.2	Electrophysiological setup.....	35
2.3.3	Extracellular field recordings .....	37
2.3.4	Analysis of evoked field recordings.....	38
2.3.5	Induction of epileptiform activity .....	39
2.4	Imaging .....	40
2.4.1	Two-photon excitation fluorescence microscopy .....	40
2.4.2	Monitoring astrocyte morphology .....	40
2.4.3	Analysis of astrocyte volume fraction .....	41
2.4.4	Monitoring dynamic astrocyte morphology changes .....	42
2.4.5	Astrocyte volume fraction in incubated acute slices.....	43
2.5	Osmotic stress .....	43
2.6	Statistics .....	44
<b>3.</b>	<b>Results .....</b>	<b>45</b>
3.1	Dynamic morphology changes of astrocytes and synaptic transmission in response to osmotic stress .....	45
3.1.1	Astrocyte morphology .....	45
3.1.2	Synaptic transmission .....	49
3.2	Astrocyte morphology changes occur acutely after onset of epileptiform activity .....	50
3.3	The role of TNF $\alpha$ in astrocyte morphological plasticity .....	54
3.3.1	Incubation of slices with TNF $\alpha$ alone or in combination with Interleukin 1b .....	57
3.3.2	The effect of epileptiform activity on astrocyte morphology in a TNFR1-deficient mouse line .....	59
3.4	The role of Brain derived neurotrophic factor in astrocyte morphological plasticity .....	64

3.5	The role of norepinephrine in astrocyte morphological plasticity .....	65
<b>4.</b>	<b>Discussion .....</b>	<b>68</b>
4.1	Osmotic stress in acute hippocampal slices .....	68
4.1.1	Effect of osmotic stress on astrocyte morphology.....	68
4.1.2	The effect of osmotic stress on the neuronal population.....	70
4.2	Astrocyte morphological plasticity induced by epileptiform activity .....	72
4.2.1	Induction of epileptiform activity in acute brain slices .....	72
4.2.2	Epileptiform activity induces rapid astrocyte morphology changes.....	74
4.3	Is inflammation responsible for rapid morphology changes during epileptiform activity? .....	75
4.3.1	The role of TNF $\alpha$ in astrocyte morphological plasticity .....	75
4.3.2	The role of TNF $\alpha$ and Interleukin 1b in astrocyte morphological plasticity.....	78
4.3.3	The role of TNFR1 in remodeling of the astroglial cytoskeleton during epileptiform activity.....	80
4.3.4	The role of brain-derived neurotrophic factor in the regulation of astrocyte morphology .....	84
4.4	The role of norepinephrine in the acute regulation of astrocyte morphology ...	86
4.5	The role of inflammatory pathways in rapid astrocyte morphology changes induced by epileptiform activity .....	88
<b>5.</b>	<b>Summary .....</b>	<b>92</b>
<b>6.</b>	<b>List of figures .....</b>	<b>93</b>
<b>7.</b>	<b>List of tables .....</b>	<b>94</b>
<b>8.</b>	<b>References .....</b>	<b>95</b>
<b>9.</b>	<b>Acknowledgements .....</b>	<b>125</b>

**List of Abbreviations**

AC	adenylyl cyclase
ACSF	artificial cerebrospinal fluid
AED	antiepileptic drug
AQP	aquaporin
AR	adrenergic receptors
BBB	blood brain barrier
BDNF	brain-derived neurotrophic factor
BSA	bovine serum albumin
CA	cornu ammonis
cAMP	cyclic adenosine monophosphate
CNS	central nervous system
CSF1R	colony-stimulating factor 1 receptor
DBH	dopamine b-hydroxylase
DG	dentate gyrus
EC	entorhinal cortex
ECM	extracellular matrix
ECS	extracellular space
EGFP	enhanced green fluorescence protein
FADDs	Fas-associating proteins with death domain
fEPSP	field excitatory synaptic potential
FV	fiber volley
GABA	$\gamma$ -aminobutyric acid
GAP	GTPase-activating protein
GDI	guanine nucleotide dissociation inhibitors
GEF	guanine nucleotide exchange factor
GFAP	glial fibrillary acidic protein
GPCRs	G-protein-coupled receptors
IL	interleukin
IL1R	interleukin-1 receptor
LC	locus coeruleus
LIMK	Lin-11, Isl-1, and Mec-3 kinases

LPS	lipopolysaccharide
LTP	long term potentiation
MLC	myosin light chain
MTLE	mesial temporal lobe epilepsy
NE	norepinephrine
NMDA	N-Methyl-D-Aspartate-receptors
PAP	perisynaptic astroglial processes
PKC	serine–threonine protein kinase C
PLC	phospholipase C
ROCK	RhoA associated coiled-coil kinase
ROI	region of interest
SC	Schaffer collaterals
SE	status epilepticus
solTNF	soluble TNF $\alpha$
Str.	stratum
TACE	TNF $\alpha$ converting enzyme
TIM	TRAF interacting motif
TKRs	tyrosine kinase receptors
tmTNF	transmembrane bound TNF $\alpha$
TNF $\alpha$	Tumor necrosis factor $\alpha$
TNFR	TNF $\alpha$ receptor
TRADDs	TNFR1-associated death domain proteins
TRAF	TNF receptor adaptor factor
TrkB	tropomyosin-related kinase B
VF	volume fraction

## 1. Introduction

### 1.1 Hippocampus

The hippocampus is a C-shaped brain structure located within the mesial temporal lobe (Schultz and Engelhardt, 2014). It plays a crucial role in various important brain functions, with memory formation being a primary one (Andersen et al., 2006). The hippocampus is also extensively studied in the context of pathophysiological conditions such as epilepsy (Engel, 2001; Prince, 1978; Stafstrom, 2005). Its highly organized (cyto-) architecture renders to the hippocampus a particularly interesting model structure to study basic principles of neurophysiology.

The hippocampus in its narrow sense can be referred to synonymously as the 'hippocampus proprius' or '*Cornu Ammonis*' (CA) (Walther, 2002). The term "*Cornu Ammonis*" is derived from Latin, and it translates to 'Ammon's Horn'. It refers to the curved shape of the hippocampus, which resembles the horns of the Egyptian god Amun. The hippocampus is further divided into layered subfields, namely, the CA1, CA2 and CA3 region (Lorente De Nó, 1934) (Fig.1). It has a distinct layered organization, with the most prominent layer being the *stratum (str.) pyramidale* comprising the cell bodies of the excitatory pyramidal neurons. The basal dendrites of these cells are located in the deep layer called the *str. oriens*. Apical dendrites in turn are found just above the *str. pyramidale* and extend through the *str. radiatum* and the *str. lacunosomoleculare* along the apical axis of the *str. pyramidale*. While the hippocampus is densely packed with neurons it contains other cell types, including astrocytes, which play important roles in supporting and modulating neuronal function and maintaining the overall health of the hippocampal circuitry.

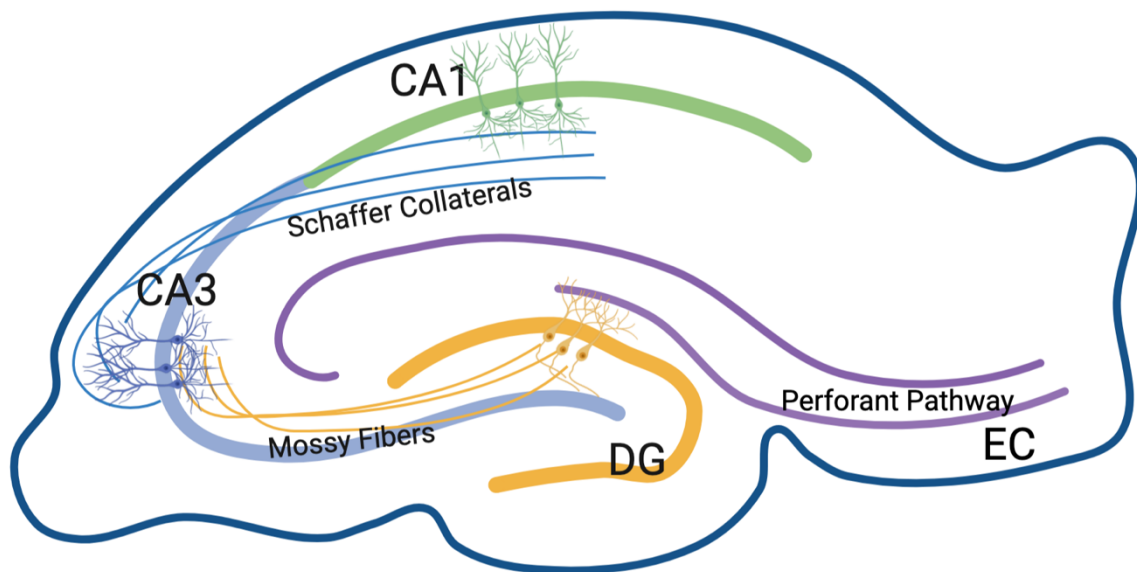


**Fig. 1:** Neuronal tri-synaptic circuit in the hippocampus

The hippocampus receives input from the entorhinal cortex through the perforant path to the dentate gyrus. The dentate granule (DG) cells project to CA3 neurons, which transmit information via the Schaffer collaterals to CA1 pyramidal neurons. The axons of CA1 pyramidal neurons project back to the entorhinal cortex directly or indirectly through the subiculum. This circuit forms the tri-synaptic pathway in the hippocampus.

The hippocampal formation consists of not only the hippocampus itself but also neighboring structures including the dentate gyrus (DG), the subiculum, presubiculum, parasubiculum, and the entorhinal cortex (EC) (Andersen et al., 2006). These structures are involved in a complex circuit known as tri-synaptic circuit, which plays a crucial role in memory processing (Andersen et al., 2006).

The major input to the hippocampal formation originates from cells of the EC through a pathway called the perforant pathway. The axons from the EC cells project to the DG primarily, but some also terminate in the subiculum and the hippocampus itself. From the DG the granule cells give rise to axons called mossy fibers which form connections with the pyramidal cells in the CA3 region (Fig. 1). The CA3 pyramidal neurons then project via Schaffer collaterals to the CA1 region. CA1 pyramidal neurons in turn project directly back to the EC or indirectly through projections to the subiculum which is also connected

to the EC. These connections from the subiculum and the CA1 hippocampal field close the hippocampal processing loop (Deng et al., 2010; van Strien et al., 2009).

Dysregulation of hippocampal function which can result from neuronal hyperexcitability is often associated with epilepsy (Schwartzkroin, 1986). Understanding the role of the hippocampus in epilepsy can provide insights into the mechanisms of seizure generation and potentially lead to new therapeutic approaches.

## 1.2 Epilepsy

Epilepsy is a serious, chronic noncommunicable neurological disease affecting about 65 million people of all ages worldwide (Thurman et al., 2011). It is characterized as an “enduring predisposition of the brain to generate epileptic seizures, with neurobiological, cognitive, psychological, and social consequences” (Fisher et al., 2005). An epileptic seizure is defined by the International League Against Epilepsy as “a transient occurrence of signs and/or symptoms due to abnormal excessive or synchronous neuronal activity in the brain” (Fisher et al., 2005). Seizure types are classified into focal onset, generalized onset, and unknown onset based on the origin site (Scheffer et al., 2017).

The diagnosis of epilepsy comprises clinical examination including information regarding seizure semiology obtained from individual and witness histories (National Clinical Guideline Centre (UK), 2012). In addition, electroencephalogram (EEG) and magnetic resonance imaging of the brain is commonly employed during epilepsy diagnosis. Specifically, epilepsy syndromes often show distinct EEG features or are accompanied by structural lesions which carries prognostic and treatment implications and, thus, provide important information for diagnostics (Wirrell et al., 2022). For example, brain/neuronal activity recorded by the EEG can be categorized as ictal (i.e., during a seizure), postictal (i.e., after a seizure) and interictal (i.e., between seizures) (Fisher and Engel, 2010) and thereby allows a further characterization of the type and/or status of the disease. The importance of a detailed characterization of the type of epilepsy becomes particularly relevant when searching for novel treatment options and/or finding the optimal treatment for the individual epilepsy patient.

Epilepsy is primarily treated with antiepileptic drugs (AEDs). Generally, said AEDs act via a facilitation of neuronal inhibition, an attenuation of neuronal excitation, or a prevention of aberrant burst-firing of neurons. Examples of AEDs which enhance the inhibitory  $\gamma$ -

aminobutyric acid (GABA)-system are benzodiazepines, barbiturates, tiagabine and vigabatrin (Davies, 1995). Other AEDs reduce neuronal excitability/excitation via an use-dependent block of sodium channels, e.g., carbamazepine, oxcarbazepine, lamotrigine, and phenytoin (Davies, 1995). Although many AEDs with different modes of actions are available, one third of patients suffering from epilepsy do not respond properly to AED treatment and continue to experience seizures (Kwan et al., 2010; Sultana et al., 2021). Drug resistance is a particular problem in patients suffering from focal epilepsies such as mesial temporal lobe epilepsy (MTLE) (Duncan et al., 2006; Pati and Alexopoulos, 2010), wherein seizures originate from the temporal lobe, the most epileptogenic region of the brain which includes the hippocampus (see above).

#### 1.2.1.1 Mesial temporal lobe epilepsy

MTLE is the most common type of focal epilepsy characterized by recurrent focal seizures originating from the mesial temporal lobe, primarily involving the hippocampus and amygdala, and potentially neighboring cortical regions (King and Spencer, 1995).

MTLE can develop after an initial event such as febrile seizures during childhood, trauma, hypoxia, brain infection, status epilepticus following a latent period (French et al., 1993). The most prevalent pathological substrate in MTLE is hippocampal sclerosis (Blumcke et al., 2017; Cavanagh and Meyer, 1956; Thom, 2014), a damage pattern that comprises segmental neuronal cell loss of the hippocampus and concomitant astrogliosis (Thom, 2014).

Although aberrant neuronal activity is the main pathophysiological feature of MTLE, it is recognized that severe changes of non-neuronal cells especially astrocytes, are strongly associated with epilepsy (Steinhäuser et al., 2016; Vezzani et al., 2011; Zhao et al., 2018). Astrocytes are known to be involved in many homeostatic functions in the central nervous system (CNS) (see section 1.3) and their malfunction has been implicated in the generation of epilepsy, especially MTLE (Bedner et al., 2015; Coulter and Steinhäuser, 2015; de Lanerolle et al., 2010; Oberheim et al., 2008) (see section 1.3.2).

Moreover, there is increasing evidence that epilepsy is highly associated with activation of microglial cells which are involved in inflammation and immune protection of the CNS (see section 1.4). Particularly, the release of cytokines by activated microglia has been

proposed to be a key driver of epileptogenic processes (Henning et al., 2023; Hiragi et al., 2018; Li et al., 2011; Vezzani et al., 2011) (see section 1.4.1).

Despite increasing knowledge about the involvement of non-neuronal cell types in epileptogenesis, the exact mechanisms are still poorly understood. Conventional antiepileptic drugs primarily target neurons, and their effectiveness may be limited, particularly in pharmacoresistant MTLE patients for whom surgical options are often the only remedy (Blumcke et al., 2017).

Uncontrolled epileptic seizures can have devastating consequences, significantly reducing patients' quality of life. Common side effects and comorbidities reported in refractory epilepsy patients include intolerable toxicity from AEDs, impaired memory function, and depressive symptoms (Juvale and Che Has, 2021; Luoni et al., 2011). Therefore, further research into the molecular mechanisms underlying epilepsy, especially the development of epilepsy (epileptogenesis) is crucial to identify additional targets for more effective pharmacological treatments. Especially astrocytes represent an interesting target for further research as there is increasing evidence that their strongly altered phenotype and function contributes to epileptogenesis.

### 1.3 Astrocytes

Astrocytes are a highly abundant type of glial cell, constituting approximately 20 – 40 % of the total number of brain cells (Verkhatsky and Nedergaard 2018). Within the CNS, astrocytes are characterized by the expression of glial fibrillary acidic protein (GFAP), which is widely used as a marker for astrocytes (Bignami et al., 1972; Kimelberg and Norenberg, 1989). Astrocytes derive their name from their star-like appearance, as “astro” means star in Greek. This characteristic morphology was first observed by pioneering neuroscientists Camillo Golgi and Ramon y Cajal through Golgi staining techniques in the early 20<sup>th</sup> century (Fig. 2 A). Despite their common stellate feature, astrocytes exhibit a remarkable diversity in their morphology (Zhang and Barres, 2010).

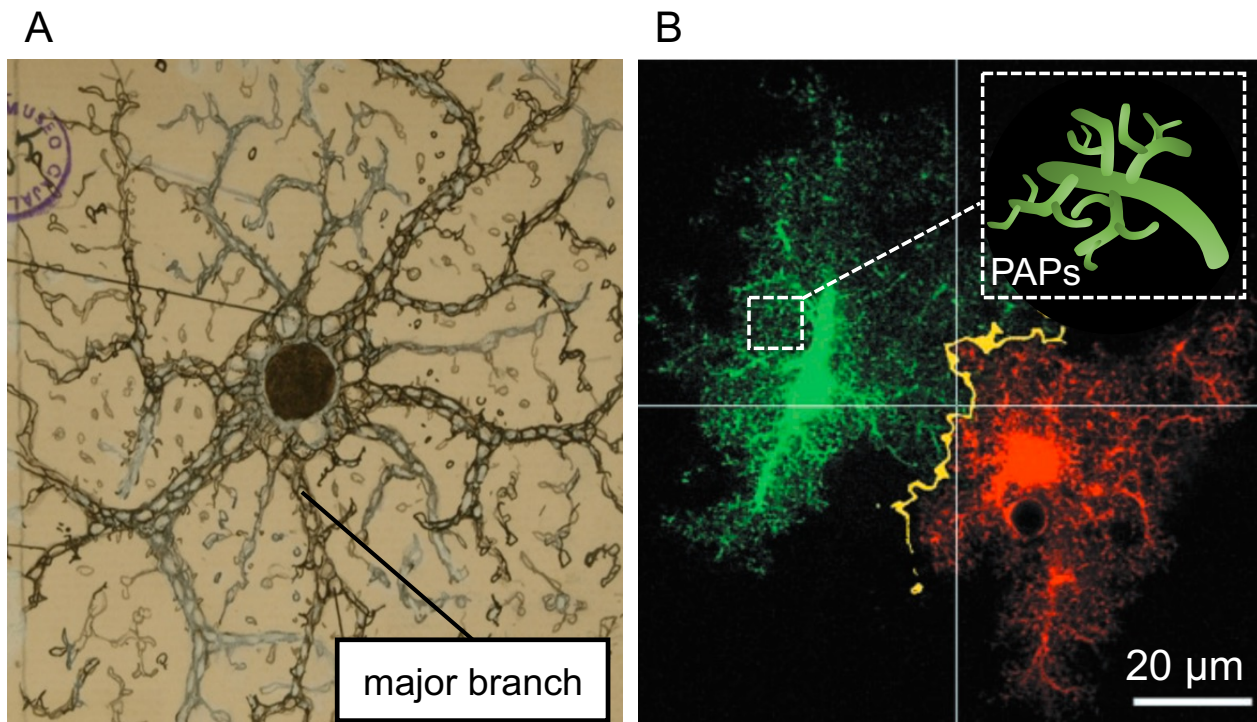


**Fig. 2:** Protoplasmic astrocytes

A) Illustration by Cajal depicting an astrocyte with its major branches, derived from the pyramidal layer of the hippocampus in an adult human brain based on Golgi staining (adopted from Ramón y Cajal, 1909). Only major and midsized processes are visualized. B) Protoplasmic astrocytes from a rodent brain visualized by intracellular fluorescent dye fill (adopted from Bushong et al., 2002). Fluorescent dye filling allows to visualize the finest peripheral processes (PAPs) revealing the actual bush-like astrocytic morphology. Even though astrocytes are extensively coupled in astroglial networks they are organized in barely overlapping territories, as indicated by the yellow line representing their discreet region of interaction.

Based on their morphology they can be broadly classified into two main categories: fibrous astrocytes, primarily found in white matter, and protoplasmic astrocytes, more abundant in grey matter (Kettenmann and Verkhratsky, 2008).

Advanced visualization techniques have revealed that astrocytes have a bush- or sponge-like morphology, situated between endothelial cells and neurons (Fig. 2 B) (Bushong et al., 2002; Ogata and Kosaka, 2002). A typical protoplasmic astrocyte consists of 5 to 8 major branches emanating from the soma, which further ramify into fine leaflet-like protrusions (Sofroniew and Vinters, 2010). Protoplasmic astrocytes typically have a diameter of 40 to 60  $\mu\text{m}$  with about 80 % of the total membrane surface of each cell being formed by processes (Khakh and Sofroniew, 2015; Robertson, 2013; Zhou et al., 2019). Each astrocyte occupies a specific territory with minimal overlap (less than 5 %) with

neighboring astrocyte processes (Fig. 2 B) (Bushong et al., 2002; Ogata and Kosaka, 2002).

Astrocytes have specialized processes called perisynaptic astroglial processes (PAPs) that enwrap synapses (Ventura and Harris, 1999) while larger astrocytic endfeet surround vessels (Sofroniew and Vinters, 2010). In the hippocampus, approximately more than half of the synaptic clefts are in contact with astrocyte protrusions (Witcher et al., 2007) and coverage of synapses is regulated dynamically (Bernardinelli et al., 2014b; Henneberger et al., 2020).

The complex morphology of astrocytes reflects their diverse functions. In healthy brain tissue, astrocytes contribute to various homeostatic processes including potassium buffering, energy supply and neurotransmitter uptake and recycling (Kimelberg, 2010). Extensive gap junction coupling between astrocytes facilitates the rapid dissipation of small molecules like glutamate or potassium (Giaume et al., 2010). Astrocytes also play an active role in bidirectional signaling at synapses thereby shaping neuronal information processing (Araque et al., 2014). A single hippocampal astrocyte and its processes can contact approximately 100,000 synapses (Bushong et al., 2002), exerting modulatory effects on various neuronal processes through direct and indirect pathways at the molecular, synaptic, cellular, and network levels (Anderson et al., 2016; Santello and Volterra, 2012; Walz, 2000). Consequently, astrocytes play a significant role in modulating neuronal function.

Although astrocytes do express voltage dependent and independent potassium and sodium channels, they are not able to propagate action potentials along their processes as neurons do (Nedergaard et al., 2003). However, they can respond biochemically to stimuli such as ions and neurotransmitters. Astrocytes can communicate through regulated elevations in intracellular calcium concentration, which propagate along astrocyte processes and even between neighboring astrocytes (Cornell-Bell et al., 1990; Dani et al., 1992; Jensen and Chiu, 1990). These calcium elevations can be triggered by neurotransmitters such as glutamate and purines released during neuronal activity (Bennett et al., 2006; Cornell-Bell et al., 1990; Porter and McCarthy, 1996). Notably, calcium release from intracellular stores also occurs without neuronal activity, indicating that astrocytes even serve as an independent modulator of neuronal excitability (Nett et al., 2002).

Variations in intracellular calcium levels in astrocytes can trigger the release of various active substances, known as gliotransmitters including ATP, and D-serine (Bezzi and Volterra, 2001). These gliotransmitters can signal to both other astrocytes and neurons, thereby influencing neuronal function in several ways, such as modulating synaptic transmission and affecting neuronal excitability (Araque et al., 2014). This bidirectional signaling between astrocytes and neurons has led to the concept of the “tripartite synapse” (Araque et al., 1999).

While significant progress has been made in understanding the roles of astrocytes in both physiological and pathological brain function, there has been relatively little investigation of the signaling pathways to and within astrocytes, particularly those involved in altering astrocyte morphology.

### 1.3.1 Morphological plasticity of astrocytes

Astrocytes demonstrate two significant phenomena of structural plasticity: Motility, which involves highly dynamic movements, and changes in their coverage of synapses (Bernardinelli et al., 2014a; Haber et al., 2006; Hirrlinger et al., 2004).

The extent of ensheathment of spines varies considerably across different brain regions, ranging from around 60% in the hippocampus (Ventura and Harris, 1999) to 100% in the Bergmann glia of the cerebellum (Lippman et al., 2008). Notably, the coverage of synapses by astrocytes can be modified in a neuronal activity-dependent manner. For instance, lactation or consolidation of short-term memory into long-term memory, leads to decreased coverage of synapses by PAPs in the supraoptic nucleus and the amygdala respectively (Oliet et al., 2001; Ostroff et al., 2014).

The dynamics of synaptic ensheathment by astrocytes are believed to be closely related to the motility of PAPs (Bernardinelli et al., 2014a; Haber et al., 2006). Studies employing simultaneous imaging of dendritic spines and astrocytic processes have shown that astrocytic processes exhibit dynamic extension and retraction on the order of minutes in live cells (Hirrlinger et al., 2004). In fact, astrocyte motility is influenced by the organism’s physiological conditions, such as parturition, lactation, chronic dehydration, starvation or voluntary exercise (Procko et al., 2011; Tatsumi et al., 2016; Theodosis, 2002). A particularly prominent trigger of PAP motility appears to be the induction of synaptic plasticity both *in vivo* and *in vitro* (Bernardinelli et al., 2014b; Henneberger et al., 2020).

Moreover, two photon excitation imaging of astrocytes in acute hippocampal slices and *in vivo* astrocytes has revealed that long term potentiation (LTP) induces shrinkage of PAPs which ultimately boosts glutamate escape from the synaptic cleft, thus enhancing N-Methyl-D-Aspartate-receptors (NMDAR) activation away from the release site, potentially at nearby synapses (Henneberger et al., 2020). Intriguingly, the withdrawal of PAPs alone can also boost glutamate escape (Henneberger et al., 2020), underscoring the functional significance of the precise spatial relationship between synapses and PAPs.

The plasticity of perisynaptic astroglial processes (PAPs) is widely recognized to modulate synaptic efficacy, spine stability, and synaptic maturation under physiological conditions (Bernardinelli et al., 2014b; Nishida and Okabe, 2007). Consequently, it is conceivable that morphological alterations of astrocytes during pathophysiological conditions play a crucial role as well. Indeed, many neurological or psychiatric disease including Alzheimer's disease, Huntington's disease, Multiple sclerosis, and epilepsy are accompanied by severe changes of in astrocyte morphology and function (Booth et al., 2017; Oberheim et al., 2008; Simpson et al., 2010; Williams et al., 2007). This observation has led to the hypothesis that not only neuronal dysfunction, but also glial dysfunction contributes to the development and the progression of these diseases.

However, the mechanisms underlying the induction of alterations in astrocyte morphology and function remain poorly understood. It is crucial to further investigate these mechanisms to enhance our understanding of how astrocytes specifically contribute to conditions such as epilepsy. Exploring the function and dysfunction of astrocytes represents an intriguing approach to develop drugs that more precisely target the underlying pathomechanisms of epilepsy.

### 1.3.2 Alterations of astrocyte morphology in epilepsy

Under physiological conditions, astrocytes are organized in exclusive territories infiltrating distinct volumes of the neuropil (Bushong et al., 2002). However, in response to injury and other pathological conditions, astrocytes undergo a process called astrogliosis becoming reactive (Anderson et al., 2014; Sofroniew, 2015; Zhou et al., 2019). Astrogliosis involves alterations in gene and protein expression, as well as changes in their secretome (Anderson et al., 2014; Sofroniew, 2015). During this process, astrocytes undergo morphological changes and exhibit hypertrophy of the cell body and major processes as

well as modified branching and outgrowth of particularly long processes (Sofroniew, 2015).

Astrogliosis is a well-recognized defense mechanism that serves to regulate and maintain the integrity of the blood-brain barrier (BBB) (Heithoff et al., 2021). In addition to its role in BBB regulation, astrogliosis also plays a crucial role in isolating non-injured tissue from damaged areas and providing support for neuronal circuitry and tissue regeneration (Burda et al., 2016; Robel, 2017). As the distance from the injury increases, the characteristic features of astrogliosis, such as hypertrophy and elevated levels of GFAP, tend to decrease (Sofroniew, 2015). Compared to microglia, which rapidly respond to insults in the CNS within minutes, the development of astrogliosis is relatively slow. Hypertrophy of astrocytes and upregulation of GFAP typically occur around 2-3 days after the initial injury (Nimmerjahn et al., 2005). Astrogliosis has been observed in various pathological conditions including Alzheimer's disease, Parkinson's disease and epilepsy (Pekny et al., 2016). It is frequently found in surgical tissue from patients with pharmaco-resistant MTLE and in various experimental epilepsy models (Binder and Steinhäuser, 2006; Witcher et al., 2010). Interestingly, experimental models have shown that the increase in cell volume is accompanied by the loss of fine processes and disruption of spatial domain organization (Oberheim et al., 2008). While it remains unclear whether astrocyte morphology is altered in the early stages of diseases such as Alzheimer's, recent findings have demonstrated that morphological alterations of astrocytes can be detected as early as 10-20 minutes after the induction of epileptiform activity in *in vitro* models as well as after induction of status epilepticus (SE) in *in vivo* models (Anders et al., 2024).

To understand functional mechanisms underlying the acute phases of epileptogenesis, epileptiform activity often is induced by pharmacological treatment (Akdogan and Yonguc, 2011). Although such simplified models do not fully replicate all features of epilepsy, they provide valuable insights into cellular alterations related to the condition. Common pharmacological epilepsy models involve targeting the inhibition of  $\gamma$ -aminobutyric acid (GABA<sub>A</sub>) receptors using substances like picrotoxin, bicuculline or penicillin, which shift the balance towards neuronal excitation (Akdogan and Yonguc, 2011). Additionally, low concentrations of extracellular magnesium ions (Mg<sup>2+</sup>) can be used to facilitate activation

of the ionotropic glutamate receptor NMDA, further promoting excitation (Akdogan and Yonguc, 2011).

Recent studies have shown that epileptiform activity induced by different pharmacological agents can prompt rapid restructuring, particularly in the peripheral regions of astrocytes, with a high likelihood of occurring in PAPs (Anders et al., 2024). Intriguingly, these changes have been shown to persist and even exacerbate epileptiform activity, suggesting that astrocytes may contribute to abnormal neuronal activity at the earliest stage of epileptogenesis (Anders et al., 2024). Although some intracellular pathways involved in the rapid morphological changes of astrocytes have been identified (see 1.3.2.1), the specific extracellular signal that triggers these changes remains unknown. Further research is needed to unravel the signaling mechanisms underlying these rapid morphological alterations in astrocytes and their role in epileptic activity.

#### 1.3.2.1 Molecular Basis of rapid astrocytic morphology changes induced by epileptiform activity

Recent studies have demonstrated that astrocytes undergo rapid changes in morphology within minutes after onset of epileptiform activity (Anders et al., 2024). Changes of astrocyte morphology can be mediated by passive mechanisms like water flux across the astrocyte membrane facilitated by aquaporins (AQP, Fig. 3), but also by active remodeling of the actin cytoskeleton (Reichenbach et al., 2010).

The cytoskeleton, composed of actin microfilaments, microtubules, and intermediate filaments, plays a critical role in maintaining cell shape and plasticity, as well as in facilitating various cellular functions including cell motility, signal transduction, phagocytosis, migration, and adhesion (Fletcher and Mullins, 2010; Zigmond, 1996). In the context of astrocytes, the actin cytoskeleton is particularly vital for mediating rapid morphological changes (Schiweck et al., 2018).

Notably, morphology changes induced by epileptiform activity were prevented by inhibition of the RhoA associated coiled-coil kinase (ROCK) a key regulator of the actin cytoskeleton (Anders et al., 2024). ROCK is involved in regulating the myosin light chain (MLC) which is necessary for the formation and maintenance of stress fibers and focal adhesions (Amano et al., 2010). Additionally, ROCK can phosphorylate Lin-11, Isl-1, and Mec-3 kinases (LIMK) 1 and 2 which in turn increase actin dynamics by regulating cofilin

phosphorylation (Midori et al., 1999; van Rheenen et al., 2009). Cofilin-1, a pH-dependent regulator of actin filament polymerization, controls the remodeling of thin cell protrusions (Kanellos and Frame, 2016).

The activity state of ROCK is regulated by the small GTPase RhoA (Nakagawa et al., 1996). RhoA is a member of the Rho GTPase family, which comprises approximately 20 subtypes, with Rho, Rac, and Cdc42 being the most extensively studied. These small GTPases play crucial roles in regulating cytoskeletal reorganization in different cellular processes (Burridge and Doughman, 2006).

Small GTPases act as binary molecular switches transitioning between an active GTP-bound and an inactive GDP-bound state (Etienne-Manneville and Hall, 2002). They possess a conserved amino acid sequence necessary for GDP/GTP binding, enabling their characteristic GTPase activity, which involves the hydrolysis of GTP to GDP (Takai et al., 1992). The cycling between the two conformational states is tightly regulated by guanine nucleotide exchange factors (GEFs) that catalyze the exchange of GDP for GTP, leading to activation, and GTPase-activating proteins (GAPs) that enhance GTP hydrolysis, resulting in inactivation (Bos et al., 2007).

In the GTP bound state RhoA is inserted in the plasma membrane where it can interact with and signal through its downstream effectors. The cycling between membrane and cytosol is controlled by guanine nucleotide dissociation inhibitors (GDIs), which can form stable complexes with both the GDP- and GTP-bound forms of RhoA (Mosaddeghzadeh and Ahmadian, 2021).

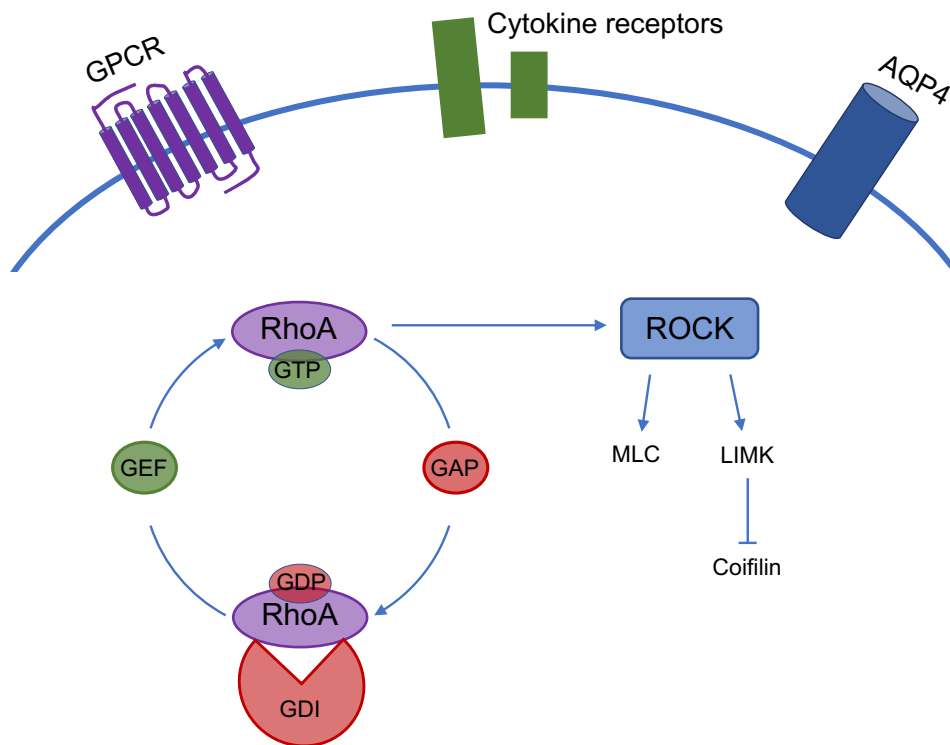


**Fig. 3:** Regulators of astrocyte morphology

Astrocyte morphology changes can occur via passive mechanisms, such as AQP-facilitated water flux, or through active actin cytoskeleton remodeling. A key regulatory mechanism of the astroglial cytoskeleton is RhoA/ROCK signaling. RhoA is a small GTPase that shifts between an active GTP-bound and an inactive GDP-bound state. The shift between the two activity states is regulated by GEFs (guanine nucleotide exchange factors), GAPs (GTPase-activating proteins) and GDIs (guanine nucleotide dissociation factors). The GDP/GTP cycle of RhoA is further modulated by signals from various classes of surface receptors including G-protein-coupled receptors (GPCRs) and cytokine receptors. GTP-bound RhoA activates ROCK which in turn phosphorylates its substrates MLC (myosin light chain) and LIMK (Lim kinase 1 and 2).

The GDP/GTP cycle of RhoA is regulated by signals originating from various classes of surface receptors including G-protein-coupled receptors (GPCRs), tyrosine kinase receptors (TKRs), cytokine receptors, and adhesion receptors (Kjøller and Hall, 1999). However, preliminary work suggested that common signaling pathways such as inducing astroglial calcium signals or activating endocannabinoid or metabotropic glutamate receptors alone is insufficient to reproduce the observed rapid morphology changes in astrocytes during epileptiform activity (Henneberger et al., 2020). This indicates that the signaling cascades previously proposed to regulate astrocyte morphology may not be mediating the rapid changes observed during epileptiform activity. This could suggest that a different signaling cascade induces these rapid astrocyte morphology changes.

Alternatively, it could also imply that more than one signaling cascade is involved in driving these rapid changes in astrocyte morphology.

Interestingly, previous studies from cell cultures have shown that inflammatory cytokines such as Interleukin-1b (IL1b) or tumor necrosis factor alpha (TNF $\alpha$ ) can modulate astrocyte morphology (Henning et al., 2023; John et al., 2004; Liddelow et al., 2017; Sano et al., 2021). Strong evidence from both animal and human studies demonstrates elevated expression of inflammatory mediators, particularly TNF $\alpha$  and IL1b, in epileptic brain tissue linking epilepsy to inflammation (Aronica and Crino, 2011; Devinsky et al., 2013; Vezzani et al., 2011). Inflammation in the CNS is characterized by an increase of cytokines including TNF $\alpha$  and IL1b released almost exclusively by microglia the resident immune cells in the CNS parenchyma (Perry and Gordon, 1988). Astrocytes express receptors for almost all cytokines released by microglia (Tada et al., 1994). Therefore, it is tempting to hypothesize that the release of inflammatory cytokines may link epileptiform activity to rapid astrocyte morphology changes.

#### 1.4 Inflammation in the central nervous system

Neuroinflammation refers to the inflammatory response that occurs within the brain or spinal cord. This response involves the production of various molecules such as cytokines, chemokines, reactive oxygen species, and secondary messengers (Estes and McAllister, 2014). These mediators are provided by both the innate and the adaptive immune system. The innate immune system is responsible for fast and non-specific immune responses. In the context of neuroinflammation, activation of the innate immune system leads to the recruitment and activation of cells from the adaptive immune system, including B-lymphocytes and T-lymphocytes, which can target specific antigens (Waisman et al., 2015). In pathological condition like epilepsy, there is evidence that components especially of the innate immune system are activated (Beach et al., 1995; Hiragi et al., 2018; Shapiro et al., 2008).

Within the CNS, the innate immune system is primarily represented by resident glial cells, namely microglia (Waisman et al., 2015). Microglia are the resident immune cells of the CNS and are considered the main mediators of the innate immune response in the brain (Kreutzberg, 1996; Perry and Gordon, 1988). They have the ability to secrete various

soluble factors, including chemokines, cytokines, and neurotrophic factors, which can modulate the immune response and contribute to tissue repair processes.

Under normal physiological conditions, microglia remain in a “resting” or surveillance state, where they continuously monitor the microenvironment. In this state, microglia contribute to synaptogenesis and neurogenesis by releasing neurotrophic factors and maintaining cholesterol homeostasis (Miyamoto et al., 2016; Mosser et al., 2017).

However, in response to injury, infection, or disrupted homeostasis, microglia undergo activation and transition into an activated phenotype (Streit and Kreutzberg, 1987). Microglial activation is characterized by various biological responses, including migration to the site of injury or inflammation, proliferation, phagocytosis, antigen presentation, and secretion of diffusible factors (Garden and Möller, 2006; Hanisch, 2002). These activated microglia can secrete various factors that serve as communication signals with surrounding cells, particularly astrocytes, to regulate the inflammatory response following insult or infection (Matejuk and Ransohoff, 2020).

Astrocytes are also important players in neuroinflammation. They express receptors for cytokines released by microglia and can respond to these signals by producing their own inflammatory mediators (Sofroniew, 2014). This communication between microglia and astrocytes helps regulate and amplify the inflammatory response in the CNS. Thus, the interaction between microglia and astrocytes is crucial in coordinating the inflammatory response in the CNS (Garland et al., 2022; Linnerbauer et al., 2020).

Importantly, inflammation and microglia activation have been implicated in various neurological and psychiatric diseases, including Alzheimer's disease, Parkinson's disease, depression, and epilepsy (Amor et al., 2010; DiSabato et al., 2016; Vezzani et al., 2011). The dysregulation of microglial activation and the subsequent inflammatory response are thought to contribute to the pathogenesis and progression of these disorders (Colonna and Butovsky, 2017).

In summary, microglia, as resident immune cells in the CNS, play a critical role in the innate immune response and neuroinflammation. Their activation and secretion of diffusible factors influence the communication with surrounding cells, including astrocytes, to regulate the inflammatory response in various physiological and pathological conditions in the CNS.

#### 1.4.1 Inflammation in the epileptic brain

Over the last twenty years, extensive clinical and experimental evidence has strongly supported the hypothesis that inflammatory processes in the brain play a crucial role in the pathophysiology of seizures and epilepsy (Vezzani and Granata, 2005).

Initial insights into the involvement of inflammation in epilepsy came from studies demonstrating the antiepileptic effects of anti-inflammatory drugs (Steinhauser and Hertting, 1981). Subsequent investigations have revealed increased markers of inflammation in the serum, cerebrospinal fluid (CSF) of patients with epilepsy (Aronica and Crino, 2011; Crespel et al., 2002; Peltola et al., 2000). Specifically, elevated expression of proinflammatory molecules such as  $TNF\alpha$ , IL1b and IL6 has been observed in neurons and glial cells in brain tissue obtained from individuals with drug-resistant epilepsy (Aronica and Crino, 2011; Vezzani et al., 2011).

These findings prompted further investigations into the role of inflammation in experimental models of epilepsy. In fact, experimentally induced seizures in rodents elicit a prominent inflammatory response in brain areas that are involved during the onset and propagation of epileptic activity (Eriksson et al., 1999; Plata-Salamán et al., 2000; Turrin and Rivest, 2004). Concomitant increase of inflammatory mediators is largely attributed to microglial activation as minocycline, a microglia-inhibitor, can block the seizure-induced rise in cytokine concentrations in the hippocampus (Wang et al., 2015).

Notably, prominent examples of cytokines whose expression is often increased in the brains of epilepsy patients and in animal models include the inflammatory mediators IL1b and  $TNF\alpha$  (Ashhab et al., 2013; De Simoni et al., 2000; Annamaria Vezzani et al., 1999). In addition to classical inflammatory cytokines, other molecules such as norepinephrine (NE) and brain-derived neurotrophic factor (BDNF) which are not primarily associated with neuroinflammation but also modulate the neuroimmune-axis, have also been found to be dysregulated in epileptic conditions (Hara et al., 1993; Isackson et al., 1991; Meierkord et al., 1994).

It is well-established that these inflammatory cytokines as well as BDNF and NE, can directly influence neuronal excitability and contribute to epileptogenesis (Dubé et al., 2005; Michev et al., 2021; Vezzani et al., 2011). However, emerging evidence suggests that inflammatory cytokines also exert indirect effect on astrocytes and contribute to epileptogenesis through such mechanisms (Bedner et al., 2015). For instance, it has been

shown that changes in the coupling properties of astroglial networks, commonly observed in animal models of MTLE, can be replicated by the application of cytokines derived from microglia (Bedner et al., 2015; Henning et al., 2023). This has further strengthened the hypothesis that inflammatory cytokines contribute to epileptogenesis not only by signaling to neurons but also through their interactions with astrocytes.

While the impact of these cytokines on the neuronal population in the context of epilepsy has been extensively studied in recent years, our understanding of how these cytokines affect the astroglial population is still limited. However, it is known that astrocytes express receptors for various soluble factors, including TNF $\alpha$ , IL1b, BDNF, and NE, making them critical targets for signaling by activated microglia (Holt et al., 2019; Sofroniew, 2014).

In summary, epilepsy is strongly associated with immune system activation, and inflammatory cytokines are believed to play a significant role in epileptogenesis. TNF $\alpha$ , IL1b, BDNF and NE are among the most prominent inflammation related molecules implicated in this process (Iughetti et al., 2018; Vezzani et al., 2011).

#### 1.4.1.1 Tumor necrosis factor alpha

TNF $\alpha$  was named for its ability to cause tumor cell death *in vitro* and induce hemorrhagic necrosis in solid tumors *in vivo* (Carswell et al., 1975). It is a highly pleiotropic cytokine that can affect various types of cells, engaging in a variety of cellular responses, including the induction of inflammatory gene expression programs, stimulation of cellular proliferation and differentiation, and activation of cell death pathways such as apoptosis and necroptosis (Baud and Karin, 2001).

In the CNS, TNF $\alpha$  is expressed by neurons, astrocytes, and oligodendrocytes, but the main source is activated microglial cells (Renno et al., 1995). TNF $\alpha$  exists in two forms: a transmembrane bound (tmTNF) form and a soluble form (solTNF) (Kriegler et al., 1988). The soluble form is released from the transmembrane form through proteolytic cleavage by the metalloprotease TNF $\alpha$  converting enzyme (TACE) (Black et al., 1997). Both forms of TNF $\alpha$  mediate their biological activities by interacting with the two structurally related receptors: TNF $\alpha$  receptor 1 (TNFR1) and TNF $\alpha$  receptor 2 (TNFR2), which belong to the TNF receptor superfamily (Locksley et al., 2001). This superfamily comprises two groups: one group that harbors a death domain in their cytoplasmic region and another group

without a death domain. TNFR1 belongs to the first group, while TNFR2 belongs to the second group (Song and Buchwald, 2015).

TNFRs do not possess intrinsic kinase activity and transduce signaling through binding to adaptor proteins (Cabal-Hierro and Lazo, 2012). Adaptor proteins can be classified into two groups: one group with a death domain such as TNFR1-associated death domain proteins (TRADDs) or Fas-associating proteins with death domain (FADDs), which are involved in death receptor signaling and can only bind to TNFR1, and a second group without death domain (Xie, 2013). The second group includes TNF receptor adaptor factor (TRAF) proteins which can interact with the receptors either directly through the TRAF interacting motif (TIM) domains present in the receptors or indirectly with other adaptor proteins acting as intermediates (Xie, 2013). The binding of these adaptor proteins to the TNFRs induces the activation of different pathways leading to the activation of NF- $\kappa$ B and various kinases, and the initiation of cell death processes such as apoptosis or necroptosis (Wajant et al., 2003).

TNFR1 is constitutively expressed in most tissues of the body, whereas expression of TNFR2 is highly regulated and is typically found only in cells of the immune system (Wajant et al., 2003). Activated NF- $\kappa$ B in turn induces the expression of many other pro-inflammatory factors (Liu et al., 2017).

There is emerging evidence that TNF $\alpha$  plays a crucial role in epileptogenesis. First, TNF $\alpha$  levels increase quickly after seizure induction in animal models for epilepsy (Ashhab et al., 2013; Vezzani and Granata, 2005). Second, there is evidence that TNF $\alpha$  alters seizure susceptibility and severeness (Patel et al., 2017). This is most likely due to the ability of TNF $\alpha$  to activate glutamatergic neurons and promote the formation of excitatory synapses (Pan et al., 1997; Santello and Volterra, 2012). Moreover, TNF $\alpha$  is a powerful inducer of apoptosis (Rath and Aggarwal, 1999). Both, overexcitation and apoptosis are believed to be crucial in epileptogenesis. However, there is increasing evidence that TNF $\alpha$  promotes epileptic activity not only by acting on neurons but also on astrocytes (Bedner et al., 2015; Henning et al., 2023; Sano et al., 2021). Specifically, it was shown that TNF $\alpha$  reduces the network coupling strength in the astroglial network (Bedner et al., 2015). Astrocytic uncoupling in turn is likely to be crucial for epileptogenesis (Steinhäuser et al., 2012).

#### 1.4.1.2 Interleukin 1b

IL1b is a key signaling molecule in the innate immune response and plays a crucial role in the regulation of innate immunity in both the central nervous system (CNS) and the periphery (Mantovani et al., 2019). IL1b, along with IL1a, was the first cytokine discovered in the IL1 family, named for their capacity to communicate between leukocytes, even though today it is evident that IL1 exerts its effects on a much wider range of cells (Garlanda et al., 2013). IL1b induces the expression of inflammatory cytokines and chemokines, enhances phagocytic capacity and tissue trafficking of leukocytes, and activates the activity of the complement and adaptive immune systems (Dinarello, 2018).

In the CNS, IL1b is primarily produced as a pro-protein form and is largely provided by microglia. In order to become biologically active, pro-IL1b must be cleaved by the cytosolic enzyme caspase-1 (Schumann et al., 1998), which is activated when assembled into an inflammasome complex (Sollberger et al., 2014).

The primary receptor for IL1b is interleukin-1 receptor 1 (IL1R1) which is abundantly expressed in most cell types in the CNS including neurons, astrocytes, and endothelial cells (Liu et al., 2019). Upon binding of IL1b to IL1R1, a structural change occurs that allows for the recruitment of the coreceptor IL1R3 which is required for signal transduction (Fields et al., 2019). This leads to the assembly of intracellular signaling proteins, such as myeloid differentiation primary response gene 88 (MYD88) and interleukin-1 receptor-activated protein kinase (IRAK) (Brikos et al., 2007), followed by activation of tumor necrosis factor receptor-associated factor 6 (TRAF6). This activation ultimately results in the release and nuclear translocation of NF- $\kappa$ B, leading to enhanced transcription of NF- $\kappa$ B-dependent genes, including various cytokines, complement factors, adhesion molecules, and interferons (Weber et al., 2010).

IL1b has gained increasing attention in epilepsy research, due to its critical contribution to fever-induced neuronal hyperexcitability, which underlies febrile seizures and may promote development of MTLE (Dubé et al., 2005). Furthermore, enhanced expression of IL1b has been observed in experimental models of epilepsy, which correlates with increased electrographic (Vezzani et al., 1999).

In summary, epilepsy is strongly associated with microglial activation and the release of inflammatory cytokines such as IL1b (Hiragi et al., 2018; Ravizza et al., 2008; Vezzani et al., 2011). However, not only are classical inflammatory molecules like TNF $\alpha$  and IL1b

increased under epileptic conditions, but molecules such as NE and BDNF have also been shown to be elevated in epileptic conditions (Hara et al., 1993; Isackson et al., 1991).

#### 1.4.1.3 Brain derived neurotrophic factor

BDNF is a homodimeric protein synthesized and released by neurons, astrocytes, and microglia (Brigadski and Leßmann, 2020). It plays a critical role as a growth factor in the development, maturation, and maintenance of the CNS (Huang and Reichardt, 2001). Notably, during inflammation, BDNF can act as a neurotrophic factor for astrocytes, promoting their survival and supporting their functions in the CNS. Moreover, the release of BDNF is regulated by microglia and therefore, BDNF is closely related to the neuroimmune-axis (Gomes et al., 2013; Jin et al., 2019).

BDNF signals through the tropomyosin-related kinase B (TrkB) receptor (Barbacid, 1994). In the CNS, TrkB exists in two main isoforms. The full-length receptor (TrkB.FL) and the two truncated receptor isoforms TrkB.T1 and TrkB.T2. The full-length receptor possesses a tyrosine kinase domain that becomes autophosphorylated upon binding of BDNF, while the truncated receptors lack this kinase domain (Barbacid, 1994). Neurons predominantly express the full-length receptor, whereas astrocytes solely express TrkB.T1 (Holt et al., 2019; Ohira et al., 2007).

Although pathways mediated by TrkB.T1 have been increasingly studied not all of these cascades have been fully characterized to date (Cao et al., 2020; Fenner, 2012). The intracellular domain of TrkB.T1 interacts with G-proteins that activate protein kinase C (PKC), which is crucial for cell maturation (Deinhardt and Chao, 2014; Fenner, 2012). BDNF may also control  $Ca^{2+}$  release in astrocytes through the stimulation of phospholipase C (PLC) (Deinhardt and Chao, 2014; Fenner, 2012). Additionally, TrkB.T1 interacts with a GDI, thereby influencing astrocyte morphology (Ohira et al., 2005).

Imbalances in BDNF levels have been linked to neurological and psychiatric disorders, such as schizophrenia, post-traumatic stress disorder, Alzheimer's disease, Parkinson's disease, and Huntington's disease (Dou et al., 2022). Interestingly, both BDNF and its associated receptor have been found to be increased in animal models and humans with epilepsy (Nawa et al., 1995) (Ernfors et al., 1991; Isackson et al., 1991; Nibuya et al., 1995; A. Vezzani et al., 1999). Multiple lines of evidence support the hypothesis that BDNF contributes to epileptogenesis by modulating the balance between synaptic inhibition and

excitation. Furthermore, BDNF may induce slower time-scale changes in dendritic or axonal sprouting, synaptic morphology, and synapse formation (Lu, 2003). However, most investigations into the role of BDNF in epilepsy have focused on neuronal mechanisms, and the potential epileptogenic effects of BDNF on astrocyte morphology remain relatively unexplored.

#### 1.4.2 The role of norepinephrine in the epileptic brain

The immune system and the sympathetic nervous system are closely interconnected (Lorton and Bellinger, 2015). The sympathetic nervous system regulates various biological processes, and the neurotransmitters epinephrine and norepinephrine (NE) are well-studied regulators of this system. NE plays a crucial role in regulation of arousal, attention, cognitive function, and stress reactions (McCormick et al., 1991). In response to infection, tissue injury and inflammation sympathetic nerves increase their firing rates leading to an increased release of NE (Molina, 2005; Pongratz and Straub, 2014). Within the CNS, NE is diffusely released by axons originating from neurons in the locus coeruleus (LC) in the brain stem.

In humans, actions of NE are mediated by three major classes of adrenergic receptors (ARs): alpha1, alpha2, and beta receptors each having again three subtypes (Bylund, 2013). ARs are G protein-coupled receptors (GPCRs) activated by binding of the endogenous ligands epinephrine and NE, which differ in their affinity (McPherson et al., 1985). The receptor types differ mainly in their associated G-proteins. Alpha1 adrenoceptors activate phospholipid metabolism through  $G_{q/11}$  G-proteins, leading to the activation of phospholipase C (PLC) and, ultimately, serine-threonine protein kinase C (PKC) (Hein and Kobilka, 1995). In contrast, alpha2 adrenoceptors inhibit cyclic adenosine monophosphate (cAMP) production by binding to membrane-bound adenylyl cyclase (AC) via  $G_i$  proteins. Meanwhile, the three families of beta adrenoceptors promote an increase in cAMP levels by activating the stimulatory G-protein  $G_s$  (Hein and Kobilka, 1995).

It is a consistent finding throughout the literature that adrenergic signaling regulates the morphology of cultured astrocytes via cAMP-dependent and -independent mechanisms (Kitano et al., 2021; Sherpa et al., 2016; Vardjan et al., 2014).

Dysregulation of NE within the CNS has been implicated in neurodegenerative disorders such as Alzheimer's disease and Parkinson's disease (Peterson and Li, 2018).

Interestingly, the concentration of NE as well as epinephrine rapidly increase in serum of patients after seizures (Simon et al., 1984). Moreover, NE levels in the brains of spontaneously epileptic rats are reported to be higher than in control rats (Hara et al., 1993). While the effect of increased levels of NE on the neuronal population has been extensively studied, less is known about how NE affects the astrocytic population during epileptogenesis.

In summary, NE represents an interesting potential mediator of rapid astrocyte morphology changes upon epileptiform activity.

### 1.5 Aim of the study

Astrocytes within the hippocampal formation appear to detect and respond to epileptiform activity (Fig. 4). Yet, the precise signaling cascade triggering morphological changes in astrocytes shortly after the onset of epileptiform activity remains elusive. Intriguingly, expression of inflammatory cytokines such as TNF $\alpha$  and IL1 $\beta$  escalates acutely following the induction of epileptiform activity. Notably, both of these cytokines have been associated with morphological changes in astrocytes in different contexts in the past. However, the connection between inflammatory cytokines and early morphological changes in astrocytes after the onset of epileptiform activity remains unexplored.

Furthermore, besides classical inflammatory mediators, modulators such as NE and BDNF also increase under epileptiform conditions. Interestingly, both NE and BDNF have been implicated in signaling cascades leading to morphological changes in astrocytes.

This study aims to investigate the mechanisms underlying rapid changes in astrocyte morphology in response to epileptiform activity within the hippocampal formation.

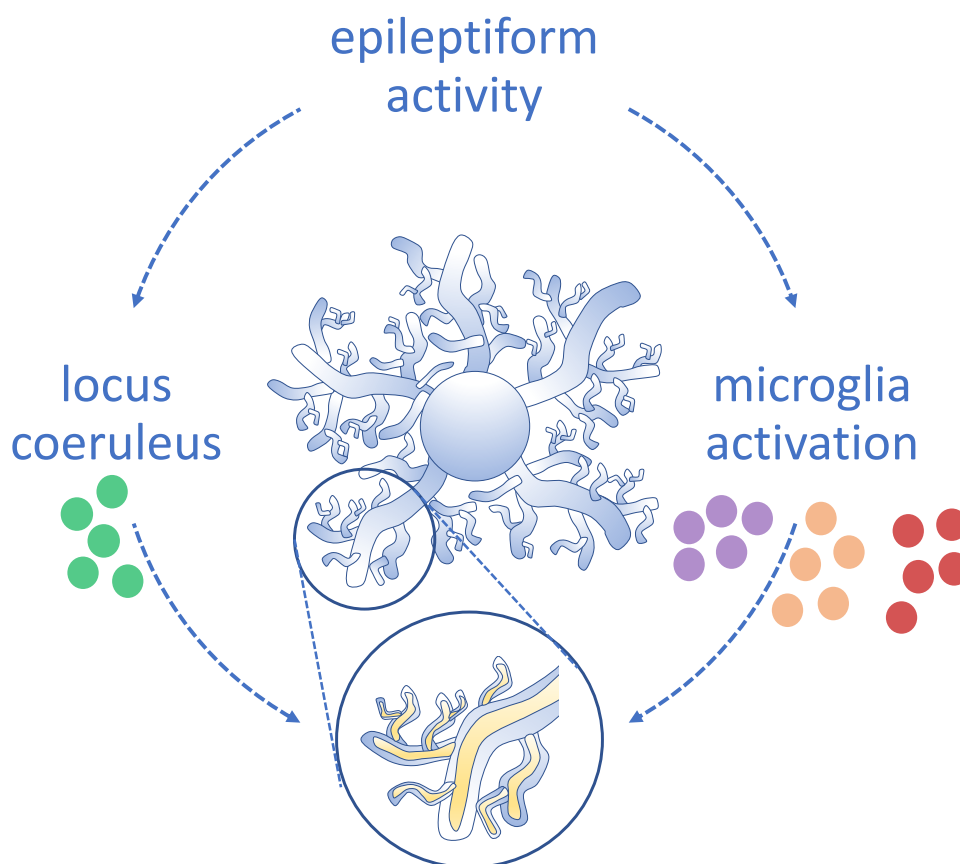


**Fig. 4:** Signaling molecules that could potentially induce rapid astrocyte morphology changes during acute onset of epileptiform activity

Epileptiform activity induces a decrease of the volume of the finest peripheral astrocyte processes. It remains unknown to date, how the astrocyte senses epileptiform activity and which signaling cascade upstream from RhoA/ROCK triggers these morphology changes. In the current study we will test if molecules released among others by activated microglia such as TNF $\alpha$  (red dots), IL1b (orange dots) or BDNF (purple dots) induces morphology changes in astrocytes of acute hippocampal slices. Furthermore, we will test whether NE which is released by neurons originating from the locus coeruleus alters the astrocyte morphology in acute hippocampal slices.

Specifically, the study aims to:

1. Determine whether inflammation, particularly the proinflammatory cytokine TNF $\alpha$ , can induce immediate changes in astrocyte morphology.
2. Examine the influence of extended TNF $\alpha$  exposure on astrocyte morphology changes
3. Examine the impact of TNF $\alpha$  on astrocyte morphology in an epilepsy model using a TNFR1-deficient mouse line, which lacks the TNF $\alpha$  receptor 1.
4. Explore the involvement of other factors, such as BDNF and NE, in mediating acute astrocyte morphology changes

By conducting these investigations, the study aims to provide new insights into the signaling cascades and mechanisms underlying rapid astrocyte morphology changes in response to epileptiform activity. The findings have the potential to enhance our understanding of the role of astrocytes in epileptogenesis and may contribute to the development of new therapeutic strategies for epilepsy.

## 2. Materials and methods

### 2.1 Animal models

Mice from either gender were used throughout the study. Their age ranged from 28 to 40 days. Animals were housed under 12 h light/dark conditions with food and water ad libitum. All animal procedures were conducted in accordance with the regulations of the European Commission and all relevant national and institutional guidelines and requirements. All procedures have been approved by the Landesamt für Natur, Umwelt und Verbraucherschutz Nordrhein-Westfalen (LANUV, Germany) where required.

#### 2.1.1 hGFAP-EGFP mice

To visualize astrocytes, we took advantage of transgenic mice with FVB-background (Friend leukemia virus B). This mouse line has an enhanced green fluorescence protein (EGFP) which is expressed under the control of the human glial fibrillary acidic protein (hGFAP) (Nolte et al., 2001). In the CNS, GFAP is almost exclusively expressed by astrocytes and therefore serves as a label for astrocytes. EGFP-expressing, fluorescent cells of the transgenic mouse line are abundant in all regions of the brain, e.g., the cortex, cerebellum, hippocampus, retina, and the spinal cord (Nolte et al., 2001). With a molecular weight of 26.9 kDa, EGFP freely diffuses into all cytoplasmic compartments (Nolte et al., 2001).

#### 2.1.2 EGFP-TNFR1<sup>-/-</sup> mice

To study the astrocyte morphology in absence of the TNF $\alpha$  receptor 1 (TNFR1), the hGFAP-EGFP mouse line was crossbred with a TNFR1 deficient mouse line. The TNFR1 knockout line derived from the C57BL/6 strain. In the knockout line (TNFR1<sup>-/-</sup>), a phosphoglycerate kinase-neomycin resistance cassette replaced exons 2–5 of the TNFR1 gene via homologous recombination, preventing the expression of functional TNFR1 on the surface of all cell types (Peschon et al., 1998). Simultaneous EGFP expression and complete TNFR1 deficiency was achieved by crossbreeding TNFR1<sup>-/-</sup> mice with hGFAP-EGFP mice (see section 2.1.1). The F1 generation expressed EGFP under the GFAP promotor and showed heterozygous expression of the TNFR1 gene (EGFP-TNFR1<sup>+/-</sup>). Animals from the F1 generation were mated with each other, resulting in an offspring of EGFP-expressing mice with either heterozygous (EGFP-TNFR1<sup>+/-</sup>), homozygous (EGFP-

TNFR1<sup>+/+</sup>), or no expression (EGFP-TNFR1<sup>-/-</sup>) of functional TNFR1. The different genotypes were identified by PCR. EGFP-TNFR1<sup>-/-</sup> mice were used in order to study the role of TNFR1 on astrocyte morphology upon epileptiform activity. Littermates with the TNFR1 wildtype gene (EGFP-TNFR1<sup>+/+</sup>) served as control.

## 2.2 Materials

### 2.2.1 Chemicals

**Tab. 1:** Chemicals

Compound	Supplier
Ascorbic acid	AppliChem GmbH, Darmstadt, Germany
BDNF	Abcam, Cambridge, UK
Glucose	AppliChem GmbH, Darmstadt, Germany
Isofluran (Forene <sup>®</sup> )	AbbVie, Mainz, Germany
KCl	AppliChem GmbH, Darmstadt, Germany
MgCl <sub>2</sub> (6 x H <sub>2</sub> O)	AppliChem GmbH, Darmstadt, Germany
MgSO <sub>4</sub> (7 x H <sub>2</sub> O)	AppliChem GmbH, Darmstadt, Germany
NaCl	AppliChem GmbH, Darmstadt, Germany
NaH <sub>2</sub> PO <sub>4</sub>	AppliChem GmbH, Darmstadt, Germany
Norepinephrine	Tocris, Bristol, UK
Penicillin G (sodium salt)	Sigma, Aldrich, St. Louis, US
Sodium pyruvate	AppliChem GmbH, Darmstadt, Germany
Sucrose	AppliChem GmbH, Darmstadt, Germany
TNF $\alpha$	Tocris, Bristol, UK

### 2.2.2 Solutions

**Tab. 2:** Artificial cerebrospinal fluid (ACSF)

	Concentration (mM)	Osmolarity (mOsm/kg)	MW (g/mol)
NaCl	131.00	262.00	58.44
KCl*	3.00 (4.00)	6.00 (8.00)	74.56
MgSO <sub>4</sub> 7H <sub>2</sub> O	1.30	2.60	246.48
NaH <sub>2</sub> PO <sub>4</sub>	1.25	2.50	119.98
NaHCO <sub>3</sub>	21.00	42.00	84.01
Glucose	10.00	10.00	180.16
+ 2 mM CaCl <sub>2</sub> (1 M stock solution), osmolarity 297-303 mOsm/kg, pH 7.4			

**Tab. 3:** Hyposmolar ACSF

	Concentration (mM)	Osmolarity (mOsm/kg)	MW (g/mol)
NaCl	61.44	122.88	58.44
KCl*	3.00 (4.00)	6.00 (8.00)	74.56
MgSO <sub>4</sub> 7H <sub>2</sub> O	1.30	2.60	246.48
NaH <sub>2</sub> PO <sub>4</sub>	1.25	2.50	119.98
NaHCO <sub>3</sub>	21.00	42.00	84.01
Glucose	10.00	10.00	180.16
+ 2 mM CaCl <sub>2</sub> (1 M stock solution), osmolarity 200 mOsm/kg, pH 7.4			

**Tab. 4:** Hyperosmolar ACSF

	Concentration (mM)	Osmolarity (mOsm/kg)	MW (g/mol)
NaCl	131.00	262.00	58.44
KCl*	3.00 (4.00)	6.00 (8.00)	74.56
MgSO <sub>4</sub> 7 x H <sub>2</sub> O	1.30	2.60	246.48
NaH <sub>2</sub> PO <sub>4</sub>	1.25	2.50	119.98
NaHCO <sub>3</sub>	21.00	42.00	84.01
Glucose	10.00	10.00	180.16
Sucrose	100.00	100.0	17.115
+ 2 mM CaCl <sub>2</sub> (1 M stock solution), osmolarity 400 mOsm/kg, pH 7.4			

**Tab. 5:** Slicing solution

	Concentration (mM)	Osmolarity (mOsm/kg)	MW (g/mol)
Sucrose	105.00	105.00	342.30
NaCl	60.00	120.00	58.44
KCl	2.50	50.00	74.56
MgCl <sub>2</sub> 6 x H <sub>2</sub> O	7.00	21.00	203.30
NaH <sub>2</sub> PO <sub>4</sub>	1.25	2.50	119.98
Ascorbic acid	1.30	1.30	176.12
Sodium pyruvate	3.00	6.00	110.00
NaHCO <sub>3</sub>	26.00	52.00	84.01
Glucose	10.00	10.00	180.16
+ 0.5 mM CaCl <sub>2</sub> (1 M stock solution), osmolarity 300-310 mOsm/kg, pH 7.4			

## 2.3 Electrophysiology

### 2.3.1 Preparation of acute hippocampal slices

1 ml of Isoflurane was dropped on a tissue inside a 10 l glass cylinder. After the isoflurane vaporized, the animals were transferred into the cylinder for anesthesia. To verify the depth of anesthesia, reflexes were tested by pinching the hind paw. When no more motor reaction could be observed, the mice were decapitated with a pair of scissors. In order to expose the skull, the skin of the head was cut coronary with a pair of scissors. Next, the head was put into ice-cold slicing solution, which was supplied with carbogen (95% O<sub>2</sub>/5% CO<sub>2</sub>) for 15 minutes before use. The brain was extracted on a petri dish filled with ice-cold slicing solution by cutting through the skull with small scissors along the coronary line. As soon as the brain was removed from the skull, the forebrain and the cerebellum were cut off using a steel blade. Afterwards, the two hemispheres were separated from each other. On each hemisphere, a ventral and a dorsal cut was performed respectively creating thereby even planes. The dorsal plane was glued to a metal platform. The glued hemispheres were inserted into the slicing chamber which was filled with carbogen-bubbled ice-cold slicing solution. Once the brain was positioned, horizontal slices of 300 µm were cut starting from the ventral hippocampus and moving towards the dorsal hippocampus using a vibratome (Campden Instruments, UK) equipped with a ceramic blade. After slicing was completed, all slices were transferred into a beaker containing slicing solution in a water bath (Grant Instruments, UK) at 34°C for 15 minutes on a net in a custom-made holder. Finally, the slices were transferred into a beaker filled with carbogen-bubbled artificial cerebrospinal fluid (ACSF) and stored at room temperature for at least one hour before being used for experiments.

### 2.3.2 Electrophysiological setup

The electrophysiological setup was placed on a vibration isolated table in a Faraday cage in order to minimize mechanical disturbance and to keep the electrical noise levels as low as possible. The submerged chamber was constantly perfused with carbogen-bubbled ACSF via a perfusion system consisting of an ACSF reservoir connected to the chamber by a silicon tube. With help of an in-line heater (Warner Instruments, US) ACSF was heated up to 34°C. The temperature was monitored by a sensor in the chamber. The ACSF was removed from the chamber by a peristaltic pump and returned through a tube

back to the reservoir. To prevent the slice from moving, a 'harp' (nylon-twines between a U-shaped platinum wire) was placed on top of the slice (Fig. 5). The two-photon excitation laser scanning microscope (see section 2.4.1) was equipped with a camera (Watec Incorporated, US) to display the light microscopy view on a monitor (Dell, US). A grounding pellet (WPI, US) was fixed in the bath and connected to a grounding point, with which also the headstages (Molecular Devices, US) were connected. The headstage including pipette holder controlled by an electrically-driven micromanipulator was placed on one side of the recording chamber. On the other side, a concentric bipolar stimulation electrode (FHC, US) was placed. The stimulation electrode was controlled by a stimulus isolator (Digitimer, US), which was triggered by the Clampex software (pClamp version 10, Molecular Devices, US). Electrical signals were recorded with a teflon-coated silver wire (WPI, US) with a chloride tip which was inserted into a glass pipette, i.e., a field pipette (Science Products, Germany), filled with 5  $\mu$ l ACSF. The field pipette was mounted onto the pipette holder (G23 Instruments, UK) of the headstage (Multiclamp 700b, Molecular Devices, US). The headstage was connected to an amplifier and the incoming signals were cleared from 50 Hz electrical interferences (HumBug, Quest Scientific Instruments, CA). Incoming signals were digitalized by an analogue digital (AD) converter (Digidata 1440A, Molecular Devices, US). The AD converter was connected to the computer (Dell, US). Recordings and stimulations were controlled by the software Clampex (Molecular Devices, San Jose, USA) and stored on the computer for further analysis.

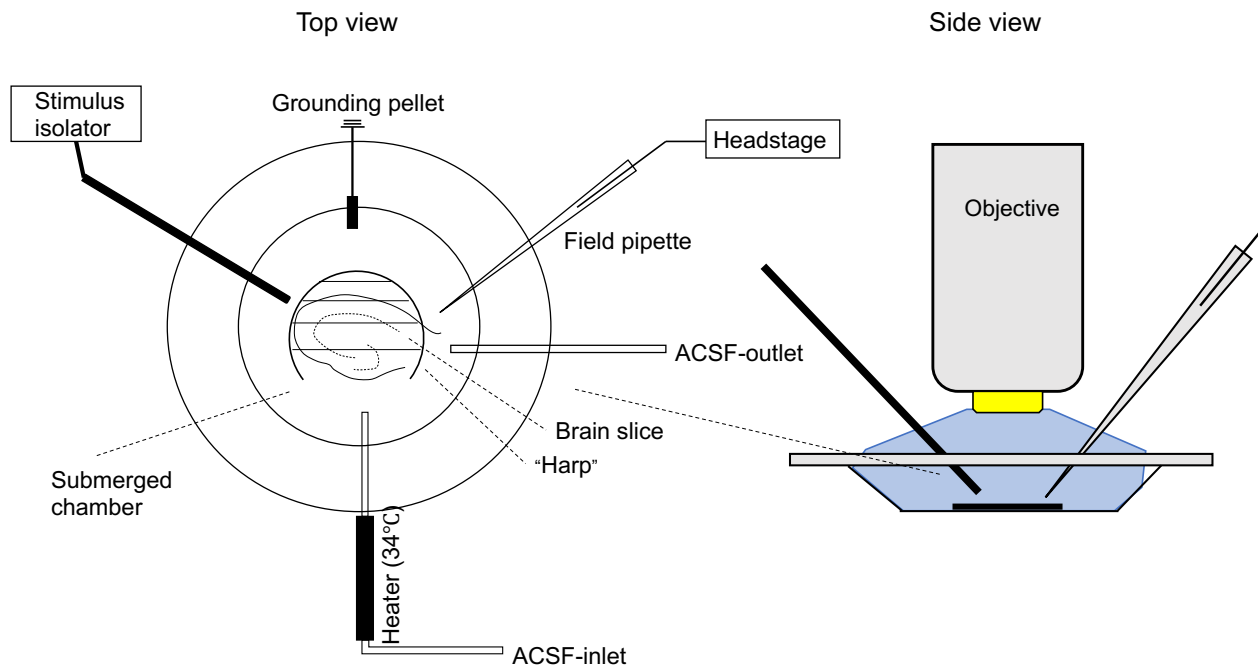


**Fig. 5:** Electrophysiological setup

The hippocampal slice in the submerged chamber was fixed with a “harp”. The supplied ACSF was heated to 34°C and removed by a peristaltic pump on the other side of the chamber. Electrical signals from a population of neurons were recorded via the field pipette.

### 2.3.3 Extracellular field recordings

A slice was transferred into the submerged recording chamber in order to perform electrophysiological recordings. The recording chamber was constantly perfused with ACSF that was carbogen-bubbled and heated to 34°C. Evoked and spontaneous field potentials were recorded with a field pipette that was placed in CA1 *stratum radiatum* or *pyramidale*. The field pipette was mounted on the pipette holder equipped with a Teflon coated silver wire with silver-chloride coated tip. This wire connected the ACSF with the headstage. Glass pipettes were produced using a micropipette puller (Model P-1000, Sutter Instruments, US). To record evoked field potentials (Fig. 6) a bipolar stimulation electrode was placed in the CA2/3 stratum radiatum and Schaffer collaterals projecting to CA1 were stimulated. In order to estimate the stimulation intensity required to evoke the half maximal electrical response, before each experiment a series of stimuli from 25 to 300  $\mu\text{A}$  was applied to the Schaffer collaterals and the corresponding response of the neuronal population was recorded in CA1 stratum radiatum or pyramidale. During the experiments Schaffer collaterals were stimulated every 30 seconds with the half maximal

intensity established beforehand. The corresponding neuronal responses were recorded either in CA1 stratum radiatum or pyramidale.

#### 2.3.4 Analysis of evoked field recordings

For quantification of evoked neuronal activity, characteristic properties of evoked field potentials, such as the extracellularly recorded fiber volley (FV) and the field excitatory postsynaptic potential (fEPSP) were used (Fig. 6). The FV is a sum potential of the axonal (presynaptic) action potential arriving at the recording side. The amplitude of the FV was used as a readout for the number of axons activated by stimulation and is defined by the most negative potential deflection relative to baseline. The FV is followed by the fEPSP which is a manifestation of the synaptic depolarization of the CA1 pyramidal neurons and thus reflects the synaptic transmission following the axonal activation. The slope of the fEPSP was used as readout for the strength of synaptic transmission, as it reflects postsynaptic currents indirectly. The fEPSP slope was measured during the linear rising (recorded in str. oriens close to str. pyramidale) or falling phase (recorded in str. radiatum) of the evoked fEPSP as illustrated by the following equation (see also Fig. 6):

$$fEPSP = \frac{y_2 - y_1 (mV)}{x_2 - x_1 (ms)}$$

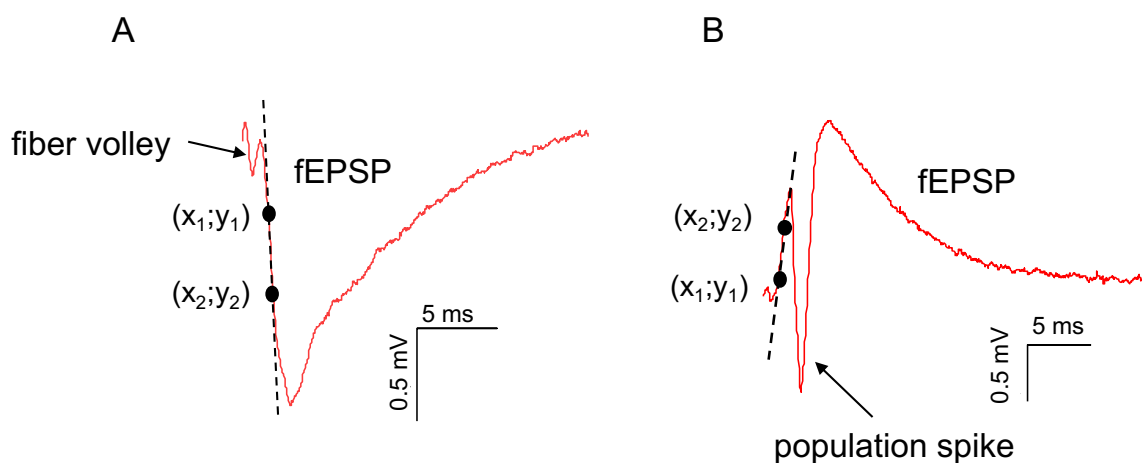


**Fig. 6:** Properties of evoked fEPSPs in CA1 stratum radiatum and pyramidale

Examples of evoked field potentials by Schaffer collateral (SC) stimulation recorded in the CA1 *str. radiatum* (A) and *str. pyramidale* (B) (Stimulation artifacts were removed. In the *str. radiatum*, a fiber volley (FV), representing the axonal activation, and a fEPSP of negative polarity were recorded upon SC stimulation. In the *str. pyramidale*, axonal stimulation evoked field excitatory postsynaptic potentials (fEPSP) consisting of a positive voltage deflection and a population spike of negative polarity. The slopes (dashed lines) were determined in the linear rising or falling phase (between the two black dots) of the fEPSPs. The amplitude of the FV (A) was determined from baseline level to the most negative voltage deflection before the onset of the fEPSP.

### 2.3.5 Induction of epileptiform activity

Evoked and spontaneous epileptiform discharges were recorded as described above in the CA1 stratum pyramidale. In all experiments comprising the induction of epileptiform activity, hippocampal slices were placed on a self-made nylon grid to improve perfusion of the hippocampal slice with ACSF and, in turn, to facilitate the induction of epileptiform activity. Experiments in which epileptiform activity was induced consisted of a 10-minute-long baseline period followed by pharmacological induction of epileptiform activity by bath-application of penicillin. In similar experiments conducted by our laboratory, the penicillin model has proven to be reliable and to induce epileptiform discharges (Anders, 2017). Since this project is based on these previous experiments, we also relied on this model to keep the conditions as comparable as possible. 4 mM penicillin G sodium salt was bath-applied for 30 minutes after the baseline period. In control recordings, no penicillin was applied after baseline recordings. It was shown in previous experiments that for stable induction of epileptiform activity it is necessary to slightly increase the extracellular  $K^+$

concentration (to 4 mM) (Anders, 2017).  $K^+$  concentration was adapted also in control- and baseline recordings to rule out an effect of  $K^+$  on the astrocyte morphology. The frequency of epileptiform discharges was calculated by counting the number of discharges per minute.

## 2.4 Imaging

### 2.4.1 Two-photon excitation fluorescence microscopy

The electrophysiological setup for field recordings was integrated in a Scientifica two-photon system (Scientifica, UK) optically linked to a femtosecond Ti:sapphire pulse laser Vision S (Coherent, US; 73 fs pulse width). EGFP was excited using a wavelength of 800 nm. The setup was equipped with a 40x (NA 0.8) objective (Olympus, Tokyo, Japan). The emissions of the fluorescent signal were separated by a dichroic mirror which reflected wavelengths smaller than 565 to a green filter (band-pass 500 to 550 nm, "green channel"). Subsequently the fluorescence signals were detected and amplified by photomultiplier tubes (PMTs). The system was controlled with help of the Matlab-based (MathWork, Natick, USA) software Scanimage (Scientifica, UK). For light microscopy of the brain slice, the microscope was equipped with an infrared light source and Dodt optics, so that the slices could be displayed on a monitor via a camera (Watec Incorporated, Pine Bush, USA).

### 2.4.2 Monitoring astrocyte morphology

Astrocyte morphology was monitored in parallel to electrophysiological recordings. In all experiments addressing astrocyte morphology, transgenic mice were used that express EGFP under the GFAP promotor (see 2.2.1). EGFP freely diffuses through the cytoplasm. With a size of 26.9 kDa EGFP reaches also the smallest branches in the periphery but cannot diffuse into adjacent astrocytes via gap junctions which are only permeable for molecules smaller than 1 kDa. Therefore, EGFP can be used to visualize single astrocytes morphology (Nolte et al., 2001). Astrocytes with moderate fluorescence intensity in the soma, located at a depth of 50 to 100  $\mu\text{m}$ , were chosen for imaging to ensure consistency and avoid astrocytes with very low or very high EGFP expression. This selection criteria aimed to maintain an astrocyte in the same z-plane throughout the experiment. The deeper the imaged astrocytes are in the tissue, the less is the excitation laser power that

reaches the cell due to attenuation within the tissue. To secure constant laser power at the imaged cells independent of their depth in the tissue, the laser power was adjusted so that the fluorescence intensity was comparable to the intensity measured with 2 mW at the slice surface in order to achieve a sufficient EGFP fluorescence while reducing the risk of photo damage due to a too high laser power. The depth (i.e., the z-position) of the imaged cell was adjusted so that the soma, but also thick and fine branches were visible in a single optical plane. It was adjusted carefully each time before taking a picture to ensure that the z-position was stable throughout the whole experiment. The cells were imaged at a nominal resolution of 0.1  $\mu\text{m}/\text{pixel}$ .

### 2.4.3 Analysis of astrocyte volume fraction

The astrocyte morphology was monitored to capture changes primarily occurring in the periphery of the astrocyte. With a size, smaller than 1  $\mu\text{m}^3$  peripheral branches are smaller than the diffraction limit of two-photon microscopy (Heller and Rusakov, 2017). To capture morphology changes occurring at this spatial range, an indirect read-out of the morphology was used (Medvedev et al., 2014; Minge et al., 2021). A statistical measure to describe astrocyte morphology is the volume fraction (VF). It reflects the fraction of tissue volume that is occupied by an astrocyte in a distinct region of interest (ROI, Fig.7). This concept has been extensively validated as a reliable indicator of local astrocyte structure, providing valuable insights into the spatial organization and morphological characteristics of astrocytes (King et al., 2020; Medvedev et al., 2014; Minge et al., 2021). The assumption for the calculation of the astrocyte volume fraction is that the fluorescence intensity  $F$  at defined pixel coordinates  $(i, j)$  in the  $x - y$  plane is proportional to the local volume of the fluorescent astrocyte branches. The averaged fluorescence  $F(i, j)$  of a region of interest containing all the thick and fine branches is determined (Fig.7). To calculate the volume fraction,  $F(i, j)$  is normalized to a second ROI placed on the soma where fluorescence intensity corresponds to a volume fraction of 100% ( $F_{\text{soma}}$ ). Both, the averaged fluorescence of the ROI and the soma fluorescence are corrected for background fluorescence ( $F_0$ ) which is determined in a region without any labeled structure.

$$A_{VF} = \frac{F_{ROI} - F_0}{F_{soma} - F_0}$$

$A_{VF}$  = astrocyte volume fraction;  $i, j$  = pixel coordinates in the  $x - y$  plane;  $F$  = fluorescence intensity;  $F_0$  = background fluorescence;  $F_{\text{soma}}$  = fluorescence inside the soma

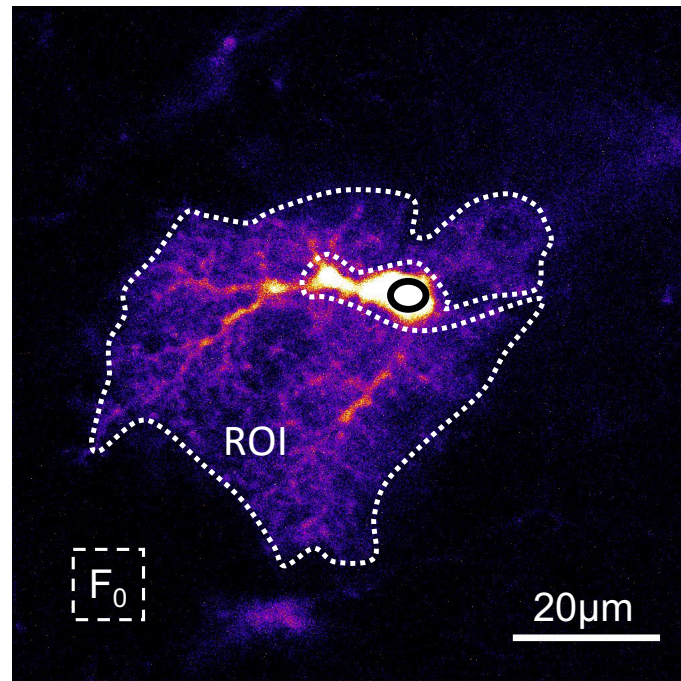


**Fig. 7:** Example of a fluorescent astrocyte in CA1

Astrocytes could be visualized due to EGFP expression under the GFAP promoter. The ROI (region of interest) includes the fine and thick branches of the astrocyte. Fluorescence intensity was normalized to the soma fluorescence ( $F_{\text{soma}}$ , black circle), where 100% of the tissue is occupied by the astrocyte.

#### 2.4.4 Monitoring dynamic astrocyte morphology changes

To assess astrocyte morphology changes in response to different triggers, individual astrocytes expressing EGFP were tracked over a 40-minute period, including a 10-minute baseline. After the initial 10 minutes, various pharmacological agents were applied through bath application for 30 minutes. The pharmacological agents used were penicillin (4 mM),  $\text{TNF}\alpha$  (10 ng/ml), or NE (100  $\mu\text{M}$ ). For the  $\text{TNF}\alpha$  experiments, baseline and control recordings were conducted in the presence of bovine serum albumin (BSA), which was necessary for  $\text{TNF}\alpha$  dilution. Throughout the experimental duration, an image of an astrocyte was captured every five minutes.

The volume fraction of the astrocyte was then calculated for each time point, using the same region of interest (ROI) for consistency. The astrocyte volume fraction was

normalized as a percentage of the average volume fraction during the baseline period. In experiments focusing on astrocyte morphology during epileptiform activity, only slices that exhibited epileptiform activity induced by penicillin were included for morphological analysis.

#### 2.4.5 Astrocyte volume fraction in incubated acute slices

For the incubation with TNF $\alpha$  (10 ng/ml) alone or in combination with Interleukin 1b (IL1b, 10 ng/ml), the acute brain slices were transferred to a beaker filled with carbogen-bubbled ACSF. The control condition consisted of ACSF containing 1% bovine serum albumin (BSA), which was used to dilute TNF $\alpha$  for treatment conditions. The slices were incubated in the respective solutions for a minimum of 2 hours prior to conducting the experiments. For incubation with BDNF (100 ng/ml), the acute hippocampal slices were transferred into chambers of an 8-well plate immediately after preparation. All chambers were supplied with carbogen-bubbled ACSF. The control slices were incubated in regular ACSF. The slices were incubated for at least 1 hour in the well plates since the maximal storage time to maintain slice viability was shorter in well plates compared to beakers.

To characterize astrocyte morphology, images of approximately three different astrocytes per slice were captured, and the volume fraction was calculated. The astrocyte volume fraction of the treated slices was compared to the astrocyte volume fraction of astrocytes from the corresponding control condition to assess any morphological changes.

## 2.5 Osmotic stress

To monitor astrocyte volume fraction and neuronal network properties simultaneously, a combination of two-photon excitation microscopy and electrophysiological recordings was employed.

During the initial 10-minute baseline period, acute hippocampal slices were perfused with isosmotic ACSF with an osmolarity of 300 mOsm/kg. After this baseline period, the isosmotic ACSF was replaced with either hyperosmolar (400 mOsm/kg) or hyposmolar (200 mOsm/kg) ACSF, as indicated in table 3 and 4. The alterations in osmolarity were achieved by either reducing the concentration of NaCl (to decrease osmolarity) or adding sucrose (to increase osmolarity). It should be noted that neither sucrose nor NaCl can

passively cross the cell membrane, so changes in their concentrations result in effective osmotic pressure.

Since changes in  $\text{Na}^+$  concentration alone can affect neuronal excitability,  $\text{Na}^+$  concentration was also reduced during the baseline condition for the hyposmolar recordings to avoid potential effects on synaptic transmission (Huang et al., 1997). To compensate for the lower osmolarity during the baseline period, sucrose was added.

Astrocyte morphology was monitored by capturing an image of an EGFP-expressing astrocyte in the CA1 region every 5 minutes. The volume fraction of the astrocyte was then calculated for each time point. After induction of osmotic stress, the astrocyte volume fraction was normalized as a percentage of the baseline volume fraction for each individual astrocyte. This normalization allows for the comparison of changes in astrocyte morphology across different time points and experimental conditions.

## 2.6 Statistics

All statistical analysis were performed with Origin (OriginLab, 2017, US). The data sets were tested for normal distribution with the Shapiro-Wilk test. The data is presented as mean  $\pm$  standard error of the mean (SEM) followed by n as the number of samples. To test the statistical difference between normally distributed samples Student's t-tests were used. When samples were not normally distributed, the Mann-Whitney U test was used. Statistical significance is indicated in figures with asterisks (\*  $p < 0.05$ ; \*\*  $p < 0.01$ ; \*\*\*  $p < 0.001$ ) and the exact values are given in the figure legend and text.

### 3. Results

#### 3.1 Dynamic morphology changes of astrocytes and synaptic transmission in response to osmotic stress

##### 3.1.1 Astrocyte morphology

In recent years, evidence has emerged that astrocytes are capable of morphological plasticity (Bernardinelli et al., 2014a; Minge et al., 2021; Oliet et al., 2001; Theodosis et al., 2004). Especially the finest perisynaptic astroglial processes (PAPs) undergo structural remodeling in an activity-dependent manner (Bernardinelli et al., 2014b). However, capturing dynamic changes in PAPs has been challenging due their nanoscopic size. A tool that is well established to determine morphology changes in PAPs is the volume fraction (Henneberger et al., 2020; Medvedev et al., 2014; Minge et al., 2021).

The astrocyte volume fraction corresponds to how much of the imaged volume is occupied by the astrocyte (Henneberger et al., 2020; Medvedev et al., 2014). This measurement has been used to monitor rapid morphology changes in astrocytes (Anders, 2017; Henneberger et al., 2020). To demonstrate the effectiveness of volume fraction measurements in capturing such changes, astrocytes were exposed to hypotonic (200 mOsm) and hypertonic (400 mOsm) conditions. These results were published in Minge et al., 2021.

The osmolarity of fluids is determined by the solutes within the fluid. Physiologically, the intra- and extracellular fluids equally have an osmolarity of approximately 300 mOsm/kg (Zidek, 2020). Altering the osmolarity of the extracellular or intracellular compartment by adding (sucrose) or withdrawing (NaCl) solutes that cannot cross the cell membrane, generates osmotic pressure. In response to osmotic pressure, water moves into the compartment with higher osmolarity or out of the compartment with lower osmolarity to establish a new ionic equilibrium. For instance, when cells are exposed to a hypotonic extracellular solution, water moves into the intracellular department, resulting in increased cell volume and a decrease in the volume of the extracellular space (ECS). Conversely, under hypertonic conditions, water flows out of the cells, leading to cell shrinkage and expansion of the ECS. Water-flux across the cell membrane is facilitated by aquaporins (AQP) (Verkman, 2013). Astrocytes show high expression for AQP4, particularly in their processes (Papadopoulos and Verkman, 2013). Therefore, astrocytes are expected to respond to osmotic stress by changing their volume especially in the periphery.

To reconfirm that volume fraction measurements can capture dynamic morphology changes in response to hypo- or hyperosmotic conditions, single EGFP-expressing astrocytes were visualized using two-photon-excitation microscopy (Fig. 8). Baseline recordings were obtained for 10 minutes in isoosmolar ACSF (300 mOsm). Following the baseline period, the ACSF was replaced by either a hypo- or hyperosmolar ACSF for a duration of 30 minutes. During this period, the astrocyte volume fraction was measured at regular intervals, typically every 5 minutes, using two-photon-excitation microscopy, and the volume fraction was calculated for each time point.

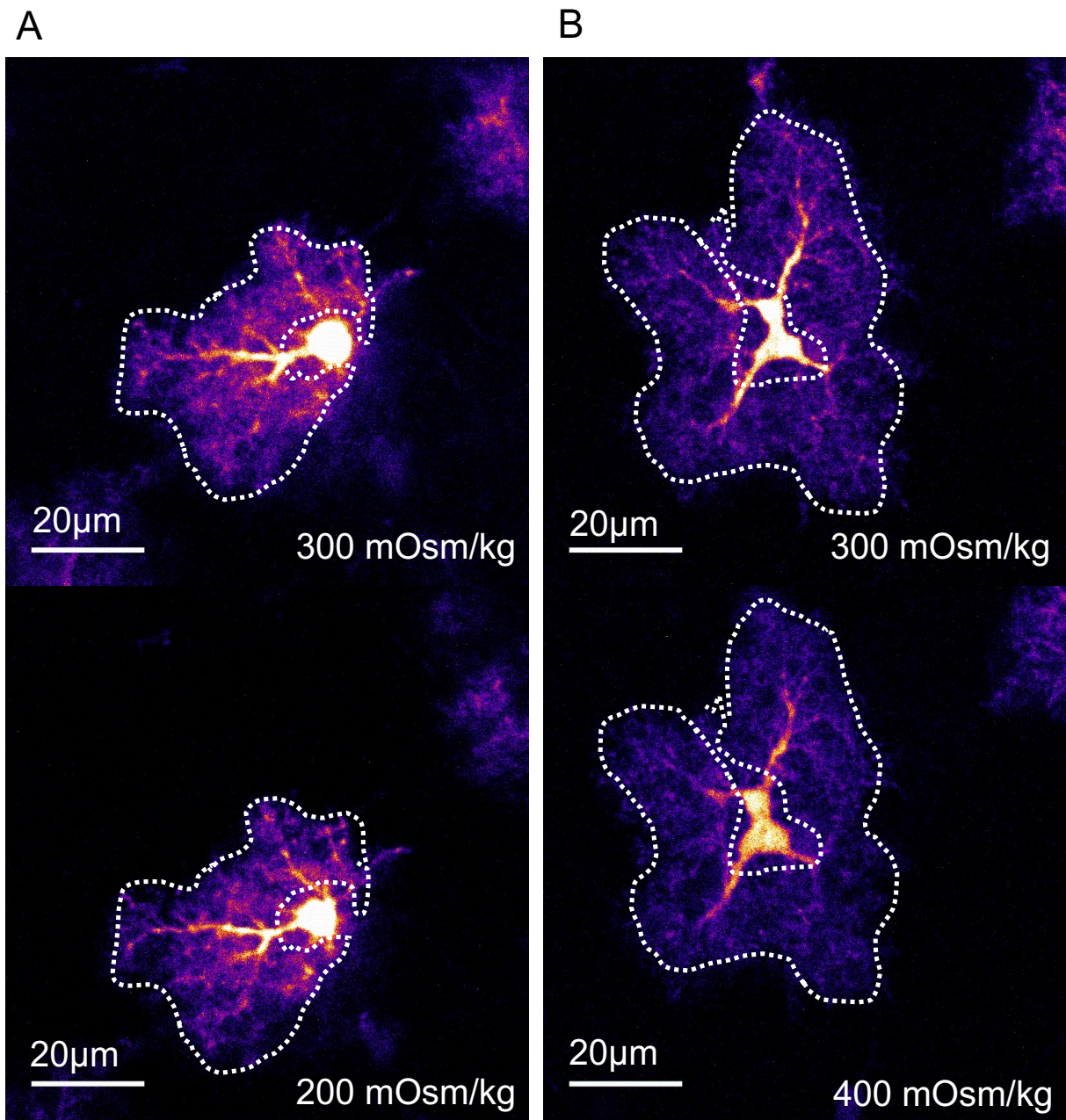


**Fig. 8:** Exemplary EGFP-expressing astrocytes exposed to osmotic stress  
 EGFP-expressing astrocytes before (top) and after osmotic stress (bottom). The ROI (dashed lines) which is required to calculate astrocyte volume fraction was determined before osmotic stress and kept the same during the experiment. In response to hyperosmotic stress (A), the volume of the astroglial soma as well as of the major branches decreased. In turn, in response to hypoosmotic condition (B) the volume of the soma and major branches increased.

Fig. 9 A depicts the astrocyte volume fraction normalized to baseline over time. The average baseline volume fraction of both conditions was  $4.52 \pm 0.27$  % ( $n = 13$ ). In the case of hyperosmolar ACSF exposure, the astrocyte volume fraction decreased

significantly to  $82.73 \pm 2.69$  % after 20 minutes (Fig. 9 B,  $n = 7$ , one-sample t-test,  $p = 0.00067$ ). This indicates a reduction in astrocyte volume in response to increased osmolarity. Conversely, when exposed to hyposmolar ACSF, the average volume fraction increased significantly to  $136.57 \pm 8.11$  %. ( $n = 6$ , one-sample t-test,  $p = 0.0064$ ) after 20 minutes (Fig. 9 B). This suggests an expansion in astrocyte volume under decreased osmolarity conditions. The statistical analysis showed a significant overall difference of  $53.84 \pm 8.01$  % between the two conditions (two sample t-test,  $p=0.000033$ ) between the cells of the two conditions.

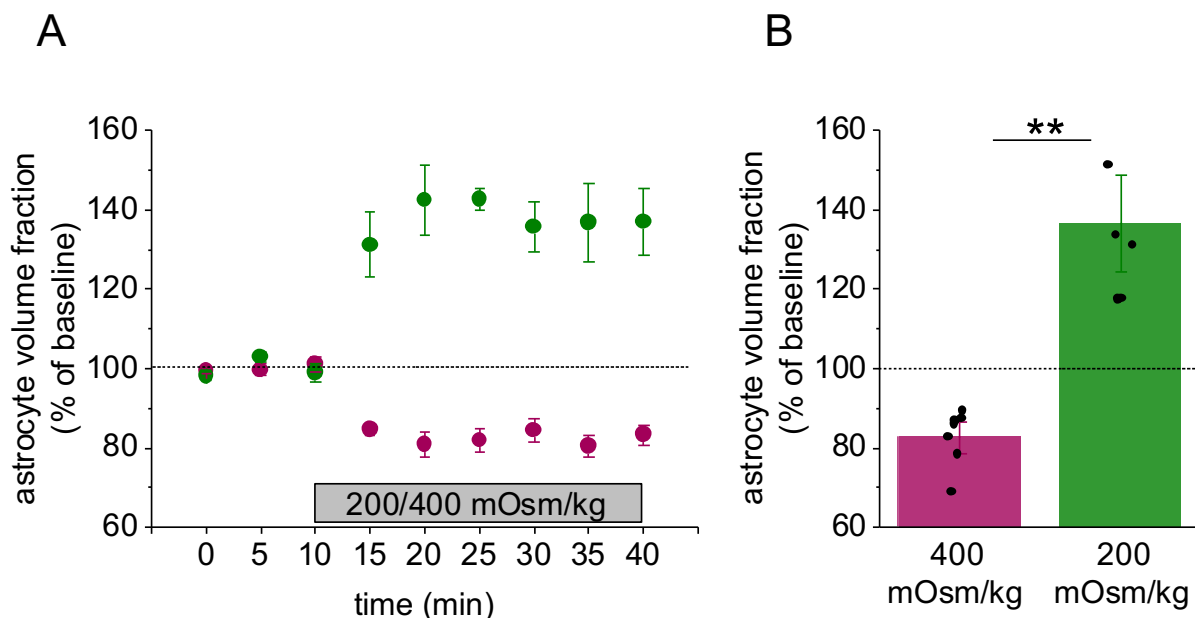


**Fig. 9:** Astrocyte volume fraction changes upon osmotic stress in acute hippocampal slices (A) Time course of normalized astrocyte volume fraction. After 10 minutes of baseline (300 mOsm/kg) osmotic stress was induced by replacing the ACSF with hyperosmotic (400 mOsm/kg, purple) or hyposmotic (200 mOsm/kg, green) ACSF. The normalized astrocyte volume fraction decreased upon hyperosmotic stress and increased upon hyposmotic stress. (B) 20 minutes after application of hyperosmolar solution the average normalized volume fraction was  $82.73 \pm 2.69$  % ( $n = 7$  one-sample t-test,  $p = 0.00067$ ). When hyposmolar solution (green) was applied, the average normalized volume fraction was  $136.57 \pm 8.11$  % ( $n = 6$ , one-sample t-test,  $p = 0.0064$ ). The overall difference between both conditions was  $53.84 \pm 8.01$  % (two sample t-test,  $p=0.000033$ ). Data are expressed and displayed as mean  $\pm$  s.e.m.

In summary, these findings demonstrate that volume fraction measurements are a suitable tool to detect dynamic morphology changes of astrocytes in response to changes in osmolarity (Minge et al., 2021). Hyperosmolar conditions cause astrocytes to shrink, while hyposmolar conditions cause them to expand, as indicated by the changes in the astrocyte

volume fraction. These findings are consistent with previous reports in the literature (Chvátal et al., 2007; Dudek et al., 1990; Risher et al., 2009).

Accordingly, the use of volume fraction analysis in combination with the experimental settings employed in the study allows for the monitoring of dynamic astrocyte morphology changes. Based on these results, the same approach was used in subsequent experiments to investigate astrocyte morphology in response to other stimuli, such as the administration of cytokines. This methodology provides a valuable tool for studying astrocyte plasticity and its modulation by different factors.

### 3.1.2 Synaptic transmission

In addition to investigating the sensitivity of astrocyte morphology to changes in extracellular osmolarity, the current study also aimed to assess whether the chosen experimental setting could detect changes in synaptic transmission concurrent with the osmolarity manipulations.

Synaptic transmission was measured by stimulating Schaffer collaterals (SCs) in the CA3 stratum radiatum (interstimulus interval of 30 seconds) and recording the corresponding neuronal responses in the CA1 stratum radiatum (Fig. 10 A). After a 10-minute baseline period in isoosmolar ACSF, the hippocampal slices were exposed to either hyperosmolar or hyposmolar ACSF.

As illustrated in Fig. 10 A, stimulation of SCs evoked a fiber volley (representing the sum potential of the axonal action potentials) followed by a fEPSP (representing the sum potential of the synaptic activation). It is further illustrated in Fig. 10 A that the fEPSP amplitude is reduced and increased in response to hyperosmolar and hypoosmolar conditions, respectively. To quantify the synaptic activity in response to stimulation, the slope of the fEPSP was analyzed. The slope is commonly used as read-out for synaptic transmission as it is proportional to the postsynaptic currents.

The results indicated that changes in extracellular osmolarity had an impact on synaptic transmission. In response to hyperosmolar ACSF, the fEPSP slope, which reflects synaptic activation, decreased significantly to  $19.00 \pm 2.91$  % compared to baseline ( $n = 9$ , one-sample t-test,  $p = 0.0092$ ). Conversely, the application of hypoosmolar solution led to a significant increase in the fEPSP slope to  $244.80 \pm 52.41$ % compared to the initial response ( $n = 6$ , one-sample t-test,  $p = 0.040$ ) (see Fig. 10 B).

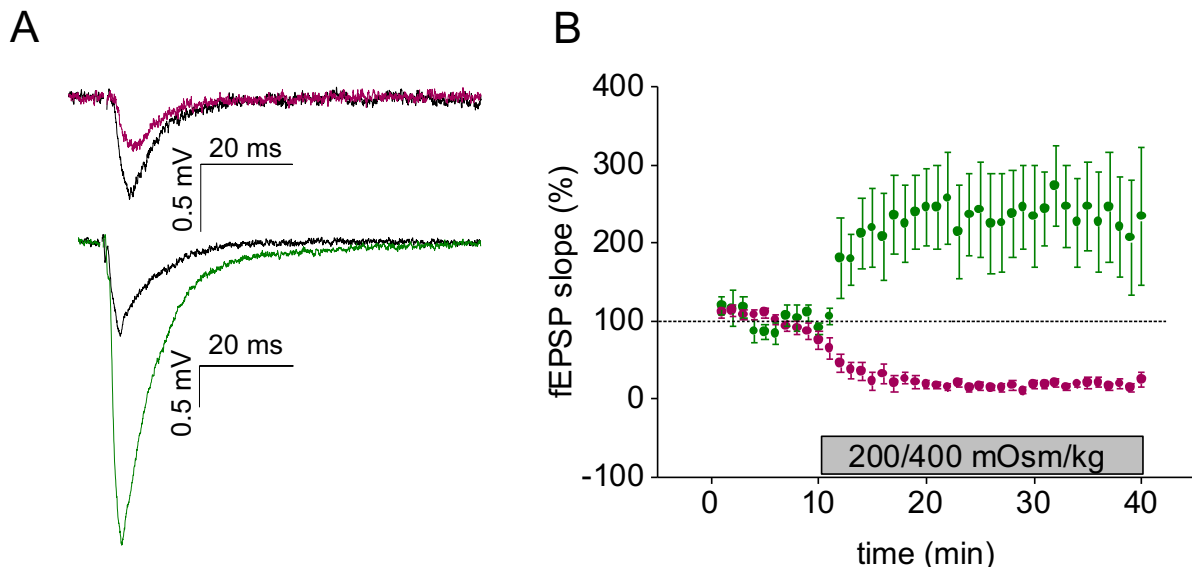


**Fig. 10:** Altered extracellular osmolarity modulates synaptic transmission in CA1 neuron populations

(A) Example trace of evoked fEPSPs in response to Schaffer collateral stimulation recorded in the CA1 stratum radiatum in hGFAP-EGFP mice before (black) and after wash-in of hyperosmolar solution (purple) or hyposmolar solution (green). (B) The graph shows the mean slope of the evoked fEPSPs in CA1 stratum radiatum over time normalized to the baseline. The mean slope after hypoosmolar treatment (green) was increased to  $244.80 \pm 52.41\%$  ( $n = 6$ , one sample t-test,  $p=0.040$ ). The mean normalized slope after hyperosmolar treatment (purple) was decreased  $19.00 \pm 2.91\%$  ( $n = 9$ , one-sample t-test,  $p= 0.0092$ ). Data are expressed and displayed as mean  $\pm$  s.e.m.

In conclusion, these results successfully demonstrated that osmotic stress can modulate synaptic transmission, consistent with previous literature findings (Huang et al., 1997). This suggests that the chosen experimental setting is capable of detecting changes in synaptic transmission induced by osmotic alterations. Furthermore, these findings highlighted the effectiveness of combining two-photon excitation microscopy with electrophysiological recordings. This integrated approach allowed for the simultaneous assessment of astrocyte morphology changes and changes in synaptic transmission, and it will be particularly useful in further experiments involving the induction of epileptiform activity.

### 3.2 Astrocyte morphology changes occur acutely after onset of epileptiform activity

We demonstrated that our indirect approach to calculate the astrocyte volume fraction can be used to monitor astrocyte morphology changes in response to osmotic stress (see

section 3.1.1). In addition, previous work from our laboratory has found that astrocytes also change their morphology in response to epileptiform activity (Anders et al., 2024). Although these morphology changes were of much smaller scale, they had important proepileptiform consequences. However, the exact mechanism underlying said proepileptiform astrocyte morphology changes remains elusive.

We hypothesized that cytokines may be involved in the induction of astrocyte morphology changes during epileptiform activity. In order to test this hypothesis, we first reproduced the previous findings in our experimental settings.

Anders et al. found that astrocyte morphology changes occurred during epileptiform activity induced by different models of epilepsy. In this work, we relied on induction of epileptiform activity by bath-application of penicillin. Besides its antimicrobial properties, penicillin has a proconvulsive effect due to inhibition of GABA<sub>A</sub> receptor-mediated chloride influx (Tsuda et al., 1994). The application of penicillin to acute hippocampal slices is known to elicit interictal epileptiform activity (Akdogan and Yonguc, 2011). The astrocyte morphology was monitored simultaneously with the induction of epileptiform activity using the penicillin model in order to examine how astrocytes respond to epileptiform activity. EGFP-labeled astrocytes were visualized using two-photon excitation microscopy, while simultaneous electrophysiological recordings were performed. Specifically, evoked and spontaneous fEPSPs were recorded in CA1 stratum pyramidale using a field pipette while astrocytes in CA1 were imaged.

After a 10-minute baseline recording period, penicillin (4 mM) was bath-applied to induce epileptiform activity, and the morphology of a single astrocyte per slice was imaged over a period of 30 minutes. In the control condition, single astrocytes were also imaged without exposure to penicillin, to serve as a comparison.

In the control and baseline conditions, no spontaneous discharges were observed (Fig. 11 B). However, typical spontaneous discharges (Fig. 11 A) occurred in 85% of slices after application of penicillin (11 out of 13 slices). Epileptiform activity started generally 5 to 10 minutes after application of penicillin (Fig. 11 B, left) with a mean frequency of  $2.10 \pm 0.74 \text{ min}^{-1}$  (Fig. 11 B, right) 10 minutes after penicillin application.

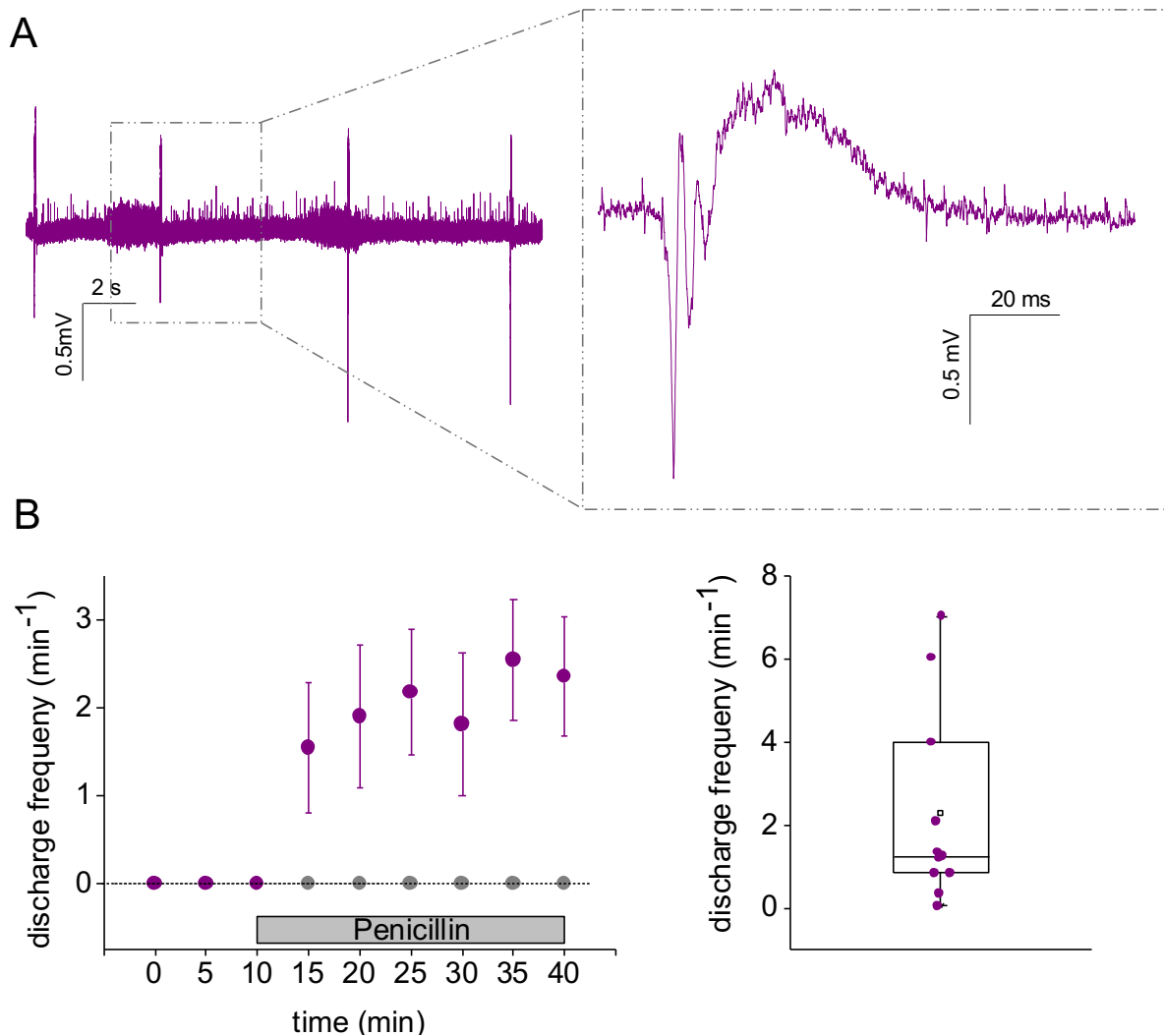


**Fig. 11:** Application of penicillin induces epileptiform activity in acute hippocampal slices (A) Example trace of penicillin recordings. Application of 4 mM penicillin reliably led to epileptiform activity with typical spontaneous discharges. (B) Discharge frequency per minute reached a stable level 5 to 10 minutes after application of penicillin (left) with a mean frequency of  $2.10 \pm 0.74 \text{ min}^{-1}$  (right). Data are expressed and displayed as mean  $\pm$  s.e.m.

During the entire time-course of the experiment (40 minutes), single astrocytes were imaged every five minutes alongside electrophysiological recordings. The average baseline volume fraction of all imaged astrocytes was  $4.53 \pm 0.36 \%$  ( $n = 13$  cells). To compare changes in astrocyte volume fraction over time, the volume fractions at each time point were normalized to the respective average volume fractions during baseline conditions (Fig. 12 A). After induction of epileptiform activity using bath application of penicillin the normalized astrocyte volume fraction decreased significantly by  $13.6 \pm 1.94\%$

compared to baseline ( $n = 7$ , one sample t-test,  $p = 0.00043$ ) and  $11.10 \pm 2.24$  % compared to control conditions (control  $n = 6$ , penicillin  $n = 7$ , two sample t-test,  $p = 0.00041$ ) (Fig. 12 B). Under control conditions (no penicillin application), the volume fraction of astrocytes decreased by only  $2.41 \pm 0.74$  % compared to baseline ( $n = 6$ , one sample t-test,  $p = 0.030$ ). This indicates that the decrease of the astrocyte volume fraction is specifically mediated by the induction of epileptiform activity via penicillin application and not due to a general decrease of the astrocyte volume fraction over the experimental time course.

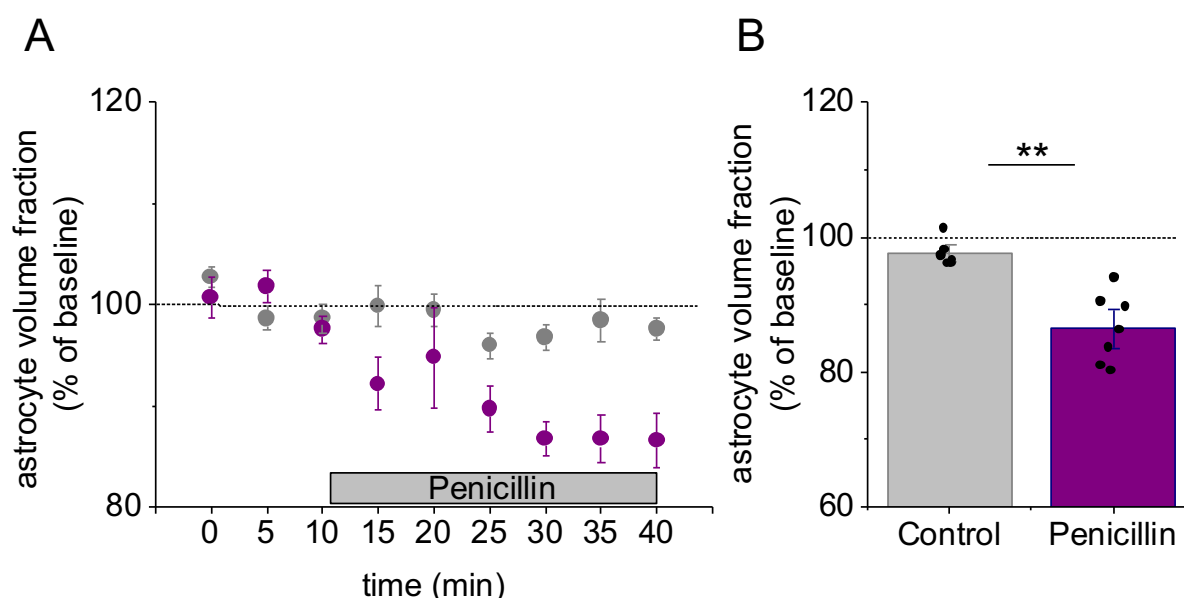


**Fig. 12:** Epileptiform activity induces rapid astrocyte morphology changes

(A) Time course of the normalized astrocyte volume fraction over 40 minutes, induction of epileptiform activity (purple) led to a decrease of astrocyte volume fraction compared to control (grey) (B) Bar graph of the average astrocyte volume fraction (normalized to baseline) during the last 10 minutes. In control conditions the average volume fraction was  $97.60 \pm 0.80$  % (grey,  $n = 6$ , one sample t-test,  $p = 0.030$ ) and in penicillin recordings the average volume fraction was  $86.45 \pm 1.94$  % (purple,  $n = 7$ , one sample t-test,  $p = 0.00043$ ) compared to baseline. The overall difference between both conditions is  $11 \pm 2.24$  % (two sample t-test,  $p = 0.00041$ ). Data are expressed and displayed as mean  $\pm$  s.e.m.

In summary, this study successfully replicated the previous findings from our laboratory, demonstrating that astrocyte volume fraction remains stable over the entire experimental duration under control conditions, while the induction of epileptiform activity leads to a significant decrease in astrocyte volume fraction. Building upon these findings, we further investigated the underlying mechanisms of astrocyte morphology changes. Specifically, we explored the involvement of various cytokines using different experimental approaches to examine their impact on astrocyte morphology changes in acute murine brain slices.

### 3.3 The role of TNF $\alpha$ in astrocyte morphological plasticity

Previous work showed that onset of epileptiform activity in acute hippocampal slices is accompanied by rapid astrocyte morphology changes (see section 3.2). Furthermore, epilepsy is highly associated with increase of inflammatory cytokines such as TNF $\alpha$  (Ravizza et al., 2008; Vezzani et al., 2011). Intriguingly, it has been shown repeatedly that the pleiotropic cytokine engages signaling pathways that lead down to RhoA/ROCK signaling and concomitant morphology changes in different cell types (Hunter and Nixon, 2006; Kant et al., 2011a; Wójciak-Stothard et al., 1998). Previous experiments suggested that rapid astrocyte morphology changes upon epileptiform activity depend on RhoA/ROCK signaling. It has not been shown specifically whether TNF $\alpha$  modulates RhoA/ROCK signaling in astrocytes of acute hippocampal slices. However, TNF $\alpha$  is a promising candidate that could link the onset of epileptiform activity to rapid astrocyte morphology changes. Part of these findings has been previously published in Anders et al., 2024.

In this experiment, the goal was to investigate whether TNF $\alpha$  modulates astrocyte morphology and whether these potential changes could be observed within a short time frame. Acute hippocampal slices were treated with TNF $\alpha$  at a concentration of 10 ng/ml, a concentration known to induce TNF $\alpha$  signaling in astrocytes based on previous research (Bedner et al., 2015).

To monitor changes in astrocyte morphology, EGFP-expressing astrocytes (Fig. 13) were visualized using two-photon excitation microscopy, as described earlier (see 3.1.1). The imaging allowed for the visualization and analysis of astrocyte morphology over a 40-minute period.

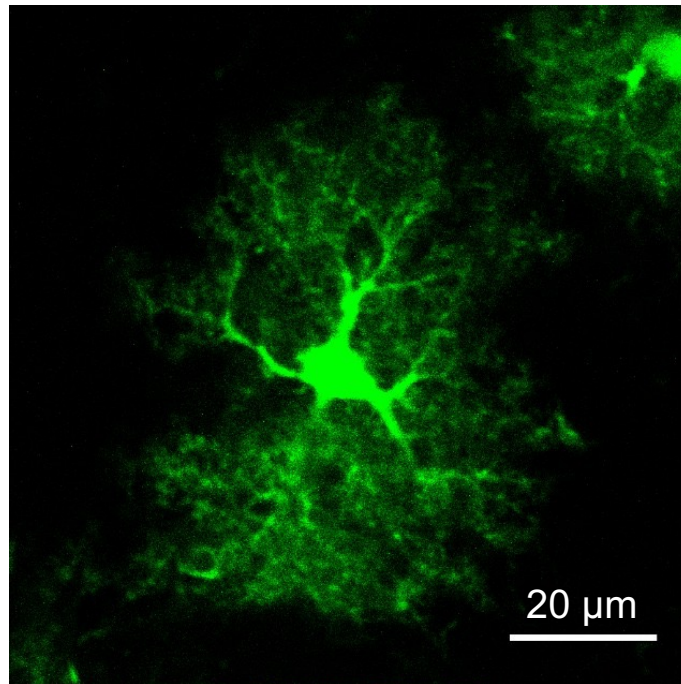


**Fig. 13:** Representative EGFP-expressing astrocyte in CA1

After a 10-minute baseline, 10 ng/ml TNF $\alpha$  was bath-applied. The baseline volume fraction of all recordings was  $7.00 \pm 0.49$  % ( $n = 26$  cells). In the control group, where no TNF $\alpha$  was applied, the volume fraction remained stable over the 40-minute recording period (Fig. 14, left grey), with a final volume fraction of  $96.80 \pm 2.03$ % of the baseline ( $n = 12$ , one sample t-test,  $p = 0.14$ , Fig. 14). Interestingly, the volume fraction of astrocytes treated with TNF $\alpha$  was not significantly different from the control condition. The final volume fraction after TNF $\alpha$  application was  $99.95 \pm 2.18$  % of the baseline ( $n = 14$ , one sample t-test,  $p = 0.98$ ). Statistical analysis indicated that there was no significant difference between the TNF $\alpha$ -treated group and the control group (two-sample t-test,  $p = 0.31$ ). These findings suggest that the acute application of TNF $\alpha$  did not have an effect on astrocyte volume fraction under the experimental conditions used in this study (Anders et al., 2024).

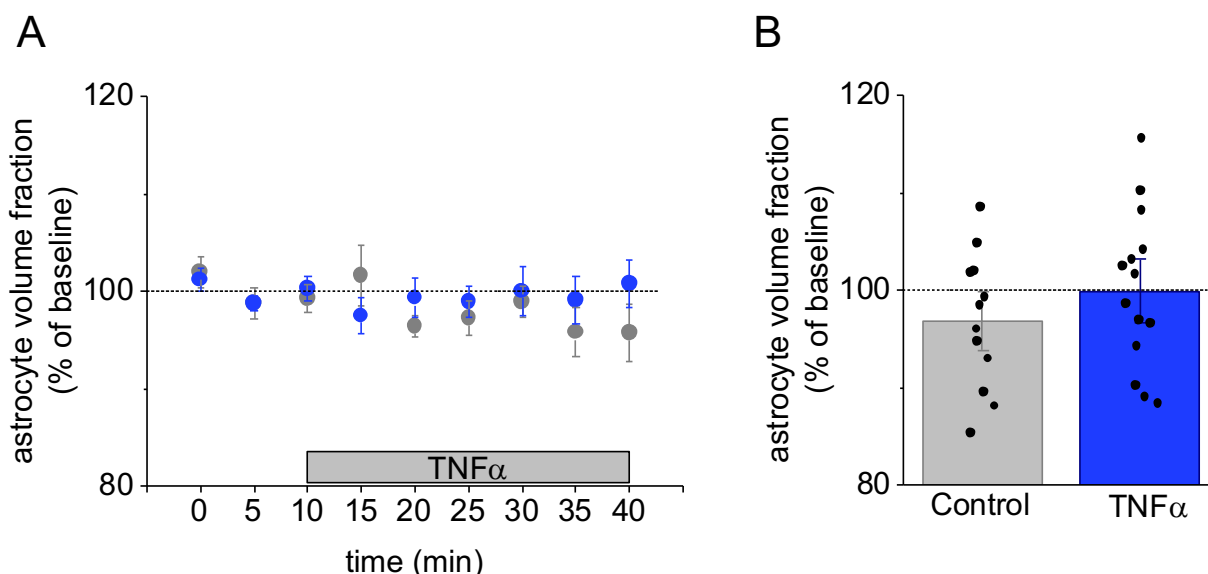


**Fig. 14:** The acute effect of 10 ng/ml TNF $\alpha$  on astrocyte morphology

(A) Time course of the normalized astrocyte volume fraction over 40 minutes, after 10 minutes of baseline 10 ng/ml TNF $\alpha$  was applied (blue), the average astrocyte volume fraction (normalized to baseline) of slices treated with TNF $\alpha$  (blue) and control slices (grey) stayed stable over 40 minutes. (B) Bar graph of the average astrocyte volume fraction (normalized to baseline) during the last 10 minutes. In control conditions the average astrocyte volume fraction was  $96.80 \pm 2.03$  % ( $n = 12$  one sample t-test,  $p = 0.14$ ) and  $99.95 \pm 2.18$  % ( $n = 14$ , one sample t-test,  $p = 0.98$ ) in TNF $\alpha$  condition compared to baseline. There was no significant difference between the final astrocyte volume fraction of control and TNF $\alpha$  condition (two sample t-test,  $p = 0.31$ ). Data are expressed and displayed as mean  $\pm$  s.e.m.

This is in contrast with findings from other cell types indicating that TNF $\alpha$  alters cell morphology by inducing RhoA/ROCK signaling (Hunter and Nixon, 2006; Kant et al., 2011). However, we hypothesized that several factors could determine whether TNF $\alpha$  has an influence on astrocyte morphology. First, we used a concentration of 10 ng/ml in the above-described experiments which may not be sufficient to induce astrocyte morphology changes within the employed application phase of 30 minutes. Second, TNF $\alpha$  is a cytokine that is known to be present for long periods during epilepsy and therefore may exhibit its effects over a longer time scale (Ashhab et al., 2013). Accordingly, it cannot be ruled out that the presently used incubation phase of 30 minutes may not be long enough to observe the potential morphology changes. Third, cytokines such as TNF $\alpha$  generally act within large cytokine networks. Accordingly, further co-stimuli may be required to promote the TNF $\alpha$  effects in astrocyte morphology.

The role of these factors for potential TNF $\alpha$ -induced astrocyte morphology changes was then tested in the following experiments.

### 3.3.1 Incubation of slices with TNF $\alpha$ alone or in combination with Interleukin 1b

In our subsequent experiment, we aimed to investigate the effects of prolonged exposure to TNF $\alpha$  on astrocyte morphology compared to the acute application used in the previous experiment. Previous studies have reported astrocytic network decoupling after 4 hours of incubation with TNF $\alpha$  (Bedner et al., 2015). However, the morphology of astrocytes was not examined in periods longer than 30 minutes (see section 3.3), and shorter than four hours. Therefore, it is intriguing to investigate whether TNF $\alpha$  would induce astrocyte morphology changes after a latent period. Additionally, we examined the impact of TNF $\alpha$  in combination with IL1b on astrocyte morphology. IL1b is known to modulate astrocyte morphology in cultures and has been shown to be a strong modulator of inflammation (John et al., 2004). Interestingly, previous studies indicated that the decoupling of astrocyte networks induced by TNF $\alpha$  depended on IL1b co-signaling (Bedner et al., 2015). Rapid astrocyte morphology changes were suggested to be correlated with astrocyte network coupling (Anders, 2017).

To investigate this, hippocampal slices were incubated with TNF $\alpha$  alone or in combination with IL1b. Following the methodology of Bedner et al. (2015), acute hippocampal slices were treated with TNF $\alpha$  (10 ng/ml) or TNF $\alpha$  and IL1b (10 ng/ml each). For the control condition, slices were incubated with ACSF containing 1% bovine serum albumin (BSA), which served as the diluent for TNF $\alpha$ . After a two-hour incubation period, astrocytes in the CA1 region were imaged (Fig. 15 A), and the astrocyte volume fraction was calculated.

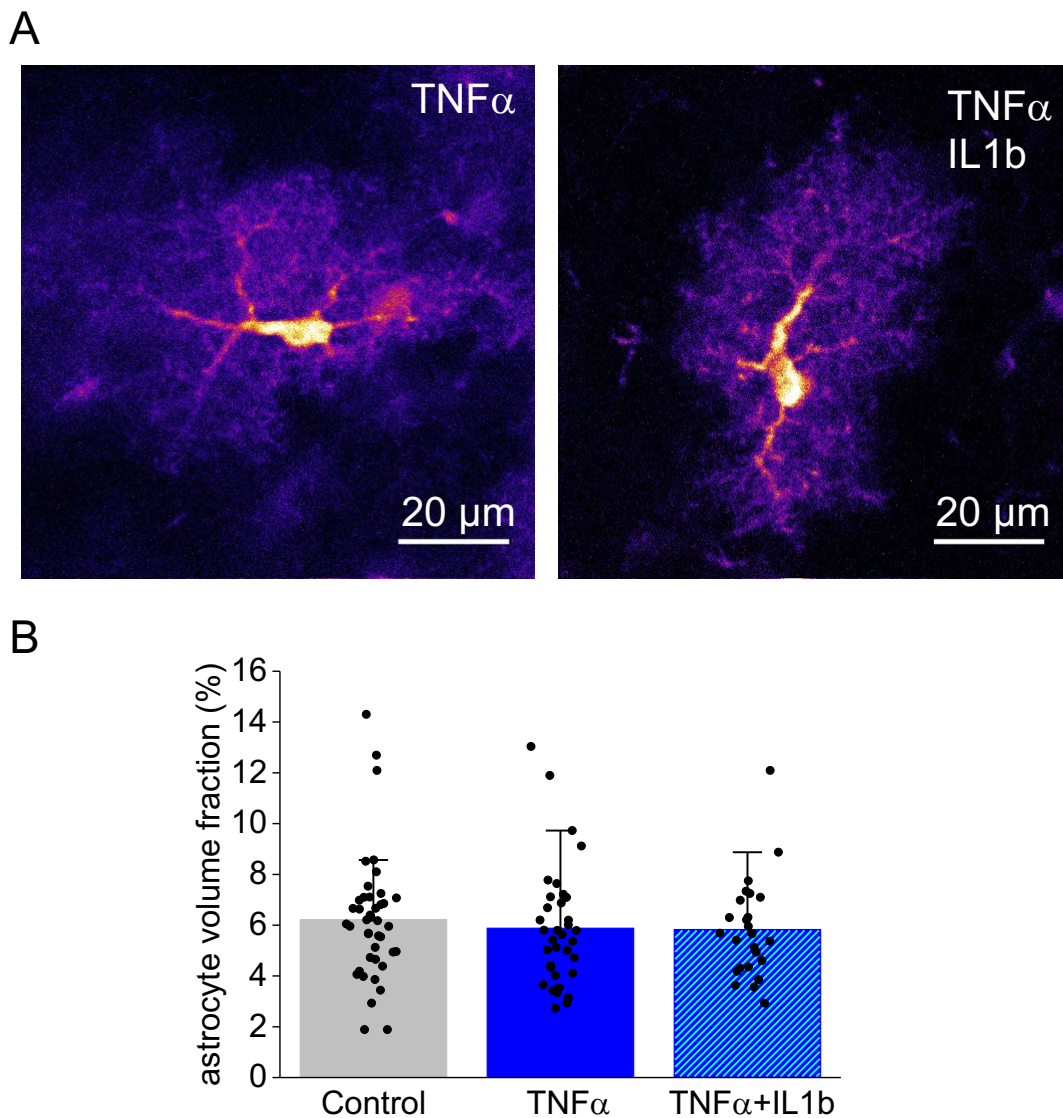


**Fig. 15:** Astrocyte morphology in slices incubated with TNF $\alpha$  or TNF $\alpha$  and IL1b

(A) Representative EGFP-expressing astrocytes that were incubated for two hours with TNF $\alpha$  (10 ng/ml) alone (left) or with TNF $\alpha$  and IL1b (10 ng/ml each) (right) (B) Comparison between the astrocyte volume fraction of astrocytes under control condition, TNF $\alpha$  and TNF $\alpha$  and IL1b. The average astrocyte volume fraction under control condition was  $6.24 \pm 0.83$  % (n=42). The average astrocyte volume fraction under control condition was  $6.24 \pm 0.83$  % (n=42). The average astrocyte volume fraction of astrocytes treated with TNF $\alpha$  ( $5.88 \pm 0.40$  %, n = 35,) was not significantly different from control astrocytes (Mann-Whitney-test, p = 0.39). The average astrocyte volume fraction of astrocytes treated with TNF $\alpha$  and IL1b ( $5.83 \pm 0.39$  %, n = 25) was also not different from control astrocytes (Mann-Whitney-test, p = 0.47). Data are expressed and displayed as mean  $\pm$  s.e.m.

The average volume fraction of astrocytes under control conditions was  $6.24 \pm 0.83$  % (n = 42, Fig. 15 B). The average astrocyte volume fraction in slices treated with TNF $\alpha$  ( $5.88 \pm 0.40$  %, n = 35, Fig. 15 B) did not show a significant difference compared to the control

condition (Mann-Whitney-Test,  $p = 0.39$ ). Similarly, the mean volume fraction of astrocytes treated with TNF $\alpha$  and IL1b was  $5.83 \pm 0.39$  % ( $n = 25$ ). Thus, combined application of TNF $\alpha$  and IL1b did not affect the volume fraction of astrocytes compared to the control condition (Mann-Whitney-Test,  $p = 0.47$ ).

In conclusion, our results demonstrate that neither the acute application of TNF $\alpha$  nor the prolonged incubation with TNF $\alpha$ , alone or in combination with IL1b, induced detectable astrocyte morphology changes as measured by volume fraction analysis in acute hippocampal slices.

### 3.3.2 The effect of epileptiform activity on astrocyte morphology in a TNFR1-deficient mouse line

The previous experiments showed that neither acute application of TNF $\alpha$  nor incubation with TNF $\alpha$  induces astrocyte morphology changes in acute hippocampal slices. So far, we could not rule out that TNF $\alpha$  requires co-signaling molecules other than IL1b. TNF $\alpha$  signaling is mainly transduced by activation of TNFR1 which is broadly expressed by astrocytes (Dopp et al., 1997). Moreover, TNFR1 is the receptor associated with RhoA/ROCK-mediated morphology changes in other cell types (Hunter and Nixon, 2006; Kant et al., 2011b). We reasoned that if rapid astrocyte morphology changes in astrocytes in fact depend on TNF $\alpha$  signaling they should be prevented in absence of TNFR1.

To further investigate the role of TNF $\alpha$  signaling in acute astrocyte morphology changes during epileptiform activity, we utilized a TNFR1 knockout mouse model. The TNFR1 knockout mouse line, in which TNFR1 is constitutively deleted, was crossbred with the hGFAP-EGFP mouse line to obtain progenies with EGFP expression and homozygous TNFR1 knockout (EGFP-TNFR1<sup>-/-</sup>) as well as progenies with EGFP expression and wildtype TNFR1 expression (EGFP-TNFR1<sup>+/+</sup>) for control recordings.

In these experiments, we employed the same approach of combining two-photon excitation microscopy with electrophysiological recordings as in the previous experiments described above (see section 3.2). Epileptiform activity was induced by bath-application of penicillin for 30 minutes following a 10-minute baseline period. Additionally, Schaffer collaterals at the border to CA1 were stimulated every 30 seconds throughout the entire experimental duration, and both evoked and spontaneous fEPSPs were recorded in CA1 stratum pyramidale.

The results showed that spontaneous discharges occurred in 21 % of hippocampal slices (6 out of 29) from EGFP-TNFR1<sup>-/-</sup> mice and in 33 % of slices (5 out of 15) from EGFP-TNFR1<sup>+/+</sup> mice 5 to 10 minutes after bath application of penicillin (Fig. 16).

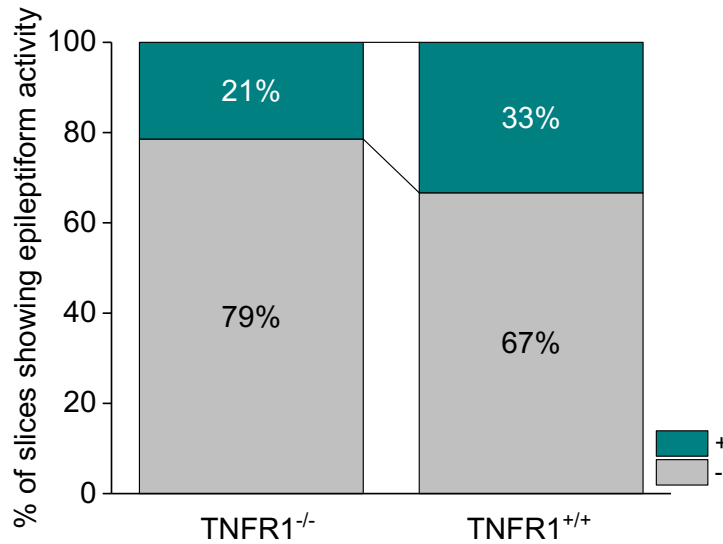


**Fig. 16:** Proportion of slices that developed epileptiform activity after penicillin treatment. Epileptiform activity was induced by application of 4 mM penicillin. In EGFP-TNFR1<sup>-/-</sup> animals, application of penicillin led to epileptiform activity (+) in 21 % of the slices (n=29). In EGFP-TNFR1<sup>+/+</sup> slices epileptiform activity occurred in 33 % of the tested slices (n=15)

The observed spontaneous discharges in hippocampal slices from EGFP-TNFR1<sup>-/-</sup> animals occurred with a mean frequency of  $1.15 \pm 0.41 \text{ min}^{-1}$  (n = 6), while in hippocampal slices from EGFP-TNFR1<sup>+/+</sup> animals, the discharges had a mean frequency of  $1.8 \pm 0.54 \text{ min}^{-1}$  (n = 5) (Fig. 17 B). Statistical analysis using a two-sample t-test revealed no significant difference in the discharges' frequency between the two genotypes ( $p = 0.35$ ). These results indicate that both EGFP-TNFR1<sup>-/-</sup> and EGFP-TNFR1<sup>+/+</sup> animals display comparable response patterns to the induction of epileptiform activity through bath-application of penicillin.

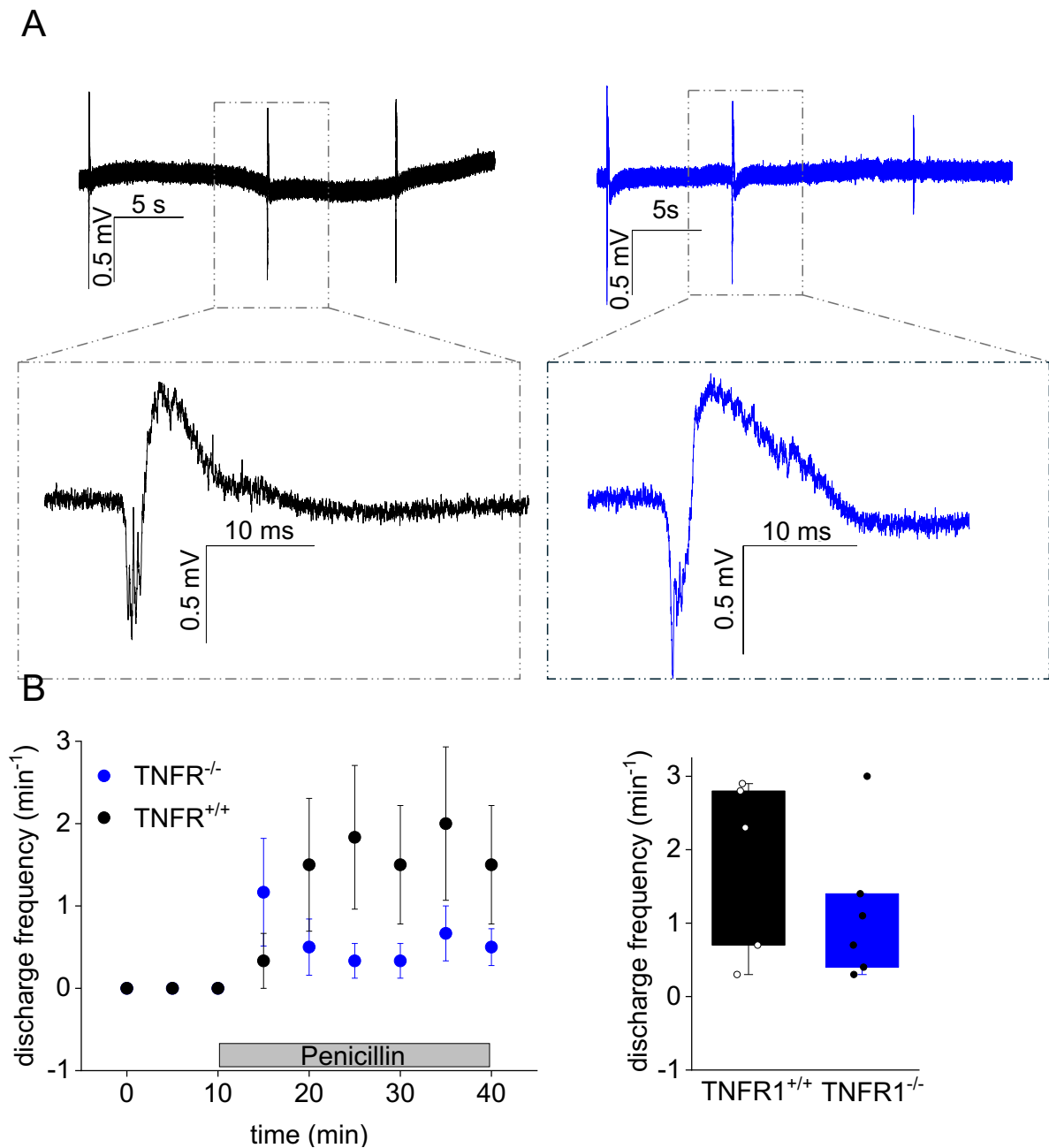


**Fig. 17:** Application of penicillin induced epileptiform activity in EGFP-TNFR1<sup>-/-</sup> and EGFP-TNFR1<sup>+/+</sup> mice

(A) Example traces of penicillin recordings in EGFP-TNFR1<sup>+/+</sup> animals (black) and EGFP-TNFR1<sup>-/-</sup> animals (blue). Application of 4 mM penicillin led to epileptiform activity with typical discharges (below). (B) Discharge frequency per minute reached a stable level 10 to 15 minutes after penicillin application with a mean frequency of  $1.8 \pm 0.54 \text{ min}^{-1}$  ( $n = 5$ ) in EGFP-TNFR1<sup>+/+</sup> animals (black) and  $1.15 \pm 0.41 \text{ min}^{-1}$  ( $n = 6$ ) in EGFP-TNFR1<sup>-/-</sup> animals (blue, two-sample-t-test,  $p = 0.35$ ). Data are expressed and displayed as mean  $\pm$  s.e.m.

In parallel to electrophysiological recordings, astrocyte morphology was assessed by measuring the volume fraction. Representative astrocytes from an EGFP-TNFR1<sup>-/-</sup> (left) and an EGFP-TNFR1<sup>+/+</sup> mouse (right) are shown in Fig. 18 A to illustrate the typical morphology. Interestingly, the mean soma fluorescence intensity in slices of the EGFP-TNFR1<sup>+/+</sup> and EGFP-TNFR1<sup>-/-</sup> mice was significantly lower compared to slices from hGFAP-EGFP mouse line used in previous experiments (Mann-Whitney-Test,  $p=0.00023$ , data not shown). However, there was no statistically significant difference in the mean soma fluorescence intensity between astrocytes from EGFP-TNFR1<sup>-/-</sup> and those from EGFP-TNFR1<sup>+/+</sup> animals (Mann-Whitney-Test,  $p=0.51$ ). The volume fraction is robust to variations in soma fluorescence intensity between cells, as it is relative to the maximal intensity of each cell itself. However, consistent z-plane maintenance is crucial for accurate morphology analysis. Therefore, only slices where astrocytes were bright enough to remain visible and stable in the same z-plane were considered. Additionally, only slices that exhibited epileptiform activity were included in the volume fraction analysis. Following a 10-minute baseline period, epileptiform activity was induced by the addition of 4 mM penicillin. The average baseline volume fraction of all astrocytes from both genotypes combined was  $4.02 \pm 0.52\%$  ( $n = 9$ ). After 30 minutes of penicillin treatment, the volume fraction of TNFR1-deficient astrocytes decreased significantly to  $78.94 \pm 3.70\%$  ( $n = 6$ , one-sample t-test,  $p = 0.0023$ ) compared to the baseline. In contrast, astrocytes with wildtype TNFR1 expression showed a mean volume fraction of  $91.020 \pm 4.14\%$  after 30 minutes of penicillin treatment, which did not exhibit a significant decrease ( $n = 3$ , one-sample t-test,  $p = 0.16$ ). However, the statistical analysis did not reveal a significant difference between the two genotypes (two sample t-test,  $p=0.086$ )

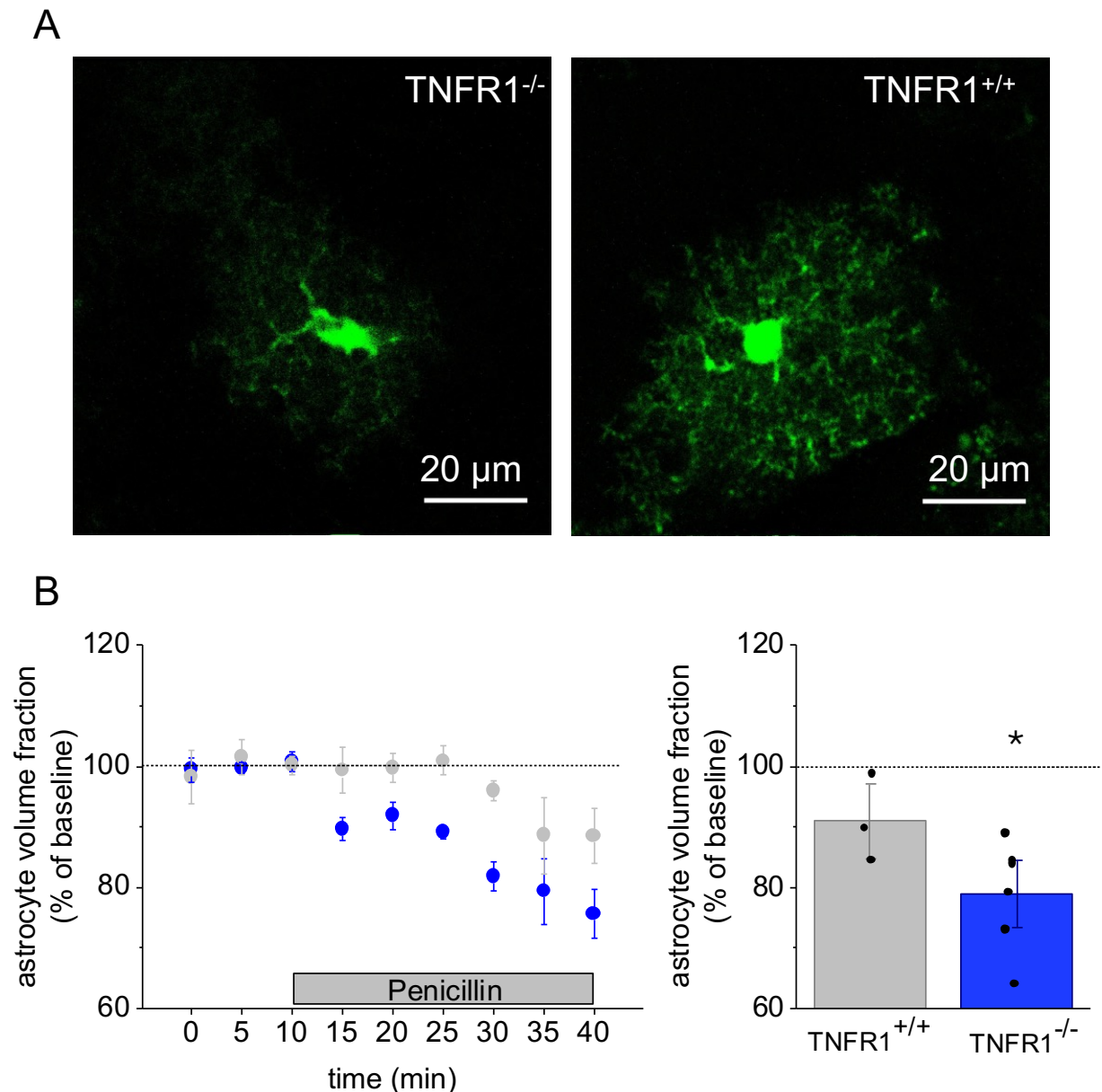


**Fig. 18:** Epileptiform activity induced astrocyte morphology changes in acute brain slices of EGFP-TNFR1<sup>-/-</sup> mice

A) Representative EGFP-expressing astrocyte in CA1 of an EGFP-TNFR1<sup>-/-</sup> mouse (left) and an EGFP-TNFR1<sup>+/+</sup> mouse (right). B) (left) The mean normalized astrocyte volume fraction over time in EGFP-TNFR1<sup>-/-</sup> animals (blue) and EGFP-TNFR1<sup>+/+</sup> animals (grey). (right) Bar graph of the average astrocyte volume fraction (normalized to baseline) during the last 10 minutes. In control conditions the average volume fraction was  $91.020 \pm 4.14$  % (n=3, one-sample t-test, p = 0.16) and in penicillin recordings the average volume fraction was  $78.94 \pm 3.70$  % (n = 6, one sample t-test, p = 0.0023) compared to baseline. The final volume fraction of EGFP-TNFR1<sup>-/-</sup> astrocytes is not significantly different from the final volume fraction of EGFP-TNFR1<sup>+/+</sup> astrocytes with expression (n = 3, two sample t-test, p = 0.086). Data are expressed and displayed as mean  $\pm$  s.e.m.

These results indicate that in the absence of TNFR1, astrocytes exhibit a significant reduction in volume fraction following the induction of epileptiform activity by penicillin similar to the astrocytes from hGFAP-EGFP animals (see section 3.2). This finding indicates, that TNFR1 is not required for the rapid restructuring of the cytoskeleton upon epileptiform activity (Anders et al., 2024).

In conclusion, our experiments provide evidence that TNF $\alpha$  does not have a direct effect on astrocyte morphology in both acute and prolonged experimental settings. Additionally, the combination of TNF $\alpha$  with IL1 $\beta$  did not induce any noticeable changes in astrocyte morphology. Furthermore, the absence of TNFR1, the primary receptor for TNF $\alpha$ , did not prevent the morphological changes observed in astrocytes during epileptiform activity. These findings suggest that TNF $\alpha$  is unlikely to mediate the rapid development of altered astrocytic morphology during the acute phase of epileptogenesis. Further studies are needed to investigate other potential mechanisms involved in astrocyte morphology changes associated with epilepsy.

#### 3.4 The role of Brain derived neurotrophic factor in astrocyte morphological plasticity

BDNF is a protein known for its involvement in brain development and recovery. It has been well established that BDNF levels increase during seizure activity (Isackson et al., 1991; Nawa et al., 1995). Astrocytes express the TrkB.T1 receptor, which is the primary receptor for BDNF in these cells. TrkB.T1 Activation of TrkB.T1 by BDNF has been shown to regulate astrocyte morphogenesis (Holt et al., 2019). Remarkably, this regulation involves RhoA/ROCK signaling in astrocyte cultures (Ohira et al., 2006) which is known to play a role in astrocyte morphology modulation. Based on these findings, we hypothesized that BDNF might influence astrocyte morphology during epileptiform activity. To test our hypothesis, we conducted experiments using acute hippocampal slices from hGFAP-EGFP mice. The slices were incubated in ACSF containing 100 ng/ml BDNF or in normal ACSF (control) for at least one hour prior to the experiments. Astrocytes expressing EGFP were visualized with two-photon excitation microscopy and the volume fraction of each astrocyte as an indicator for astrocyte morphology was calculated.

The average volume fraction of astrocytes treated with BDNF was  $5.19 \pm 0.25$  % (n = 29) which did not significantly differ from the average volume fraction in the control group ( $4.80 \pm 0.28$  %, n = 29, Mann-Whitney-Test, p = 0.20) as shown in Fig. 19. These findings

suggest that the application of BDNF for more than one hour did not have a noticeable effect on astrocyte morphology in our experimental setup.

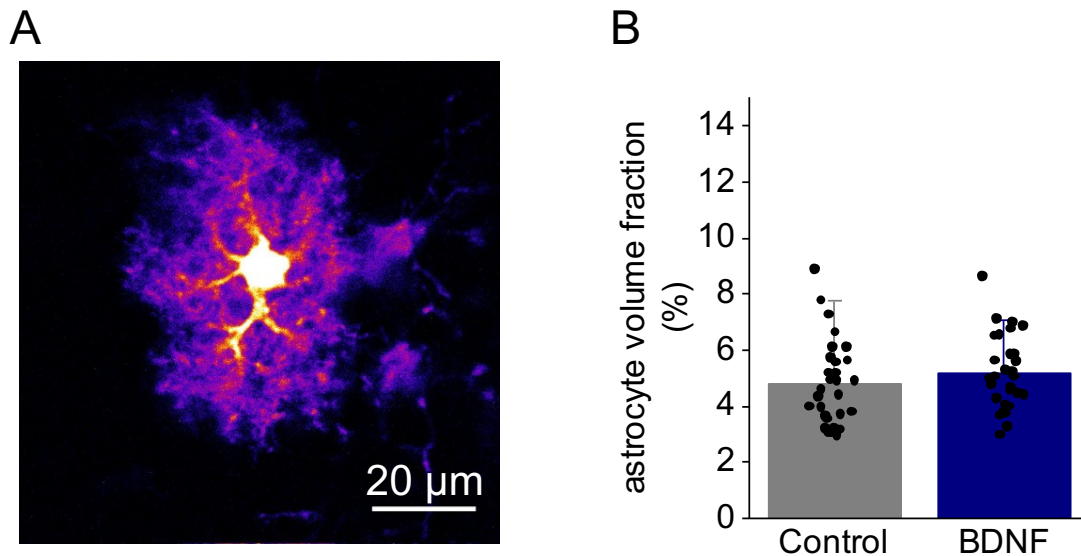


**Fig. 19:** Astrocytes exposed to BDNF do not show alterations in astrocytic volume fraction (A) Exemplary EGFP-expressing astrocyte of an acute hippocampal slice incubated with 100 ng/ml BDNF. (B) Comparison between the mean astrocyte volume fraction of astrocytes treated with BDNF (blue) and control astrocytes (grey). The mean volume fraction of astrocytes treated with BDNF ( $5.19 \pm 0.25$  %,  $n = 29$ ) was not different from control astrocytes ( $4.80 \pm 0.28$  %,  $n = 29$ , Mann-Whitney-Test,  $p = 0.20$ ). Data are expressed and displayed as mean  $\pm$  s.e.m.

Indeed, under the used experimental conditions, BDNF does not seem to alter the astrocyte morphology. Consequently, it seems unlikely that BDNF alone induces rapid changes of astrocyte morphology during epileptiform activity. These findings indicate that other signaling pathways or mechanisms may play a role in triggering the restructuring of the astroglial cytoskeleton. Further investigations are needed to elucidate the specific signaling cascade responsible for the rapid astrocyte morphology changes observed during epileptiform activity.

### 3.5 The role of norepinephrine in astrocyte morphological plasticity

NE is a catecholamine hormone that functions as neurotransmitter in the sympathetic nervous system but also in the CNS. NE acts on alpha- and beta- adrenergic receptors which are expressed by neurons, astrocytes, and microglia throughout the CNS (Salm and McCarthy, 1992). It is well established, that NE alters astrocyte morphology in cultures

and that NE levels are raised in epileptic brains of rodents (Vardjan et al., 2014). Therefore, it seemed promising to test its ability to acutely alter astrocyte morphology in hippocampal slices.

EGFP-expressing astrocytes were monitored for 40 minutes, including a 10-minute baseline period. After the baseline period, 100  $\mu$ M NE was added to the bath solution, and the volume fraction of each astrocyte was calculated every 5 minutes. For control recordings, astrocytes were monitored for 30 minutes after the 10-minute baseline recordings, without adding NE. The average astrocyte volume fraction of the last 10 minutes of the experiment were normalized to the respective baseline volume fraction.

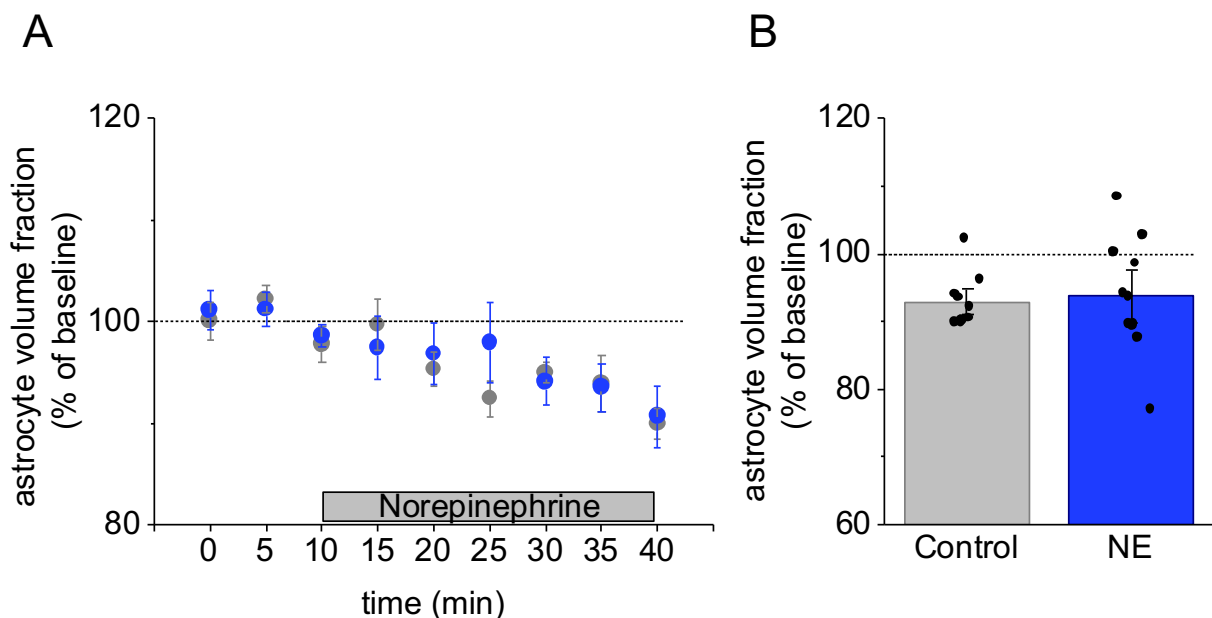


**Fig. 20:** Astrocyte morphology is not altered by 100  $\mu$ M NE

(A) Normalized astrocyte volume fraction over time when NE was bath-applied (blue) or under control condition (grey). The final normalized astrocyte volume fraction of slices treated with NE ( $n = 10$ ,  $91.85 \pm 2.37$  %) and of control slices ( $n = 10$ ,  $92.91 \pm 1.26$  %) are not significantly different (Mann-Whitney Test,  $p = 0.97$ ). Data are expressed and displayed as mean  $\pm$  s.e.m.

The average baseline volume fraction of both groups was  $5.63 \pm 0.37$  % ( $n = 20$ ) The results showed that both the NE-treated group and the control group exhibited a decline in astrocyte volume fraction over time compared to their respective baselines (Fig. 20). The astrocytes treated with NE reached a final volume fraction of  $91.85 \pm 2.37$ % ( $n = 10$ , one-sample t-test,  $p = 0.00025$ ), while the control astrocytes had a final volume fraction of  $92.91 \pm 1.26$ % ( $n = 10$ , one sample Wilcoxon-rank-test,  $p = 0.019$ ) (Fig. 20). Importantly,

there was no significant difference in the final astrocyte volume fractions between the NE-treated group and the control group (Mann-Whitney Test,  $p = 0.97$ ). Therefore, it is suggested that the observed astrocyte morphology alterations in this experimental setting are not mediated by NE.

Based on these findings, it can be concluded that bath-application of NE did not induce significant additional changes in astrocyte morphology compared to the control condition in acute hippocampal slices. This suggests that NE, at the concentration used in the study, does not play a major role in regulating rapid astrocyte morphology changes under these experimental conditions. However, it is essential to note that this study focused on acute changes, and further investigations may be needed to explore potential longer-term effects or effects under different experimental conditions.

## 4. Discussion

Over the past few decades, our understanding of astrocytes has evolved significantly. Once considered as passive support cells, we now recognize their active participation in neuronal communication within the tripartite synapse (Volterra and Meldolesi, 2005). Astrocytes play crucial roles in normal brain function and are implicated in various neurological disorders, including Alzheimer's disease, Parkinson's disease, and epilepsy (Pekny et al., 2016).

Of particular interest is the morphological plasticity of astrocytes, which has been found to be involved in both physiological and pathological processes. Long-term changes in astrocyte morphology have been observed in epilepsy for many years (Coulter and Steinhäuser, 2015; Khurgel and Ivy, 1996; Pekny et al., 2016). However, recent studies have revealed that astrocytes can undergo rapid morphology changes within minutes after the onset of epileptiform activity in animal models (Anders, 2017).

While the involvement of RhoA/ROCK signaling in the rapid restructuring of the astroglial cytoskeleton during epileptiform activity has been established, the signaling cascades upstream of RhoA have remained unknown. Therefore, the main objective of the current study was to investigate the upstream signaling pathways that activate RhoA and trigger remodeling of the astroglial cytoskeleton in response to epileptiform activity.

By identifying these upstream signaling pathways, the study aimed to enhance our understanding of the molecular mechanisms underlying astrocyte morphology changes in epilepsy.

### 4.1 Osmotic stress in acute hippocampal slices

#### 4.1.1 Effect of osmotic stress on astrocyte morphology

Capturing dynamic astrocyte morphology changes, especially in the fine peripheral astroglial processes (PAPs), which are too small to be fully resolved by diffraction-limited microscopy, is technically challenging (Heller and Rusakov, 2017). While electron microscopy has provided valuable insights into the ultra-structure of astrocytes, it is not suitable for capturing real-time changes due to the requirement for tissue fixation. Yet, characterizing morphological plasticity especially in PAPs is important, because the spatial arrangement of astrocytic processes enwrapping thousands of synapses is crucial for the bi-directional signaling between astrocytes and neurons.

In order to capture real-time changes in the astrocyte morphology volume fraction measurements were employed. It now has been established, that measuring the fraction of tissue volume occupied by astrocytes can be used as an indirect measure to obtain information about local astrocyte structure and detect changes in perisynaptic astrocyte processes (King et al., 2020; Medvedev et al., 2014; Minge et al., 2021) and to detect changes of perisynaptic astrocyte processes (Henneberger et al., 2020).

To demonstrate the efficacy of this method, in this study astrocytes were exposed to osmotic stress, a well-established model for studying volume regulation in various organisms (Kimmelberg and Kettenmann, 1990). Astrocytes have water-selective aquaporins that allow them to alter their volume in response to osmotic stress (Chvátal et al., 2007; Nagelhus and Ottersen, 2013; Risher et al., 2009). The volume fraction measurements of astrocytes exposed to hyper- or hypoosmotic stress confirmed that astrocytes shrink or swell, respectively, in response to these conditions (see 3.1.1, Fig. 9).

This is consistent with findings throughout the literature (Andrew et al., 1997; Chvátal et al., 2007; Kimmelberg and Kettenmann, 1990; Risher et al., 2009). Even though, swelling and shrinking of astrocytes in response to osmotic stress is a robust finding, the studies differ in the severity of reported morphology changes. For instance, Risher et al. (2009) report an increase of astrocytic volume in response to hypoosmotic stress of about 18 %. This is lower to the increase reported in the present study (36.57 %, see 3.1.1, Fig. 9). This can be explained by a difference of the severeness of hypoosmotic stress between the two studies. Risher et al. decreased the osmolarity of the extracellular fluid by only 40 mOsm/kg while it was decreased by 100 mOsm/kg in the current study. This is in line with previous findings suggesting a positive correlation between the severeness of the osmotic challenge and astrocytic volume changes (Andrew et al., 1997). Moreover, the tool which is used to determine astrocyte morphology is relevant. Since, aquaporins are dispersed unevenly over the astroglial surface with pronounced expression in the PAPs (Nielsen et al., 1997), it is plausible that also volume changes are irregular throughout the cell, particularly during the acute phase of osmotic stress. Indeed, this was confirmed in a study in which volume changes in the soma and the periphery were analyzed separately, revealing that volume changes are accentuated in the periphery (Chvátal et al., 2007). Consequently, the severity of the observed volume changes may not only depend on the

severity of osmotic stress, but also on the chosen analysis tool. In fact, when using volume fraction measurements, the changes may appear more severe compared to using a tool that includes the soma (cell body) in the analysis. Volume fraction measurements focus specifically on the fraction of tissue volume occupied by astrocytes, providing valuable insights into the dynamics of astrocyte morphology, particularly in the periphery, where aquaporins are highly expressed (Henneberger et al., 2020; Medvedev et al., 2014).

In conclusion, the study successfully demonstrated that astrocyte morphology changes induced by osmotic stress can be effectively captured using volume fraction measurements. This method provides valuable insights into the dynamics of astrocyte morphology, particularly in the periphery, and can be a useful tool for studying astrocyte plasticity in various physiological and pathophysiological contexts.

#### 4.1.2 The effect of osmotic stress on the neuronal population

In addition to investigating the astrocyte morphology in response to osmotic stress, the effect of osmotic pressure on the neuronal population was also investigated.

Evoked field excitatory postsynaptic potentials (fEPSPs) in the hippocampal neuronal population in the CA1 region were monitored during hypotonic and hypertonic conditions. The fEPSP slope, which reflects the postsynaptic currents, was analyzed to assess synaptic transmission.

The collected data revealed that synaptic transmission was modulated by osmotic pressure. Hypertonic conditions led to a decrease in synaptic transmission, while hypotonic conditions resulted in an increase in synaptic transmission (see section 3.1.2). These results are consistent with previous studies that have shown the modulation of neuronal network properties by changes in the osmolarity of the extracellular space (Huang et al., 1997; Li et al., 2012). Additionally, it was reported that lowered concentration of  $\text{Na}^+$  per se can increase synaptic transmission (Huang et al., 1997). This is especially important as the hypotonic ACSF was achieved by lowering the concentration of  $\text{Na}^+$ . However, the concentration of  $\text{Na}^+$  was also lowered for baseline condition of hypotonic recordings as well, so that changes in synaptic transmission can be traced back to osmolarity.

The efficiency of synaptic transmission depends on various factors, including intrinsic pre- and postsynaptic processes, as well as the spatial arrangement of the pre- and

postsynaptic elements and the surrounding astrocytes (Henneberger et al., 2020; Panatier et al., 2011; Theodosis et al., 2008).

Osmolarity is known to influence both mentioned parameters. However, as intrinsic properties of the neuronal population were not investigated specifically in the present study, we will focus on the effect of altered osmolarity on the astrocytic morphology. As discussed above, osmotic stress induces swelling or shrinkage of astroglial elements. Cellular swelling is accompanied by shrinkage of the extracellular space (Chen et al., 2021). Conversely, cell shrinkage leads to an expansion of the extracellular space. A reduced volume of the ECS can lead to the accumulation of ions or neurotransmitters, as their dilution is decreased. Additionally, a decreased ECS volume, along with potential increased tortuosity, can impede the diffusion of neuroactive substances away from their targets, promoting their accumulation within the synaptic cleft and enhancing synaptic transmission (Vargová and Syková, 2014). Conversely, expansion of the ECS can result in higher dilution of neuroactive elements, potentially leading to a decrease in synaptic transmission.

Alteration of the extracellular space volume could be crucial for the efficiency of synaptic transmission. The shifts in astrocytic volume in response to osmotic stress are driven by the redistribution of water across the cell membrane, facilitated by aquaporins, with AQP4 being the predominant aquaporin in the CNS, primarily expressed by astrocytes (Nagelhus and Ottersen, 2013). The swelling and shrinking of cells, particularly glial processes surrounding synapses, may modify the diffusion of transmitters away from the synaptic cleft, thereby influencing synaptic transmission. However, it is important to consider that osmotic stress may alter the synaptic cleft itself, leading to a dual effect: either reducing or increasing the volume of dilution and altering the distance over which transmitter molecules must diffuse.

The contribution of volume changes in neurons in response to osmotic stress is discussed controversially. For instance, there is evidence that some dendritic shafts swell in response to hypotonia after a latent period (Aitken et al., 1998). However, pyramidal neurons barely express aquaporins which facilitate fast water flux over the cell membrane (Andrew et al., 2007). Therefore, it can be assumed that rapid shifts in extracellular space volume due to water shifts are mediated by other factors. For instance, the extracellular matrix (ECM), which includes molecules like proteoglycans and glycoproteins, can absorb

or release water (Yue, 2014). Changes in ECM composition or structure in response to osmotic stress could contribute to tissue volume changes. Although this has not been explicitly tested in the present study, it is plausible. Additionally, since astrocytes alter their cell volume in response to osmotic stress, it is coherent to assume that this effect at least contributes to changes in the extracellular space (ECS) during osmotic stress.

Based on the understanding that astrocytes significantly contribute to changes in extracellular space volume in response to osmotic stress, it can be concluded that the effect of osmotic stress on synaptic transmission is at least partially influenced by the morphological changes of astrocytes. The alterations in astrocyte morphology, captured through imaging techniques, combined with electrophysiological recordings, provide valuable insights into the relationship between astrocyte dynamics, extracellular space volume, and synaptic transmission.

Taken together, combining imaging with electrophysiological recordings, we could reveal both, morphological changes in astrocytes as well as changes in synaptic transmission in response to osmotic pressure.

## 4.2 Astrocyte morphological plasticity induced by epileptiform activity

### 4.2.1 Induction of epileptiform activity in acute brain slices

For a long time, studies of epileptogenic processes relied on human surgery brain tissue. Apart from the limited availability of sufficient numbers of nonepileptic, age-matched human control brain tissue samples, surgical biopsy specimens of pharmacoresistant TLE patients are typically collected at advanced stages of the disease rather than during the early phases of epileptogenesis. Animal models for TLE offer a great opportunity to overcome the shortage of human control hippocampi and gain insights into the early stages of epileptogenesis, for which human hippocampal tissue is generally unavailable. The most frequently applied models for MTLE are post status epilepticus (SE) and kindling (Leite et al., 2002). Post SE models involve the local or systemic administration of chemoconvulsives like kainic acid, an L-glutamate analogue, or pilocarpine, a muscarinic acetylcholine receptor agonist (Becker, 2018). These models usually elicit damage patterns comprising mossy fiber sprouting, extensive cell loss, prominent reactive astrogliosis as well as blood–brain barrier (BBB) dysfunction in the hippocampus (Sharma

et al., 2007). Therefore, they are particularly well-suited to study hippocampal sclerosis (HS) which is commonly found in brain tissue of MTLE patients (Thom, 2014).

Kindling, on the other hand, relies on repeated electrical stimulation of limbic brain structures leading progressively to the onset of after-discharges and behavioral seizures (Goddard, 1967). However, significant neuropathological changes are typically observed only with prolonged kindling protocols (Cavazos et al., 1994). Both, post SE and kindling models show features of MTLE that reflect epileptogenic processes that are rather associated with chronic epilepsy (Becker, 2018).

To understand functional mechanisms underlying the acute phases of epileptogenesis, pharmacological treatments in acute brain slices are often employed. These models focus on investigating neuronal hyperexcitability rather than chronic epilepsy features. Common models for acute focal seizures in brain slices include the penicillin model and the 0  $Mg^{2+}$ /bicuculline model (Akdogan and Yonguc, 2011). The proconvulsive effects of penicillin and bicuculline are due to the inhibition of  $GABA_A$ -mediated synaptic inhibition (Tsuda et al., 1994). In the 0  $Mg^{2+}$ /Bicuculline model, the increased activation of ionotropic glutamate receptors (NMDARs) additionally contributes to the generation of epileptiform activity. Activation of NMDARs is achieved by using ACSF which is devoid of  $Mg^{2+}$  which otherwise blocks NMDARs at resting membrane potential (Akdogan and Yonguc, 2011). In the current study, the penicillin model was used to induce interictal epileptiform discharges in acute hippocampal slices. This model specifically modulates inhibition without directly affecting NMDARs, which helps prevent synaptic potentiation during the induction of epileptiform activity (Anders, 2017).

The results showed that slices from hGFAP-EGFP mice (derived from an FVB background) exhibited interictal epileptiform discharges with a typical shape in 85% of the samples (see section 3.2), whereas slices from EGFP-TNFR1<sup>-/-</sup> (C57/BL6 background) and EGFP-TNFR1<sup>+/+</sup> mice (C57/BL6 background) displayed epileptiform activity in only 21% and 33% of the samples, respectively (see section 3.3.2).

This finding indicates that slices from EGFP-TNFR1<sup>-/-</sup> animals and EGFP-TNFR1<sup>+/+</sup> animals respectively are more resistant to induction of epileptiform activity than slices from hGFAP-EGFP line. The difference in susceptibility may be attributed to the genetic backgrounds of the mouse lines, as different strains can exhibit varying seizure thresholds. The hGFAP-EGFP mouse line was derived from an FVB background while

the EGFP-TNFR1 line was derived from a C57/BL6 background. Using quantitative trait loci mapping, several different loci that contribute to seizure susceptibility could be identified (Ferraro et al. 2002). Due to different expression of the identified gene loci, the FVB-strain for instance has a lower seizure threshold than the C57/BL6 strain which is reported to be rather resistant to seizure induction (Ferraro et al. 2004). Coherent with these findings, slices from mice derived from a C57/BL6 strain developed less frequently epileptiform activity than slices from mice with an FVB-background. However, since the study compared experiments within each genotype, the results remain valid.

In summary, even though the success rate differs between the different genotypes application of penicillin elicited epileptiform activity in slices of hGFAP-EGFP, EGFP-TNFR1<sup>-/-</sup> and EGFP-TNFR1<sup>+/+</sup> animals.

#### 4.2.2 Epileptiform activity induces rapid astrocyte morphology changes

In the current study using the penicillin model, the induction of epileptiform activity resulted in a reduction of the astrocyte volume fraction, confirming previous observations of morphology changes (3.2, Fig. 12). This shows that the reported morphology changes induced by epileptiform activity can be effectively reproduced. However, the relative change observed in this study ( $11\% \pm 2.3\%$ ) was slightly lower compared to the findings of Anders (2017) ( $13.4\% \pm 2.4\%$ ). This discrepancy could be attributed to differences in experimental conditions, such as the discharge frequency of epileptiform activity. The mean discharge frequency in the current study ( $2.2 \pm 0.74 \text{ min}^{-1}$ ) was lower than that reported by Anders (2017) ( $6.78 \pm 1.38 \text{ min}^{-1}$ ), suggesting that less severe epileptiform activity induced less pronounced astrocyte morphology changes, consistent with previous finding suggesting that the strength of astrocyte morphology changes positively correlates with the discharge frequency (Anders, 2017).

Furthermore, findings from Anders et al. (2017) indicated that the RhoA/ROCK pathway might be activated upstream of astrocyte morphology changes induced by epileptiform activity. ROCK, as key regulator of the astrocyte actin-cytoskeleton, influences the phosphorylation state of cofilin, an actin depolymerizing factor. However, the exact mechanism linking epileptiform activity to rapid astrocyte morphology changes through the RhoA/ROCK pathway remains unknown. Therefore, the focus of this study was to

elucidate the specific extracellular signaling pathways involved in triggering these rapid astrocyte morphology changes.

#### 4.3 Is inflammation responsible for rapid morphology changes during epileptiform activity?

The main hypothesis of this study is that the rapid restructuring of the astrocyte cytoskeleton observed immediately after the onset of seizure activity is mediated by inflammatory molecules released by activated microglia. Previous research by Anders (2024) indicated that the observed morphology changes are linked to active restructuring of the astroglial cytoskeleton through the involvement of RhoA/ROCK signaling.

The upstream events that trigger RhoA/ROCK signaling in the context of epileptiform activity have remained unknown. However, epilepsy is commonly associated with microglia activation and subsequent inflammation. Activated microglia release various molecules, including TNF $\alpha$ , IL1b, and BDNF (Garden and Möller, 2006; Soontornniyomkij et al., 1998). Astrocytes are known to be primary targets of these signaling molecules released by microglia (Matejuk and Ransohoff, 2020). Based on these findings, the hypothesis emerged that microglia activation, accompanied by the release of inflammatory mediators like TNF $\alpha$ , plays a role in inducing rapid astrocyte morphology changes during epileptiform activity.

Therefore, the aim of this study was to investigate whether microglia activation and the release of inflammatory molecules, particularly TNF $\alpha$ , contribute to the induction of RhoA/ROCK signaling and subsequent astrocyte morphology changes observed during epileptiform activity. By exploring the interplay between inflammatory mediators, and astrocytes, the study aimed to shed light on the underlying mechanisms of rapid astrocyte cytoskeletal restructuring in response to seizure activity.

##### 4.3.1 The role of TNF $\alpha$ in astrocyte morphological plasticity

TNF $\alpha$  is a cytokine known to be a major driver of inflammation in both the CNS and the periphery. It exhibits pleiotropic effects on various cell types, ranging from the induction of inflammatory gene expression programs to the modulation of cellular proliferation,

differentiation, and even cell death processes such as apoptosis and necroptosis (Baud and Karin, 2001).

Under physiological conditions, TNF $\alpha$  levels in the CNS are almost undetectable. However, they rapidly increase following seizure activity (De Simoni et al., 2000; Ravizza et al., 2008; Vezzani et al., 2011). Previous research has shown that astrocytes express the specific receptors for TNF $\alpha$ , namely TNF receptor 1 (TNFR1) and TNF receptor 2 (TNFR2) (Choi et al., 2005). Additionally, TNF $\alpha$  has been shown to induce morphology changes in various cell types by activating the RhoA/ROCK signaling pathway (Hunter and Nixon, 2006; Kant et al., 2011a). Based on this knowledge, the hypothesis was formulated that TNF $\alpha$  may serve as a link between the onset of epileptiform activity and the rapid changes in astroglial morphology.

To investigate the effect of TNF $\alpha$  on the morphology of EGFP-expressing astrocytes in the hippocampus of acute brain slices, two experimental scenarios were conducted. First, the acute effect of TNF $\alpha$  on astrocyte morphology was examined by monitoring the astrocyte volume fraction over a period of 30 minutes while TNF $\alpha$  was introduced. Second, acute brain slices were incubated with TNF $\alpha$  for 2 hours. In both scenarios, TNF $\alpha$  did not alter the morphology of hippocampal astrocytes (see section 3.3, Fig. 14 and section 3.3.1, Fig. 15).

Previous studies have demonstrated that TNFR1 activation induces RhoA/ROCK signaling and subsequent cytoskeletal restructuring in various cell types, including airway smooth muscle cells and endothelial cells (Hunter et al., 2003; Wójciak-Stothard et al., 1998). Therefore, it is intriguing that the astrocytes in the present study exhibited a different response to TNF $\alpha$  exposure compared to these other cell types. This raises the question of why astrocytes in this study displayed distinct behavior in terms of their response to TNF $\alpha$  compared to other cell types.

The possibility that the lack of effect of TNF $\alpha$  on astrocyte morphology was due to a deficiency in functional TNFR1 receptors in the astrocytes can be considered. However, TNFR1 is known to be expressed by almost every cell type, making it unlikely that the astrocytes in the current study lacked TNFR1 (Wajant et al., 2003). This is supported by previous studies demonstrating high levels of TNFR1 expression by astrocytes (Choi et al., 2005; Dopp et al., 1997). Furthermore, it has been shown that TNF $\alpha$  induces astrocyte network decoupling in acute slices in a TNFR1-dependent manner (Bedner et al., 2015;

Henning et al., 2023). Therefore, the absence of TNFR1 expression in astrocytes is highly unlikely.

If astrocytes do express TNFR1, the next question is whether the receptor was indeed activated. TNFR1 is the high affinity receptor for TNF $\alpha$  and can be activated even at low concentration of TNF $\alpha$  (Grell et al., 1998). In the present study, the concentration of TNF $\alpha$  used was 400-fold higher than the levels observed after the induction of status epilepticus (SE) as measured by ELISA (Müller, 2018). Moreover, a previous study demonstrated that the applied concentration of TNF $\alpha$  (10 ng/ml) activates TNFR1 on astrocytes of acute hippocampal slices (Bedner et al., 2015). Therefore, it can be assumed that the chosen concentration of TNF $\alpha$  was sufficient to activate TNFR1 in the current study as well.

Another possible explanation of a lack of effect of TNF $\alpha$  could be simultaneous activation of TNFR1 and TNFR2. While both TNF $\alpha$  receptors can interact with TNF receptor-associated factors (TRAFs) to transduce signals, only TNFR1 possesses a death domain that allows it to interact with TRADDs (Xie, 2013). As a result, TNFR1 and TNFR2 may activate converging as well as distinct signaling pathways. In the context of epilepsy, these two receptors have been shown to have opposing effects. For example, mice lacking TNFR1 are less prone to develop seizures, whereas TNFR2 deficiency increases seizure susceptibility (Chen et al., 2021). Accordingly, it was reported that combined knockout of TNFR1 and TNFR2 decreased acute infection induced seizures while TNFR2 specific knockout enhanced seizure activity (Patel et al., 2017). Therefore, it is possible that also in astrocytes the two receptors mediate opposing effects regarding the morphology. In the case of smooth muscle cells, TNF $\alpha$  induces morphology changes by activation of the small GTPase RhoA (Hunter and Nixon, 2006). Small GTPases cycle between an active and an inactive state. This cycling is finely regulated by GEFs, GDIs and GAPs (Etienne-Manneville and Hall, 2002). To date it is not fully understood how exactly downstream signaling induced by cytokine receptors regulates this cycling. However, it is imaginable that TNFR1 and TNFR2 activate different RhoA regulating factors which could lead to different effects of the two receptors on the astroglial cytoskeleton. In other words, simultaneous activation of both receptors could cancel each other out. However, there is currently limited evidence regarding the downstream signaling of TNFR2 in regulating the activity of small GTPases.

Additionally, while the membrane-bound form of TNF $\alpha$  can activate both receptors, the soluble form of TNF $\alpha$  predominantly activates TNFR1 with high efficacy which makes it highly unlikely that a potential activation of TNFR2 would mask an effect mediated by TNFR1 (Wajant and Siegmund, 2019).

Indeed, the lack of effect of TNF $\alpha$  on astrocytic morphology in the current study suggests that TNF $\alpha$ /TNFR1 signaling alone is not sufficient to induce these changes. It is interesting to note that the regulation of small GTPases can vary between different cell types, and TNF $\alpha$  signaling may exhibit different effects depending on the specific cell type and the expression patterns of TNF $\alpha$  receptors (Wajant and Siegmund, 2019). This variation in response to TNF $\alpha$  could be attributed to the different expression patterns of TNF $\alpha$  receptors among cell types.

While TNF $\alpha$  alone did not induce morphology changes in astrocytes in the current study, it is worth considering that the actions of TNF $\alpha$  are often enhanced by the interaction with additional cytokines, such as IL1b. The combined effect of TNF $\alpha$  and IL1b will be discussed in the following section.

#### 4.3.2 The role of TNF $\alpha$ and Interleukin 1b in astrocyte morphological plasticity

As discussed above, TNF $\alpha$  alone does not induce rapid morphology changes in astrocytes of acute hippocampal slices. However, activation of microglia during epilepsy leads to the release of TNF $\alpha$  in combination with various other cytokines (Vezzani and Granata, 2005). These cytokines commonly act in an interconnected manner. Specifically, the two cytokines TNF $\alpha$  and IL1b share overlapping biological activities and often act synergistically (Stahl et al., 2003). We therefore hypothesized that IL1b could enhance an effect of TNF $\alpha$  on the astroglial cytoskeleton.

The results of the study indicate that the presence of TNF $\alpha$  and IL1b together did not induce changes in astrocyte morphology in acute hippocampal slices (see section 3.3.1, Fig. 15). This finding is interesting because previous studies have suggested that IL1b can regulate RhoA/ROCK signaling and modulate astrocyte morphology in cultured astrocytes (John et al., 2004). However, it is important to note that cultured astrocytes often differ significantly from astrocytes in tissue, and the mechanisms observed in culture may not necessarily apply to *in situ* conditions. The mechanisms of astrocytic morphological plasticity are commonly studied in cell cultures (Kimelberg, 1983). These

studies can give meaningful insights into the molecular mechanisms that regulate morphological plasticity. However, cultured astrocytes differ considerably from astrocytes in tissue. For instance, they typically exhibit a flat, polygonal shape, which contrasts significantly with the bushy morphology seen *in situ* (Bushong et al., 2002; Hertz et al., 1998). This limits of course the significance of results gained from culture studies regarding the applicability to *in situ* studies. In fact, it is a common finding that mechanisms regulating the astrocyte morphology reported in culture studies are not transferrable into *in situ* conditions. For instance, in cultured astrocytes, lysophosphatidic acid and sphingosine-1-phosphate induce RhoA/ROCK signaling by activation of their associated G-protein coupled receptors and thereby induce morphology changes (Moolenaar, 1999; Ramakers and Moolenaar, 1998). Still, acute application of these agents does not alter the astrocyte morphology in acute hippocampal slices (Anders, 2017). This shows, that even within the same cell type, effects of pharmacological agents vary between astrocytes in culture and *in situ*.

It is intriguing to note that TNF $\alpha$  and IL1b have been shown to decrease the network coupling strength between astrocytes, both in cell cultures and acute hippocampal slices (Bedner et al., 2015; John et al., 2004). Loss of astrocytic gap junction coupling is a characteristic feature of the sclerotic hippocampus in human and experimental TLE (Bedner and Steinhäuser, 2023). Recent studies demonstrated that seizure induced astrocyte gap junction decoupling can be mimicked by application of TNF $\alpha$  or rescued by TNF $\alpha$  knockout respectively (Bedner et al., 2015; Henning et al., 2023). Intriguingly, Anders et al. (2017) found that rapid astrocyte morphology changes induced by epileptiform activity were accompanied by a decrease in network coupling strength. This led to the hypothesis that rapid astrocyte morphology changes and network coupling strength correlate (Anders, 2017). However, in the current study, TNF $\alpha$  and IL1b did not affect astrocyte morphology (see section 3.3.1, Fig. 15) despite their ability to induce gap junction decoupling in the above mentioned studies. Notably, Henning et al. and Bedner et al. investigated gap junction coupling after 4 hours and later rather than during the early phase of epileptogenesis. This could suggest that the role of TNF $\alpha$  may be dependent on the specific timepoint observed. It could also suggest that astrocyte gap junction coupling strength and astrocyte morphology changes may be independent. This hypothesis is supported by the finding that seizure induced gap junction decoupling can be prevented

by microglia depletion which is the main source for TNF $\alpha$  (Henning et al., 2023). Astrogliosis however, is only marginally affected by microglia depletion which could indicate that astrocyte morphology changes depend on factors other than inflammation. In conclusion, we found that TNF $\alpha$  combined with IL1b do not alter the astrocyte morphology within the observed period. This suggests that TNF $\alpha$  and IL1b may not be the primary triggers of rapid astrocyte morphology changes during epileptiform activity. Furthermore, the results suggest that astrocyte network organization and single-cell morphology may be regulated independently of each other. This finding is significant as it implies that astrocyte morphology changes may be influenced by factors other than inflammation, despite the association between astrocyte network alterations and inflammation in epilepsy.

Taken together, the findings from the present study suggest that TNF $\alpha$  alone and in combination with IL1b does not induce rapid astrocyte morphology changes in acute hippocampal slices under physiological conditions. This indicates that other factors or signaling pathways may be responsible for the observed rapid changes in astrocyte morphology during normal physiological processes. However, epileptiform activity is known to involve complex and dynamic interactions between neurons, glial cells, and inflammatory mediators. Therefore, it is possible that the role of TNF $\alpha$  signaling in astrocyte morphology changes could be different under epileptic conditions compared to physiological conditions. Moreover, it is crucial to consider that rapid astrocyte morphology changes under epileptiform conditions could be driven by multiple converging pathways. To further address the question whether of TNF $\alpha$  signaling plays a role in rapid astrocyte morphology changes under epileptiform conditions, we used a TNFR1-deficient mouse line to induce epileptiform activity and monitor astrocyte morphology changes in the hippocampal formation. The results will be discussed in the following section.

#### 4.3.3 The role of TNFR1 in remodeling of the astroglial cytoskeleton during epileptiform activity

In order to investigate the role of TNFR1 signaling in astrocytes in early epileptogenesis, we took advantage of a TNFR1-deficient mouse line (see section 2.1.2). If TNFR1 is essential for the rapid restructuring of the astroglial cytoskeleton upon epileptiform activity, it should not be inducible in absence of TNFR1. Specifically, we induced epileptiform

activity by application of penicillin for 30 minutes and monitored astrocyte morphology in parallel. In fact, in astrocytes from EGFP-TNFR1<sup>-/-</sup> mice epileptiform activity induced morphology changes similar to those observed in astrocytes from hGFAP-EGFP mice (see section 3.3.2, Fig. 17).

Other than expected, in EGFP-TNFR1<sup>+/+</sup> the reduction of the astrocyte volume fraction was not significant. It seems unlikely, that the genotype contributes to a lack of effect in EGFP-TNFR1<sup>+/+</sup> mice. Even though, EGFP-TNFR1 mice are derived from a C57BL/6 strain and hGFAP-EGFP mice are derived from an FVB strain the different genetical background is not responsible for a lack of effect, because in astrocytes of EGFP-TNFR1<sup>-/-</sup> mice morphology changes could be induced by epileptiform activity. Moreover, it was shown previously that epileptiform activity induces astrocytes morphology changes also in rats suggesting that rapid astrocytes morphology changes is a robust finding throughout species (Anders, 2017). Notably, the mean soma fluorescence intensity in EGFP-TNFR1<sup>+/+</sup> and EGFP-TNFR1<sup>-/-</sup> animals was significantly lower compared to hGFAP-EGFP animals (see section 4.3.3). Although volume fraction measurements are robust to variations in soma fluorescence intensity, it remains possible that the intensity was so low that it approached the detection limit and that changes in volume fraction, preventing the detection of changes in volume fraction, particularly in the periphery. However, there was no significant difference in soma intensity between EGFP-TNFR1<sup>+/+</sup> and EGFP-TNFR1<sup>-/-</sup> animals. Given that morphological changes in astrocytes from TNFR1 animals were indeed detectable, it is unlikely that the lack of an effect in EGFP-TNFR1<sup>-/-</sup> is due to the lower mean soma fluorescence intensity

A rather likely explanation for the lack of effect in EGFP-TNFR1<sup>+/+</sup> animals is that some cells are resistant to morphology changes induced by epileptiform activity. This is supported by previous data indicating that a certain number of astrocytes are indeed non-responsive towards epileptiform activity (Anders, 2017). Indeed, in the current study the volume fraction of one astrocyte (3.3.2, Fig. 17) stayed close to 100 % relative to baseline during the last 10 minutes of the experiment. Considering the low number of cells from EGFP-TNFR1<sup>+/+</sup> mice (n=3), one outlier could mask an effect.

Astrocytes in EGFP-TNFR1<sup>-/-</sup> animals were significantly reduced in their volume fraction after induction of epileptiform activity. This finding indicates that TNFR1 is not required for the restructuring of the astroglial cytoskeleton upon epileptiform activity.

TNF $\alpha$  mainly signals via activation of TNFR1 (Wajant et al., 2003). Yet, TNFR2 can be activated by TNF $\alpha$  as well. As in the current study a TNFR1 specific knockout has been used we cannot exclude that the restructuring of the astroglial cytoskeleton is mediated by TNFR2. However, this seems unlikely for at least two reasons: First, the expression of TNFR1 is by far higher than the expression of TNFR2 (Chen et al., 2021). Second, it was shown that in airway smooth muscle cells activation of RhoA/ROCK signaling by TNF $\alpha$  depends on recruitment of TRADDs, with which only TNFR1 can interact with (Hunter and Nixon, 2006). Even though such signaling cascades have not been described specifically yet, it remains possible that TNFR2 interacts with adaptor proteins other than TRADDs that can activate RhoA.

Considering that TNF $\alpha$  alone does not induce astrocyte morphology changes and that TNFR1 is not required for the rapid restructuring of the astroglial cytoskeleton during epileptiform activity, it is indeed unlikely that TNF $\alpha$  is directly involved in the remodeling process induced by epileptiform activity.

This is an unexpected finding as several lines of evidence indicate that TNF $\alpha$  is an important driver of astrogliosis which is marked by severe changes in morphology (Abd-El-Basset et al., 2021; Liddelow et al., 2017). For instance, it was shown that TNF $\alpha$  together with other proinflammatory cytokines released from microglia induces astrogliosis (Liddelow 2017). Moreover, it was shown recently that TNF $\alpha$  promotes astrogliosis in a kainic acid (KA) epilepsy model (Henning et al., 2023). Intracortical injection of KA leads to recurrent spontaneous seizure activity and reliably reproduces key morphological and functional features of chronic human MTLE-HS, and is commonly used to study chronic aspects of epilepsy (Bedner et al., 2015). Coherently, Henning et al. investigated changes in astrocytes morphology and function within 4 hours to days after induction of seizure activity. Consequently, changes in the astrocyte morphology found in this model may be rather representative for the chronic phase of epilepsy (Leite et al., 2002; Sharma et al., 2007). In contrast, the penicillin model is used to understand functional mechanisms underlying the acute phases of epileptogenesis (Akdogan and Yonguc, 2011). In consequence, a lack of effect of TNF $\alpha$  in an acute model while having an effect in a chronic epilepsy model could indicate that TNF $\alpha$  rather promotes long-term morphology changes than acute changes. This is supported by the fact that in the brain tissue of patients suffering from chronic recurrent seizures TNF $\alpha$  levels are not only

acutely but permanently increased (Ashhab et al., 2013). Moreover, it seems conceivable that long-term changes are regulated differently than rapid morphology changes. In fact, rapid astrocyte morphology changes differ strongly in their characteristics from astrogliosis. For instance, the key feature of astrogliosis is hypertrophy of the cell body and the major branches (Sofroniew, 2015). Rapid morphology changes on the other hand seem to occur almost exclusively in the smaller peripheral protrusions (Anders, 2017). Also, it seems that during rapid astrocyte morphology changes the spatial organization in non-overlapping territories is conserved (Anders, 2017). In contrast, astrogliosis is accompanied by a disruption of the territorial organization (Oberheim et al., 2008). Rapid morphology changes are mediated by remodeling of the actin cytoskeleton in the fine perisynaptic astroglial processes (PAP). Remodeling of the PAPs is a phenomenon that occurs also under physiological conditions such as LTP (Henneberger et al., 2020) and depends on the actin-controlling protein cofilin (Henneberger et al., 2020). The key feature of astrogliosis on the other hand is hypertrophy of the cell body and major branches. This is especially driven by an increased expression of intermediate filaments such as GFAP and vimentin (Eng et al., 2000; Wilhelmsson et al., 2004). This indicates that the altered morphology in astrogliosis could be due to altered gene expression while rapid morphology changes are due to phosphorylation and dephosphorylation of the actin cytoskeleton.

In consequence, at least at first sight the phenotype encountered right after onset of epileptiform activity is quite different from the one encountered after recurrent seizure activity. This means in turn that over the time course of epilepsy astrocytes adopt different phenotypes.

In summary, the current study shows that TNF $\alpha$  does not induce rapid morphology changes in astrocytes, nor is TNF $\alpha$ /TNFR1 signaling required for rapid morphology changes induced by epileptiform activity in acute mouse brain slices. TNF $\alpha$  is a prominent inflammatory cytokine. However, so far, we could not rule out that other pathways linked to inflammation are involved in rapid astrocyte morphology changes in epilepsy. Therefore, the role of other mediators of inflammation will be discussed in the following sections.

#### 4.3.4 The role of brain-derived neurotrophic factor in the regulation of astrocyte morphology

The role of BDNF in astrocyte morphology changes in epilepsy is an important area of investigation. Dysregulation of BDNF has been implicated in various pathological conditions, including epilepsy, and increased levels of BDNF have been observed in epilepsy (Iughetti et al., 2018; Vezzani et al., 1999). Interestingly, BDNF is closely related to the neuroimmune-axis as its release can be regulated by microglia and it promotes survival of astrocytes during inflammation (Gomes et al., 2013).

In order to investigate whether BDNF links the onset of epileptiform activity to rapid astrocyte morphology changes, acute hippocampal slices were incubated with BDNF. Subsequently, the astrocyte morphology of treated slices was compared to non-treated slices with the help of volume fraction measurements. Contrary to our expectation, in this experimental setting BDNF did not alter astrocyte morphology (see section 3.4, Fig. 19). This finding contrasts with previous cell culture studies, such as the work by Ohira et al. (2007) which demonstrated that BDNF induces morphological plasticity in cultured astrocytes after 1 hour. In those studies, BDNF was shown to activate the TrkB.T1 receptor on astrocytes and induce morphology changes that are RhoA/ROCK-dependent. The lack of effect of BDNF on astrocyte morphology in the current study could be attributed to the differences between experimental settings. While cell culture studies as used by Ohira et al (2006) provide controlled and simplified conditions, investigations *in situ* or *in vivo* models, such as acute hippocampal slices, aim to capture the complexity and interactions of cells within their native environment. It is well-known that results from cell culture studies do not always translate directly to *in situ* or *in vivo* conditions. Variability in cellular properties and interactions between different cell types within the brain can contribute to these differences. The present study highlights the importance of validating findings from cell culture studies in more complex models, such as brain slices or *in vivo* models, to better understand the relevance and applicability of the results.

The possibility of species-dependent differences in TrkB.T1 function between rats and mice is an important consideration. Ohira et al. (2006) relied on astrocytes derived from rat hippocampi while we relied on astrocytes in murine hippocampi. However, the intracellular domain of TrkB.T1 is highly conserved among various species, including humans, mice, rats, and felines (Armanini et al., 1995; Middlemas et al., 1991; Shelton et

al., 1995). This suggests that the receptor is likely to mediate similar effects in astrocytes from different species. Nevertheless, further investigation is needed to confirm whether any species-specific differences exist in the response of astrocytes to BDNF and TrkB.T1 activation.

The concentration of BDNF used in the present study (100 ng/ml) was based on previous cell culture studies that demonstrated its efficacy in altering astrocyte morphology (Holt et al., 2019; Ohira et al., 2005). However, it is possible that different concentrations of BDNF are required to elicit morphological changes in acute brain slices. To address this, future experiments could be conducted using a range of BDNF concentrations to determine the optimal dosage for inducing astrocyte morphology changes in this experimental model.

Interestingly, previous studies have shown that BDNF activation of TrkB.T1 leads to the inhibition of RhoA activation by promoting the dissociation of RhoGDI (Ohira et al. 2005). This suggests that BDNF may have an opposing effect on RhoA signaling compared to the effect induced by epileptiform activity, which is known to activate RhoA.

It has been reported that effects of BDNF mediated by TrkB.FL which is predominantly expressed by neurons are time and dose dependent (Cunha et al., 2009; Suzuki et al., 2004). To date this has not been examined specifically for TRkB.T1 signaling. However, it is possible that also effects mediated by TrkB.T1 are dose dependent and different effects are mediated by different doses. Future studies could explore the dose-dependent effects of BDNF on RhoA/ROCK signaling in astrocytes to better understand its role in modulating astrocyte morphology.

Investigating the effect of BDNF on astrocyte morphology in the presence of epileptiform activity could provide valuable insights into the underlying mechanisms of epilepsy. If BDNF inhibits RhoA activation, it could potentially alter or prevent astrocyte morphology changes induced by epileptiform activity. This could help elucidate the role of BDNF in modulating neural activity and its potential contributions to either pro-convulsive or anti-convulsive actions.

In conclusion, the present study suggests that BDNF does not directly alter astrocyte morphology in acute brain slices and may even counteract RhoA activation. However, further investigations are required to better understand the role of BDNF in astrocyte morphological plasticity, including studies using different concentrations of BDNF and examining its effects in the context of epileptiform activity.

#### 4.4 The role of norepinephrine in the acute regulation of astrocyte morphology

The engagement of the stress axis and increased release of NE in the hippocampus during epilepsy have been well-documented (Hara et al., 1993; Simon et al., 1984). To investigate the potential link between increased NE levels and rapid astrocyte morphology changes, NE was applied to hippocampal slices, and astrocyte morphology was monitored. Surprisingly, NE did not alter astrocyte morphology in this experimental setting (see 3.5, Fig. 20).

Previous studies in cultured astrocytes have consistently demonstrated that NE induces morphological plasticity, specifically stellation, which is the transformation of cultured astrocytes from a flat polygonal shaped phenotype to a process-bearing phenotype. This effect is mediated through the activation of beta-adrenergic receptors, which in turn activate adenylyl cyclase (AC) and generate the second messenger cyclic adenosine monophosphate (cAMP) (Vardjan et al., 2014). However, in acute hippocampal slices, NE did not induce rapid changes in astrocyte morphology.

One possible explanation for this lack of effect could be that the concentration of NE used in the study was not sufficient to activate beta-adrenergic receptors. While NE is a potent agonist of all adrenergic receptors, the affinity of these receptors for NE varies. Alpha-adrenergic receptors are activated by nanomolar concentrations of NE, while beta receptors require micromolar concentrations (McPherson et al., 1985; Zhang et al., 2004). In this study, a concentration of 100  $\mu$ M NE was used, which should be sufficient to activate beta receptors. Therefore, it appears that, unlike in cell culture studies, beta-receptor activation does not induce morphological changes in astrocytes in acute hippocampal slices.

This finding is supported by the results from previous experiments conducted in our laboratory, investigating the role of AC, the key downstream effector of beta receptors involved in morphology changes. In these experiments, NKH477, an activator of AC, was applied to acute hippocampal slices, and astrocyte morphology was monitored simultaneously. Interestingly, in this experimental setting, the astrocyte volume fraction decreased significantly (Anders, 2017). However, as a side effect, NKH477 induced epileptiform discharges comparable to those induced by penicillin. When neuronal activity was blocked by applying tetrodotoxin (TTX), NKH477 no longer had an effect on the

astrocyte volume fraction, suggesting that activation of AC itself did not induce rapid astrocyte morphology changes (Anders, 2017).

Taken together, these results suggest that beta-receptor signaling is not involved in rapid astrocyte morphology changes in acute hippocampal slices. In consequence, it is suggested that beta receptor signaling is not the mechanistic link between the onset of epileptiform activity and astrocyte morphology changes.

As stated above, adrenergic receptors differ in their affinity for NE. Assuming that the concentration was high enough to stimulate beta receptors, it can be deduced that alpha receptors were stimulated simultaneously, as NE has a higher affinity for alpha-adrenergic than for beta-adrenergic receptors (Zhang et al., 2004). It is established that not only beta receptors regulate astrocyte morphology but also alpha-adrenergic receptors (Ruck et al., 1991). In contrast to beta receptors, alpha receptors are coupled to G-proteins that inhibit AC/cAMP signaling and therefore inhibit process formation in cultures (Enkvist et al., 1996). Hence, alpha- and beta-adrenergic receptors mediate opposing pathways regarding the regulation of astrocyte morphology in cell cultures. It was shown that the strength of the effect of NE on astrocyte morphology varies between cortical and spinal astrocytes due to different expression patterns of alpha and beta receptors (Kitano et al., 2021). It was proposed that the effect of NE on astrocyte morphology is regulated by the balance of alpha- and beta-receptor expression (Kitano et al., 2021).

In the present study, it is possible that the simultaneous activation of alpha- and beta-adrenergic receptors by NE led to opposing downstream signaling pathways. The activation of beta receptors, which promote cAMP generation and process formation, may have been counteracted by the inhibition of cAMP signaling mediated by alpha receptors. As a result, the effects of NE on astrocyte morphology may have been nullified in this experimental setting. Therefore, it could be promising to use specific agonists for alpha- or beta-adrenergic receptors in future experiments to better understand their role in astrocyte morphology.

Intriguingly, it was shown recently that alpha receptors inhibit astrocyte stellation not only by inhibiting AC/cAMP signaling but also via cAMP-independent mechanism(s) (Kitano et al., 2021). This is based on the observation that alpha receptor activation in cultured astrocytes inhibits stellation induced by the ROCK inhibitor Y27632 which is known to

induce stellation in a cAMP-independent manner (Abe and Misawa, 2003; Kitano et al., 2021). This finding indicates that alpha receptors regulate the astrocyte morphology by engaging pathways that regulate RhoA/ROCK signaling additionally to cAMP signaling (Kitano et al., 2021).

Given this new information, targeting alpha-adrenergic receptor signaling could be a promising approach to modulate astrocyte morphology during epileptogenesis. To address alpha receptor signaling specifically, lower concentrations of NE could be used as alpha-adrenergic receptors are activated by nanomolar concentrations, while beta-adrenergic receptors require micromolar concentrations for activation. Alternatively, subtype-specific agonists such as phenylephrine for alpha 1 receptors or dexmedetomidine for alpha 2 receptors could be employed (Jasper et al., 1998).

Another approach to investigate the contribution of NE signaling to morphological alterations in astrocytes during epileptiform activity could involve using a mouse model lacking dopamine b-hydroxylase (DBH) expression homozygously. DBH catalyzes the conversion of dopamine to NE. Consequently, these mouse models are NE-deficient and have been utilized in epilepsy research before (Szot et al., 1999). If morphology changes still occur in NE-deficient mice following the induction of epileptiform activity, it would suggest that NE is not involved in rapid astrocyte morphology changes.

In summary, the present study demonstrated that NE at a concentration of 100  $\mu$ M does not induce rapid astrocyte morphology changes in murine acute hippocampal slices. However, considering the complexity of the noradrenergic system in the CNS and the diverse actions mediated by adrenergic receptors in astrocytes, adrenergic receptors remain an intriguing target for modulating astrocyte morphology in acute hippocampal slices. Further investigations into the effects mediated by adrenergic receptors on astrocyte morphology, as proposed above, are warranted.

#### 4.5 The role of inflammatory pathways in rapid astrocyte morphology changes induced by epileptiform activity

In the present study, we investigated the effects of classical inflammatory mediators such as TNF $\alpha$  and IL1b, as well as modulators of the neuroimmune axis including NE and BDNF, on astrocyte morphology. Contrary to our expectations, none of these molecules induced significant changes in astrocyte morphology in our experiments. This raises the

question of whether inflammation is indeed involved in the restructuring of the astroglial cytoskeleton during epileptiform activity.

Multiple lines of evidence suggest that inflammation in early epileptogenesis is primarily driven by microglia activation. Activated microglia release various pro- and anti-inflammatory factors, including TNF $\alpha$ , IL1b, IL6, prostaglandins, which contribute to the inflammatory response (Garden and Möller 2006; Soontornniyomkij et al. 1998). However, our findings consistently showed that TNF $\alpha$ , in particular, is unlikely to mediate rapid astrocyte morphology changes during epileptiform activity. Nonetheless, it is possible that other inflammatory molecules released by activated microglia play a role in mediating these changes. Importantly, it is worth considering that rapid astrocyte morphology changes may not be driven by a single pathway, but rather by multiple converging pathways.

Cytokines commonly act in an interconnected manner, contributing to the inflammatory response. Accordingly, previous studies have shown that only the combined application of TNF $\alpha$ , IL1a, and C3, all produced by activated microglia, was sufficient to induce a reactive astrocyte phenotype in cultured astrocytes (Liddel et al. 2017). This could suggest that multiple inflammatory triggers may be necessary to induce a switch in astrocyte phenotype. To elucidate the general role of inflammation in acute astrocyte morphology changes it could be beneficial to mimic an inflammatory milieu in acute hippocampal slices. This could be achieved for instance by using lipopolysaccharide (LPS) a strong inducer of microglia activation (Holtman et al., 2015; Qiu et al., 2022). The advantage of this approach could be that the activation of microglia leads to the release of various soluble factor including cytokines and neurotrophic factors that may work in an interconnected manner. Consequently, this model would be more similar to *in vivo* conditions. Yet, the disadvantage is that such an experimental setting would not unravel a single mechanistic link as a potential effect cannot be traced back to a single triggering signal. Yet, such an experiment could give meaningful insights into the general role of inflammation in acute astrocyte morphology changes during epileptogenesis.

To further explore the role of inflammation in astrocyte morphological plasticity during epileptiform activity, additional experiments are needed. One approach is to analyze astrocyte morphology in the absence of microglia, which are considered the main drivers of inflammation during early epileptogenesis. This can be achieved using, a microglia-

deficient mouse model such as Cx3cr1 knockout mice (Paolicelli et al. 2014). This mouse line was recently used to demonstrate that microglia are responsible for the shift from resting to reactive astrocytes in cultures (Liddel et al. 2017). Drawbacks of this mouse model are that the disruption of neuron–microglia signaling severely affects synaptic properties and plasticity.

In order to investigate the role of microglia activation in linking epileptiform activity to rapid morphology changes in astrocytes, there are alternative approaches to knockout paradigms. One such approach is the use of minocycline, a tetracycline antibiotic that has been shown to have anti-inflammatory properties in the central nervous system (CNS) separate from its antimicrobial action (Kobayashi et al. 2013). Minocycline has been demonstrated to reduce initial seizure-induced microglia activation and block the increase of cytokine concentration in a KA-induced SE model (Abraham et al. 2012; Wang et al. 2015). Another approach is the pharmacological depletion of microglia by inhibiting the colony-stimulating factor 1 receptor (CSF1R) using PLX5622 (Dagher et al. 2015).

If induction of epileptiform activity in acute slices where microglia are silenced or absent leads to rapid morphology changes in astrocytes, it would strongly indicate that microglia activation is not the sole driver of these changes. Intriguingly, a study by Sano et al. (2021) demonstrated that microglia inhibition reduced activated astrocyte morphology during astrogliosis following pilocarpine-induced status epilepticus. This finding is in contrast with the results reported by Henning et al. (2023), who showed only a marginal effect of microglia depletion on astrogliosis.

Both Sano et al. and Henning et al. used post-status epilepticus models (KA and pilocarpine). It is important to note that studies using post-status epilepticus models, such as KA and pilocarpine, which attempt to recreate human temporal lobe epilepsy, may not capture immediate molecular or morphological alterations in astrocytes following the onset of epileptiform activity. The observed effects of inflammation on astrocyte morphology in these models may primarily occur during the latent and chronic phases, and it may not necessarily reflect the drivers of rapid astrocyte morphology changes in the penicillin model. Therefore, it seems mandatory to further investigate the effect of microglia silencing in a model more representative for the very early stage of epileptogenesis such as the penicillin model used in the present study.

In summary, the current study gave first insights into the contribution of inflammation to rapid astrocyte morphology changes in early epileptogenesis. However, further investigations are required to understand the specific mechanisms underlying rapid astrocyte morphology changes in different epileptic models, including the penicillin model. Silencing or absence of microglia in acute slices would provide valuable insights into the contribution of microglia activation to these rapid changes and help uncover other potential mechanisms involved.

## 5. Summary

The aim of the study was to investigate the mechanisms underlying rapid astrocyte morphology changes in the hippocampal formation in response to epileptiform activity.

The present study specifically focused on investigating the role of the inflammatory cytokine tumor necrosis factor alpha in mediating rapid astrocyte morphology changes during epileptiform activity. Inflammation has been consistently linked to epileptic processes in the brain, making tumor necrosis factor alpha an intriguing candidate for studying its effects on astrocytes.

However, contrary to expectation, the study's findings indicate that tumor necrosis factor alpha does not have an acute or delayed effect on astrocyte morphology in hippocampal slices. Moreover, we show that even in the absence of the primary receptor of tumor necrosis factor alpha, astrocytes respond with rapid morphological changes to epileptiform activity.

This suggests that tumor necrosis factor alpha, despite its association with inflammation and epileptic processes, does not directly contribute to the rapid changes in astrocyte morphology observed during epileptiform activity.

Furthermore, the study's findings indicate that the molecules norepinephrine and brain derived neurotrophic factor which are known to be associated with epileptic processes do not promote astrocyte morphology changes in acute hippocampal slices in our experimental settings.

The lack of influence especially of tumor necrosis factor alpha, brain derived neurotrophic and norepinephrine on astrocyte morphology in acute hippocampal slices suggests that other signaling pathways and molecules may play a more prominent role in mediating these morphological changes. This raises the question of whether inflammation is involved at all in astrocyte plasticity under these conditions. Future studies will be needed to uncover the complex interactions and signaling cascades involved in astrocyte plasticity during the onset of epileptiform activity and to determine the precise role, if any, of inflammation in this process.

## 6. List of figures

Figure 1: Neuronal tri-synaptic circuit in the hippocampus .....	9
Figure 2: Protoplasmic astrocytes.....	13
Figure 3: Regulators of astrocyte morphology .....	20
Figure 4: Signaling molecules that could potentially induce rapid astrocyte morphology changes during acute onset of epileptiform activity .....	30
Figure 5: Electrophysiological setup .....	37
Figure 6: Properties of evoked fEPSPs in CA1 stratum radiatum and pyramidale .....	39
Figure 7: Example of a fluorescent astrocyte in CA1 .....	42
Figure 8: Exemplary EGFP-expressing astrocytes exposed to osmotic stress.....	47
Figure 9: Astrocyte volume fraction changes upon osmotic stress in acute hippocampal slices .....	48
Figure 10: Altered extracellular osmolarity modulates synaptic transmission in CA1 neuron populations.....	50
Figure 11: Application of penicillin induces epileptiform activity in acute hippocampal slices .....	52
Figure 12: Epileptiform activity induces rapid astrocyte morphology changes.....	53
Figure 13: Representative EGFP-expressing astrocyte in CA1 .....	55
Figure 14: The acute effect of 10 ng/ml TNF $\alpha$ on astrocyte morphology.....	56
Figure 15: Astrocyte morphology in slices incubated with TNF $\alpha$ or TNF $\alpha$ and IL1b.....	58
Figure 16: Proportion of slices that developed epileptiform activity after penicillin treatment .....	60
Figure 17: Application of penicillin induced epileptiform activity in EGFP-TNFR1 <sup>-/-</sup> and EGFP-TNFR1 <sup>+/+</sup> mice .....	61
Figure 18: Epileptiform activity induced astrocyte morphology changes in acute brain slices of EGFP-TNFR1 <sup>-/-</sup> mice.....	63
Figure 19: Astrocytes exposed to BDNF do not show alterations in astrocytic volume fraction .....	65
Figure 20: Astrocyte morphology is not altered by 100 $\mu$ M NE.....	66

## 7. List of tables

Table 1: Chemicals .....	33
Table 2: Artificial cerebrospinal fluid (ACSF) .....	33
Table 3: Hyposmolar ACSF .....	34
Table 4: Hyperosmolar ACSF .....	34
Table 5: Slicing solution .....	34

## 8. References

Abd-El-Basset EM, Rao MS, Alshawaf SM, Ashkanani HK, Kabli AH. Tumor necrosis factor (TNF) induces astrogliosis, microgliosis and promotes survival of cortical neurons. *AIMS Neurosci* 2021; 8: 558–584

Abe K, Misawa M. Astrocyte stellation induced by Rho kinase inhibitors in culture. *Brain Res Dev Brain Res* 2003; 143: 99–104

Aitken PG, Borgdorff AJ, Juta AJA, Kiehart DP, Somjen GG, Wadman WJ. Volume changes induced by osmotic stress in freshly isolated rat hippocampal neurons. *Pflügers Arch* 1998; 436: 991–998

Akdogan I, Yonguc NG. Kannez FS ed. *Experimental Epilepsy Models and Morphologic Alterations of Experimental Epilepsy Models in Brain and Hippocampus*. IntechOpen, 2011: 269-281

Amano M, Nakayama M, Kaibuchi K. Rho-kinase/ROCK: A key regulator of the cytoskeleton and cell polarity. *Cytoskeleton* 2010; 67: 545–554

Amor S, Puentes F, Baker D, Van Der Valk P. Inflammation in neurodegenerative diseases. *Immunology* 2010; 129: 154–169

Anders S. Rapid astrocyte morphology changes during epileptogenesis in the rodent hippocampus. Thesis. Mathematisch-Naturwissenschaftlichen Fakultät der Universität Bonn, 2017

Anders S, Breithausen B, Unichenko P, Herde MK, Minge D, Abramian A, Behringer C, Deshpande T, Boehlen A, Domingos C, Henning L, Pitsch J, Kim Y-B, Bedner P, Steinhäuser C, Henneberger C. Epileptic activity triggers rapid ROCK1-dependent astrocyte morphology changes. *Glia* 2024; 72: 643–659

Andersen P, Morris R, Amaral D, Bliss T, O'Keefe J. *The Hippocampus Book*. New York

Oxford Academic, 2006

Anderson MA, Ao Y, Sofroniew MV. Heterogeneity of reactive astrocytes. *Neurosci Lett* 2014; 565: 23–29

Anderson MA, Burda JE, Ren Y, Ao Y, O'Shea TM, Kawaguchi R, Coppola G, Khakh BS, Deming TJ, Sofroniew MV. Astrocyte scar formation aids central nervous system axon regeneration. *Nature* 2016; 532: 195–200

Andrew RD, Labron MW, Boehnke SE, Carnduff L, Kirov SA. Physiological Evidence That Pyramidal Neurons Lack Functional Water Channels. *Cereb Cortex* 2007; 17: 787–802

Andrew RD, Lobinowich ME, Osehobo EP. Evidence against volume regulation by cortical brain cells during acute osmotic stress. *Exp Neurol* 1997; 143: 300–312

Araque A, Carmignoto G, Haydon PG, Oliet SHR, Robitaille R, Volterra A. Gliotransmitters Travel in Time and Space. *Neuron* 2014; 81: 728–739

Araque A, Parpura V, Sanzgiri RP, Haydon PG. Tripartite synapses: glia, the unacknowledged partner. *Trends Neurosci* 1999; 22: 208–215

Armanini MP, McMahon SB, Sutherland J, Shelton DL, Phillips HS. Truncated and catalytic isoforms of *trkB* are co-expressed in neurons of rat and mouse CNS. *Eur J Neurosci* 1995; 7: 1403–1409

Aronica E, Crino PB. Inflammation in epilepsy: Clinical observations. *Epilepsia* 2011; 52: 26–32

Ashhab MU, Omran A, Kong H, Gan N, He F, Peng J, Yin F. Expressions of Tumor Necrosis Factor Alpha and MicroRNA-155 in Immature Rat Model of Status Epilepticus and Children with Mesial Temporal Lobe Epilepsy. *J Mol Neurosci* 2013; 51: 950–958

- Barbacid M. The Trk family of neurotrophin receptors. *J Neurobiol* 1994; 25: 1386–1403
- Baud V, Karin M. Signal transduction by tumor necrosis factor and its relatives. *Trends Cell Biol* 2001; 11: 372–377
- Beach TG, Woodhurst WB, MacDonald DB, Jones MW. Reactive microglia in hippocampal sclerosis associated with human temporal lobe epilepsy. *Neurosci Lett* 1995; 191: 27–30
- Becker AJ. Review: Animal models of acquired epilepsy: insights into mechanisms of human epileptogenesis. *Neuropathol Appl Neurobiol* 2018; 44: 112–129
- Bedner P, Dupper A, Hüttmann K, Müller J, Herde MK, Dublin P, Deshpande T, Schramm J, Häussler U, Haas CA, Henneberger C, Theis M, Steinhäuser C. Astrocyte uncoupling as a cause of human temporal lobe epilepsy. *Brain* 2015; 138: 1208–1222
- Bedner P, Steinhäuser C. Role of Impaired Astrocyte Gap Junction Coupling in Epileptogenesis. *Cells* 2023; 12: 1669
- Bennett MR, Buljan V, Farnell L, Gibson WG. Purinergic Junctional Transmission and Propagation of Calcium Waves in Spinal Cord Astrocyte Networks. *Biophys J* 2006; 91: 3560–3571
- Bernardinelli Y, Muller D, Nikonenko I. Astrocyte-Synapse Structural Plasticity. *Neural Plast* 2014a; 2014: 232105
- Bernardinelli Y, Randall J, Janett E, Nikonenko I, König S, Jones EV, Flores CE, Murai KK, Bochet CG, Holtmaat A, Muller D. Activity-Dependent Structural Plasticity of Perisynaptic Astrocytic Domains Promotes Excitatory Synapse Stability. *Curr Biol* 2014b; 24: 1679–1688
- Bezzi P, Volterra A. A neuron–glia signalling network in the active brain. *Curr Opin*

Neurobiol 2001; 11: 387–394

Bignami A, Eng LF, Dahl D, Uyeda CT. Localization of the glial fibrillary acidic protein in astrocytes by immunofluorescence. *Brain Res* 1972; 43: 429–435

Binder DK, Steinhäuser C. Functional changes in astroglial cells in epilepsy. *Glia* 2006; 54: 358–368

Black RA, Rauch CT, Kozlosky CJ, Peschon JJ, Slack JL, Wolfson MF, Castner BJ, Stocking KL, Reddy P, Srinivasan S, Nelson N, Boiani N, Schooley KA, Gerhart M, Davis R, Fitzner JN, Johnson RS, Paxton RJ, March CJ, Cerretti DP. A metalloproteinase disintegrin that releases tumour-necrosis factor-alpha from cells. *Nature* 1997; 385: 729–733

Blumcke I, Spreafico R, Haaker G, Coras R, Kobow K, Bien CG, et al. Histopathological Findings in Brain Tissue Obtained during Epilepsy Surgery. *N Engl J Med* 2017; 377: 1648–1656

Booth HDE, Hirst WD, Wade-Martins R. The Role of Astrocyte Dysfunction in Parkinson's Disease Pathogenesis. *Trends Neurosci* 2017; 40: 358–370

Bos JL, Rehmann H, Wittinghofer A. GEFs and GAPs: Critical Elements in the Control of Small G Proteins. *Cell* 2007; 129: 865–877

Brikos C, Wait R, Begum S, O'Neill LAJ, Saklatvala J. Mass spectrometric analysis of the endogenous type I interleukin-1 (IL-1) receptor signaling complex formed after IL-1 binding identifies IL-1RAcP, MyD88, and IRAK-4 as the stable components. *Mol Cell Proteomics* 2007; 6: 1551–1559

Brigadski T, Leßmann V. The physiology of regulated BDNF release. *Cell Tissue Res* 2020; 382: 15–45

Burda JE, Bernstein AM, Sofroniew MV. Astrocyte roles in traumatic brain injury. *Exp Neurol* 2016; 275: 305–315

Burridge K, Doughman R. Front and back by Rho and Rac. *Nat Cell Biol* 2006; 8: 781–782

Bushong EA, Martone ME, Jones YZ, Ellisman MH. Protoplasmic Astrocytes in CA1 Stratum Radiatum Occupy Separate Anatomical Domains. *J Neurosci* 2002; 22: 183–192

Bylund DB. Adrenergic Receptors. In: Lennarz WJ, Lane MD, eds. *Encyclopedia of Biological Chemistry (Second Edition)*. Waltham: Academic Press, 2013, 57–60

Cabal-Hierro L, Lazo PS. Signal transduction by tumor necrosis factor receptors. *Cell Signal* 2012; 24: 1297–1305

Cao T, Matyas JJ, Renn CL, Faden AI, Dorsey SG, Wu J. Function and Mechanisms of Truncated BDNF Receptor TrkB.T1 in Neuropathic Pain. *Cells* 2020; 9: 1194

Carswell EA, Old LJ, Kassel RL, Green S, Fiore N, Williamson B. An endotoxin-induced serum factor that causes necrosis of tumors. *Proc Natl Acad Sci U S A* 1975; 72: 3666–3670

Cavanagh JB, Meyer A. Aetiological Aspects of Ammon's Horn Sclerosis Associated with Temporal Lobe Epilepsy. *BMJ* 1956; 2: 1403–1407

Cavazos J, Das I, Sutula T. Neuronal loss induced in limbic pathways by kindling: evidence for induction of hippocampal sclerosis by repeated brief seizures. *J Neurosci* 1994; 14: 3106–3121

Chen R, Xue G, Hölscher C. The role of the TNF $\alpha$ -mediated astrocyte signaling pathway in epilepsy. *Acta Epileptologica* 2021; 3: 24

Choi SJ, Lee K-H, Park HS, Kim S-K, Koh C-M, Park JY. Differential Expression, Shedding, Cytokine Regulation and Function of TNFR1 and TNFR2 in Human Fetal Astrocytes. *Yonsei Med J* 2005; 46: 818–826

Chvátal A, Anděrová M, Kirchhoff F. Three-dimensional confocal morphometry – a new approach for studying dynamic changes in cell morphology in brain slices. *J Anat* 2007; 210: 671–683

Colonna M, Butovsky O. Microglia Function in the Central Nervous System During Health and Neurodegeneration. *Annu Rev Immunol* 2017; 35: 441–468

Cornell-Bell AH, Finkbeiner SM, Cooper MS, Smith SJ. Glutamate Induces Calcium Waves in Cultured Astrocytes: Long-Range Glial Signaling. *Science* 1990; 247: 470–473

Coulter DA, Steinhäuser C. Role of astrocytes in epilepsy. *Cold Spring Harb Perspect Med* 2015; 5: a022434

Crespel A, Coubes P, Rousset M-C, Brana C, Rougier A, Rondouin G, Bockaert J, Baldy-Moulinier M, Lerner-Natoli M. Inflammatory reactions in human medial temporal lobe epilepsy with hippocampal sclerosis. *Brain Res* 2002; 952: 159–169

Cunha C, Angelucci A, D'Antoni A, Dobrossy MD, Dunnett SB, Berardi N, Brambilla R. Brain-derived neurotrophic factor (BDNF) overexpression in the forebrain results in learning and memory impairments. *Neurobiol Dis* 2009; 33: 358–368

Dani JW, Chernjavsky A, Smith SJ. Neuronal activity triggers calcium waves in hippocampal astrocyte networks. *Neuron* 1992; 8: 429–440

Davies JA. Mechanisms of action of antiepileptic drugs. *Seizure* 1995; 4: 267–271

De Simoni MG, Perego C, Ravizza T, Moneta D, Conti M, Marchesi F, De Luigi A, Garattini S, Vezzani A. Inflammatory cytokines and related genes are induced in the rat

hippocampus by limbic status epilepticus. *Eur J Neurosci* 2000; 12: 2623–2633

Deinhardt K, Chao MV. Trk Receptors. In: Lewin GR, Carter BD, eds. *Neurotrophic Factors*, Berlin, Heidelberg: Springer, 2014: 103–119

Deng W, Aimone JB, Gage FH. New neurons and new memories: how does adult hippocampal neurogenesis affect learning and memory? *Nat Rev Neurosci* 2010; 11: 339–350

Devinsky O, Vezzani A, Najjar S, De Lanerolle NC, Rogawski MA. Glia and epilepsy: excitability and inflammation. *Trends Neurosci* 2013; 36: 174–184

Dinarello CA. Overview of the IL-1 family in innate inflammation and acquired immunity. *Immunol Rev* 2018; 281: 8–27

DiSabato DJ, Quan N, Godbout JP. Neuroinflammation: the devil is in the details. *J Neurochem* 2016; 139: 136–153

Dopp JM, Mackenzie-Graham A, Otero GC, Merrill JE. Differential expression, cytokine modulation, and specific functions of type-1 and type-2 tumor necrosis factor receptors in rat glia. *J Neuroimmunol* 1997; 75: 104–112

Dou S-H, Cui Y, Huang S-M, Zhang B. The Role of Brain-Derived Neurotrophic Factor Signaling in Central Nervous System Disease Pathogenesis. *Front Hum Neurosci* 2022; 16: 924155

Dubé C, Vezzani A, Behrens M, Bartfai T, Baram TZ. Interleukin-1 $\beta$  contributes to the generation of experimental febrile seizures. *Ann Neurol* 2005; 57: 152–155

Dudek FE, Obenaus A, Tasker JG. Osmolality-induced changes in extracellular volume alter epileptiform bursts independent of chemical synapses in the rat: Importance of non-synaptic mechanisms in hippocampal epileptogenesis. *Neurosci Lett* 1990; 120: 267–270

Duncan JS, Sander JW, Sisodiya SM, Walker MC. Adult epilepsy. *Lancet* 2006; 367: 1087–1100

Eng LF, Ghirnikar RS, Lee YL. Glial fibrillary acidic protein: GFAP-thirty-one years (1969-2000). *Neurochem Res* 2000; 25: 1439–1451

Engel J. Mesial Temporal Lobe Epilepsy: What Have We Learned? *Neuroscientist* 2001; 7: 340–352

Enkvist MOK, Hämäläinen H, Jansson CC, Kukkonen JP, Hautala R, Courtney MJ, Åkerman KEO. Coupling of Astroglial  $\alpha$ 2-Adrenoreceptors to Second Messenger Pathways. *J Neurochem* 1996; 66: 2394–2401

Eriksson C, Van Dam AM, Lucassen PJ, Bol JGJM, Winblad B, Schultzberg M. Immunohistochemical localization of interleukin-1 $\beta$ , interleukin-1 receptor antagonist and interleukin-1 $\beta$  converting enzyme/caspase-1 in the rat brain after peripheral administration of kainic acid. *Neuroscience* 1999; 93: 915–930

Ernfors P, Bengzon J, Kokaia Z, Persson H, Lindvall O. Increased levels of messenger RNAs for neurotrophic factors in the brain during kindling epileptogenesis. *Neuron* 1991; 7: 165–176

Estes ML, McAllister AK. Alterations in Immune Cells and Mediators in the Brain: It's Not Always Neuroinflammation! *Brain Pathol* 2014; 24: 623–630

Etienne-Manneville S, Hall A. Rho GTPases in cell biology. *Nature* 2002; 420: 629–635

Fenner BM. Truncated TrkB: Beyond a dominant negative receptor. *Cytokine Growth Factor Rev* 2012; 23: 15–24

Fields JK, Günther S, Sundberg EJ. Structural Basis of IL-1 Family Cytokine Signaling.

Front Immunol 2019; 10: 1412

Fisher RS, Boas W van E, Blume W, Elger C, Genton P, Lee P, Engel Jr. J. Epileptic Seizures and Epilepsy: Definitions Proposed by the International League Against Epilepsy (ILAE) and the International Bureau for Epilepsy (IBE). *Epilepsia* 2005; 46: 470–472

Fisher RS, Engel JJ. Definition of the postictal state: When does it start and end? *Epilepsy Behav* 2010; 19: 100–104

Fletcher DA, Mullins RD. Cell mechanics and the cytoskeleton. *Nature* 2010; 463: 485–492

French JA, Williamson PD, Thadani VM, Darcey TM, Mattson RH, Spencer SS, Spencer DD. Characteristics of medial temporal lobe epilepsy: I. Results of history and physical examination. *Ann of Neurol* 1993; 34: 774–780

Garcia-Lopez P, Garcia-Marin V, Freire M. The Histological Slides and Drawings of Cajal. *Front Neuroanat* 2010; 4: 9

Garden GA, Möller T. Microglia Biology in Health and Disease. *J NeuroImmune Pharmacol* 2006; 1: 127–137

Garland EF, Hartnell IJ, Boche D. Microglia and Astrocyte Function and Communication: What Do We Know in Humans? *Front Neurosci* 2022; 16: 824888

Garlanda C, Dinarello CA, Mantovani A. The Interleukin-1 Family: Back to the Future. *Immunity* 2013; 39: 1003–1018

Giaume C, Koulakoff A, Roux L, Holcman D, Rouach N. Astroglial networks: a step further in neuroglial and gliovascular interactions. *Nat Rev Neurosci* 2010; 11: 87–99

Goddard GV. Development of Epileptic Seizures through Brain Stimulation at Low

Intensity. *Nature* 1967; 214: 1020–1021

Gomes C, Ferreira R, George J, Sanches R, Rodrigues DI, Gonçalves N, Cunha RA. Activation of microglial cells triggers a release of brain-derived neurotrophic factor (BDNF) inducing their proliferation in an adenosine A2A receptor-dependent manner: A2A receptor blockade prevents BDNF release and proliferation of microglia. *J Neuroinflammation* 2013; 10: 16

Grell M, Wajant H, Zimmermann G, Scheurich P. The type 1 receptor (CD120a) is the high-affinity receptor for soluble tumor necrosis factor. *Proc Natl Acad Sci U S A* 1998; 95: 570–575

Haber M, Zhou L, Murai KK. Cooperative Astrocyte and Dendritic Spine Dynamics at Hippocampal Excitatory Synapses. *J Neurosci* 2006; 26: 8881–8891

Hanisch U-K. Microglia as a source and target of cytokines. *Glia* 2002; 40: 140–155

Hara M, Sasa M, Kawabata A, Serikawa T, Yamada T, Yamada J, Takaori S. Decreased Dopamine and Increased Norepinephrine Levels in the Spontaneously Epileptic Rat, a Double Mutant Rat. *Epilepsia* 1993; 34: 433–440

Hein L, Kobilka BK. Adrenergic receptor signal transduction and regulation. *Neuropharmacology* 1995; 34: 357–366

Heithoff BP, George KK, Phares AN, Zuidhoek IA, Munoz-Ballester C, Robel S. Astrocytes are necessary for blood–brain barrier maintenance in the adult mouse brain. *Glia* 2021; 69: 436–472

Heller JP, Rusakov DA. The Nanoworld of the Tripartite Synapse: Insights from Super-Resolution Microscopy. *Front Cell Neurosci* 2017; 11: 374

Henneberger C, Bard L, Panatier A, Reynolds JP, Kopach O, Medvedev NI, Minge D,

Herde MK, Anders S, Kraev I, Heller JP, Rama S, Zheng K, Jensen TP, Sanchez-Romero I, Jackson CJ, Janovjak H, Ottersen OP, Nagelhus EA, Oliet SHR, Stewart MG, Nägerl UV, Rusakov DA. LTP Induction Boosts Glutamate Spillover by Driving Withdrawal of Perisynaptic Astroglia. *Neuron* 2020; 108: 919-936.e11

Henning L, Antony H, Breuer A, Müller J, Seifert G, Audinat E, Singh P, Brosseron F, Heneka MT, Steinhäuser C, Bedner P. Reactive microglia are the major source of tumor necrosis factor alpha and contribute to astrocyte dysfunction and acute seizures in experimental temporal lobe epilepsy. *Glia* 2023; 71: 168–186

Hertz L, Peng L, Lai JCK. Functional Studies in Cultured Astrocytes. *Methods* 1998; 16: 293–310

Hiragi T, Ikegaya Y, Koyama R. Microglia after Seizures and in Epilepsy. *Cells* 2018; 7: 26

Hirrlinger J, Hülsmann S, Kirchhoff F. Astroglial processes show spontaneous motility at active synaptic terminals in situ. *Eur J Neurosci* 2004; 20: 2235–2239

Holt LM, Hernandez RD, Pacheco NL, Torres Ceja B, Hossain M, Olsen ML. Astrocyte morphogenesis is dependent on BDNF signaling via astrocytic TrkB.T1. *ELife* 2019; 8: e44667

Holtman IR, Raj DD, Miller JA, Schaafsma W, Yin Z, Brouwer N, Wes PD, Möller T, Orre M, Kamphuis W, Hol EM, Boddeke EWGM, Eggen BJL. Induction of a common microglia gene expression signature by aging and neurodegenerative conditions: a co-expression meta-analysis. *Acta Neuropathol Commun* 2015; 3: 31

Huang EJ, Reichardt LF. Neurotrophins: Roles in Neuronal Development and Function. *Annu Rev Neurosci* 2001; 24: 677–736

Huang R, Bossut DF, Somjen GG. Enhancement of Whole Cell Synaptic Currents by Low

Osmolarity and by Low [NaCl] in Rat Hippocampal Slices. *J of Neurophysiol* 1997; 77: 2349–2359

Hunter I, Cobban H, Vandenabeele P, Macewan D, Nixon G. Tumor necrosis factor- $\alpha$ -induced activation of RhoA in airway smooth muscle cells: Role in the Ca<sup>2+</sup> sensitization of myosin light chain(20) phosphorylation. *Mol Pharmacol* 2003; 63: 714–721

Hunter I, Nixon GF. Spatial compartmentalization of tumor necrosis factor (TNF) receptor 1-dependent signaling pathways in human airway smooth muscle cells. Lipid rafts are essential for TNF- $\alpha$ -mediated activation of RhoA but dispensable for the activation of the NF- $\kappa$ B and MAPK pathways. *J Biol Chem* 2006; 281: 34705–34715

Isackson PJ, Huntsman MM, Murray KD, Gall CM. BDNF mRNA expression is increased in adult rat forebrain after limbic seizures: Temporal patterns of induction distinct from NGF. *Neuron* 1991; 6: 937–948

Iughetti L, Lucaccioni L, Fugetto F, Predieri B, Berardi A, Ferrari F. Brain-derived neurotrophic factor and epilepsy: a systematic review. *Neuropeptides* 2018; 72: 23–29

Jasper JR, Lesnick JD, Chang LK, Yamanishi SS, Chang TK, Hsu SAO, Daunt DA, Bonhaus DW, Eglen RM. Ligand Efficacy and Potency at Recombinant  $\alpha$ 2 Adrenergic Receptors: Agonist-Mediated [<sup>35</sup>S]gtpys Binding. *Biochem Pharmacol* 1998; 55: 1035–1043

Jensen AM, Chiu SY. Fluorescence measurement of changes in intracellular calcium induced by excitatory amino acids in cultured cortical astrocytes. *J Neurosci* 1990; 10: 1165–1175

Jin Y, Sun LH, Yang W, Cui RJ, Xu SB. The Role of BDNF in the Neuroimmune Axis Regulation of Mood Disorders. *Front in Neurol* 2019; 10

John GR, Chen L, Riviaccio MA, Melendez-Vasquez CV, Hartley A, Brosnan CF.

Interleukin-1 $\beta$  Induces a Reactive Astroglial Phenotype via Deactivation of the Rho GTPase–Rock Axis. *J Neurosci* 2004; 24: 2837–2845

Juvalle IIA, Che Has AT. Possible interplay between the theories of pharmacoresistant epilepsy. *Eur J Neurosci* 2021; 53: 1998–2026

Kanellos G, Frame MC. Cellular functions of the ADF/cofilin family at a glance. *J Cell Sci* 2016; 129: 3211–3218

Kant S, Swat W, Zhang S, Zhang Z-Y, Neel BG, Flavell RA, Davis RJ. TNF-stimulated MAP kinase activation mediated by a Rho family GTPase signaling pathway. *Genes Dev* 2011a; 25: 2069–2078

Kant S, Swat W, Zhang S, Zhang Z-Y, Neel BG, Flavell RA, Davis RJ. TNF-stimulated MAP kinase activation mediated by a Rho family GTPase signaling pathway. *Genes Dev* 2011b; 25: 2069–2078

Kettenmann H, Verkhratsky A. Neuroglia: the 150 years after. *Trends Neurosci* 2008; 31: 653–659

Khakh BS, Sofroniew MV. Diversity of astrocyte functions and phenotypes in neural circuits. *Nat Neurosci* 2015; 18: 942–952

Khurgel M, Ivy GO. Astrocytes in kindling: relevance to epileptogenesis. *Epilepsy Res* 1996; 26: 163–175

Kimelberg HK. Functions of Mature Mammalian Astrocytes: A Current View. *Neuroscientist* 2010; 16: 79–106

Kimelberg HK. Primary astrocyte cultures—a key to astrocyte function. *Cell Mol Neurobiol* 1983; 3: 1–16

Kimelberg HK, Kettenmann H. Swelling-induced changes in electrophysiological properties of cultured astrocytes and oligodendrocytes. I. Effects on membrane potentials, input impedance and cell-cell coupling. *Brain Res* 1990; 529: 255–261

Kimelberg HK, Norenberg MD. Astrocytes. *Sci Am* 1989; 260: 66–77

King CM, Bohmbach K, Minge D, Delekate A, Zheng K, Reynolds J, Rakers C, Zeug A, Petzold GC, Rusakov DA, Henneberger C. Local Resting Ca<sup>2+</sup> Controls the Scale of Astroglial Ca<sup>2+</sup> Signals. *Cell Rep* 2020; 30: 3466-3477.e4

King D, Spencer S. Invasive electroencephalography in mesial temporal lobe epilepsy. *J Clin Neurophysiol* 1995; 12: 32–45

Kitano T, Eguchi R, Okamatsu-Ogura Y, Yamaguchi S, Otsuguro K. Opposing functions of  $\alpha$ - and  $\beta$ -adrenoceptors in the formation of processes by cultured astrocytes. *J Pharmacol Sci* 2021; 145: 228–240

Kjøller L, Hall A. Signaling to Rho GTPases. *Exp Cell Res* 1999; 253: 166–179

Kreutzberg GW. Microglia: a sensor for pathological events in the CNS. *Trends Neurosci* 1996; 19: 312–318

Kriegler M, Perez C, DeFay K, Albert I, Lu SD. A novel form of TNF/cachectin is a cell surface cytotoxic transmembrane protein: ramifications for the complex physiology of TNF. *Cell* 1988; 53: 45–53

Kwan P, Arzimanoglou A, Berg AT, Brodie MJ, Allen Hauser W, Mathern G, Moshé SL, Perucca E, Wiebe S, French J. Definition of drug resistant epilepsy: Consensus proposal by the ad hoc Task Force of the ILAE Commission on Therapeutic Strategies. *Epilepsia* 2010; 51: 1069–1077

de Lanerolle NC, Lee T-S, Spencer DD. Astrocytes and epilepsy. *Neurotherapeutics*; 7:

424-438

Leite J.P., Garcia-Cairasco N, Cavalheiro EA. New insights from the use of pilocarpine and kainate models. *Epilepsy Res* 2002; 50: 93–103

Li G, Bauer S, Nowak M, Norwood B, Tackenberg B, Rosenow F, Knake S, Oertel WH, Hamer HM. Cytokines and epilepsy. *Seizure* 2011; 20: 249–256

Li L, Yin J, Liu C, Chen Lei, Chen Ling. Hypertonic stimulation inhibits synaptic transmission in hippocampal slices through decreasing pre-synaptic voltage-gated calcium current. *Neurosci Lett* 2012; 507: 106–111

Liddelow SA, Guttenplan KA, Clarke LE, Bennett FC, Bohlen CJ, Schirmer L, Bennett ML, Münch AE, Chung W-S, Peterson TC, Wilton DK, Frouin A, Napier BA, Panicker N, Kumar M, Buckwalter MS, Rowitch DH, Dawson VL, Dawson TM, Stevens B, Barres BA. Neurotoxic reactive astrocytes are induced by activated microglia. *Nature* 2017; 541: 481–487

Linnerbauer M, Wheeler MA, Quintana FJ. Astrocyte crosstalk in CNS inflammation. *Neuron* 2020; 108: 608–622

Lippman JJ, Lordkipanidze T, Buell ME, Yoon SO, Dunaevsky A. Morphogenesis and regulation of Bergmann glial processes during Purkinje cell dendritic spine ensheathment and synaptogenesis. *Glia* 2008; 56: 1463–1477

Liu T, Zhang L, Joo D, Sun S-C. NF- $\kappa$ B signaling in inflammation. *Signal Transduct Target Ther* 2017; 2: 17023

Liu X, Nemeth DP, McKim DB, Zhu L, DiSabato DJ, Berdysz O, Gorantla G, Oliver B, Witcher KG, Wang Y, Negray CE, Vegesna RS, Sheridan JF, Godbout JP, Robson MJ, Blakely RD, Popovich PG, Bilbo SD, Quan N. Cell-Type-Specific Interleukin 1 Receptor 1 Signaling in the Brain Regulates Distinct Neuroimmune Activities. *Immunity* 2019; 50: 317–

333.e6

Locksley RM, Killeen N, Lenardo MJ. The TNF and TNF Receptor Superfamilies: Integrating Mammalian Biology. *Cell* 2001; 104: 487–501

Lorente De Nó R. Studies on the structure of the cerebral cortex. II. Continuation of the study of the ammonic system. *Journal Für Psychologie Und Neurologie* 1934; 46: 113–177

Lorton D, Bellinger DL. Molecular Mechanisms Underlying  $\beta$ -Adrenergic Receptor-Mediated Cross-Talk between Sympathetic Neurons and Immune Cells 2015. *Int J Mol Sci* 2015; 16: 5635–5665

Lu B. BDNF and Activity-Dependent Synaptic Modulation. *Learn Mem* 2003; 10: 86–98

Luoni C, Bisulli F, Canevini MP, De Sarro G, Fattore C, Galimberti CA, Gatti G, La Neve A, Muscas G, Specchio LM, Striano S, Perucca E, Group on behalf of the SS. Determinants of health-related quality of life in pharmaco-resistant epilepsy: Results from a large multicenter study of consecutively enrolled patients using validated quantitative assessments. *Epilepsia* 2011; 52: 2181–2191

Mantovani A, Dinarello CA, Molgora M, Garlanda C. IL-1 and related cytokines in innate and adaptive immunity in health and disease. *Immunity* 2019; 50: 778–795

Matejuk A, Ransohoff RM. Crosstalk Between Astrocytes and Microglia: An Overview. *Front Immunol* 2020; 11: 1416

McCormick DA, Pape H-C, Williamson A. Chapter 22 - Actions of norepinephrine in the cerebral cortex and thalamus: implications for function of the central noradrenergic system. In: Barnes CD, Pompeiano O, eds. *Progress in Brain Research*, vol. 88, Pisa: Elsevier, 1991: 293–305

McPherson GA, Molenaar P, Malta E. The affinity and efficacy of naturally occurring catecholamines at  $\beta$ -adrenoceptor subtypes. *J Pharm Pharmacol* 1985; 37: 499–501

Medvedev N, Popov V, Henneberger C, Kraev I, Rusakov DA, Stewart MG. Glia selectively approach synapses on thin dendritic spines. *Philos Trans R Soc Lond B Biol Sci* 2014; 369: 20140047

Meierkord H, Shorvon S, Lightman S I. Plasma concentrations of prolactin, noradrenaline, vasopressin and oxytocin during and after a prolonged epileptic seizure. *Acta Neurol Scand* 1994; 90: 73–77

Michev A, Orsini A, Santi V, Bassanese F, Veraldi D, Brambilla I, Marseglia GL, Savasta S, Foadelli T. An Overview of The Role of Tumor Necrosis Factor-Alpha in Epileptogenesis and Its Therapeutic Implications. *Acta Biomed* 2021; 92: e2021418

Middlemas DS, Lindberg RA, Hunter T. trkB, a neural receptor protein-tyrosine kinase: evidence for a full-length and two truncated receptors. *Mol Cell Biol* 1991; 11: 143–153

Midori M, Ishizaki T, Shuken Boku, Naoki Watanabe. Signaling from Rho to the Actin Cytoskeleton Through Protein Kinases ROCK and LIM-kinase. *Science* 1999; 285: 895–898

Minge D, Domingos C, Unichenko P, Behringer C, Pauletti A, Anders S, Herde MK, Delekate A, Gulakova P, Schoch S, Petzold GC, Henneberger C. Heterogeneity and Development of Fine Astrocyte Morphology Captured by Diffraction-Limited Microscopy. *Front Cell Neurosci* 2021; 15: 669280

Miyamoto A, Wake H, Ishikawa AW, Eto K, Shibata K, Murakoshi H, Koizumi S, Moorhouse AJ, Yoshimura Y, Nabekura J. Microglia contact induces synapse formation in developing somatosensory cortex. *Nat Commun* 2016; 7: 12540

Molina PE. Neurobiology of the stress response: Contribution of the sympathetic

nervous system to the neuroimmune axis in traumatic injury. *Shock* 2005; 24: 3-10

Moolenaar WH. Bioactive Lysophospholipids and Their G Protein-Coupled Receptors. *Exp Cell Res* 1999; 253: 230–238

Mosaddeghzadeh N, Ahmadian MR. The RHO Family GTPases: Mechanisms of Regulation and Signaling. *Cells* 2021; 10: 1831

Mosser C-A, Baptista S, Arnoux I, Audinat E. Microglia in CNS development: Shaping the brain for the future. *Prog Neurobiol* 2017; 149–150: 1–20

Müller J. Preservation of Astrocytic Coupling Prevents Epileptogenesis. Thesis. Mathematisch-Naturwissenschaftlichen Fakultät der Universität Bonn, 2018

Nagelhus EA, Ottersen OP. Physiological Roles of Aquaporin-4 in Brain. *Physiol Rev* 2013; 93: 1543–1562

Nakagawa O, Fujisawa K, Ishizaki T, Saito Y, Nakao K, Narumiya S. ROCK-I and ROCK-II, two isoforms of Rho-associated coiled-coil forming protein serine/threonine kinase in mice. *FEBS Lett* 1996; 392: 189–193

National Clinical Guideline Centre (UK). The Epilepsies: The Diagnosis and Management of the Epilepsies in Adults and Children in Primary and Secondary Care: Pharmacological Update of Clinical Guideline 20. London: Royal College of Physicians (UK), 2012

Nawa H, Carnahan J, Gall C. BDNF Protein Measured by a Novel Enzyme Immunoassay in Normal Brain and after Seizure: Partial Disagreement with mRNA Levels. *Eur J Neurosci* 1995; 7: 1527–1535

Nedergaard M, Ransom B, Goldman SA. New roles for astrocytes: Redefining the functional architecture of the brain. *Trends Neurosci* 2003; 26: 523–530

Nett WJ, Oloff SH, McCarthy KD. Hippocampal Astrocytes In Situ Exhibit Calcium Oscillations That Occur Independent of Neuronal Activity. *J Neurophysiol* 2002; 87: 528–537

Nibuya M, Morinobu S, Duman RS. Regulation of BDNF and trkB mRNA in rat brain by chronic electroconvulsive seizure and antidepressant drug treatments. *J Neurosci* 1995; 15: 7539–7547

Nielsen S, Nagelhus EA, Amiry-Moghaddam M, Bourque C, Agre P, Ottersen OP. Specialized Membrane Domains for Water Transport in Glial Cells: High-Resolution Immunogold Cytochemistry of Aquaporin-4 in Rat Brain. *J Neurosci* 1997; 17: 171–180

Nishida H, Okabe S. Direct Astrocytic Contacts Regulate Local Maturation of Dendritic Spines. *J Neurosci* 2007; 27: 331–340

Nolte C, Matyash M, Pivneva T, Schipke CG, Ohlemeyer C, Hanisch U-K, Kirchhoff F, Kettenmann H. GFAP promoter-controlled EGFP-expressing transgenic mice: A tool to visualize astrocytes and astrogliosis in living brain tissue. *Glia* 2001; 33: 72–86

Oberheim NA, Tian G-F, Han X, Peng W, Takano T, Ransom B, Nedergaard M. Loss of Astrocytic Domain Organization in the Epileptic Brain. *J Neurosci* 2008; 28: 3264–3276

Ogata K, Kosaka T. Structural and quantitative analysis of astrocytes in the mouse hippocampus. *Neuroscience* 2002; 113: 221–233

Ohira K, Funatsu N, Homma KJ, Sahara Y, Hayashi M, Kaneko T, Nakamura S. Truncated TrkB-T1 regulates the morphology of neocortical layer I astrocytes in adult rat brain slices. *Eur J Neurosci* 2007; 25: 406–416

Ohira K, Homma KJ, Hirai H, Nakamura S, Hayashi M. TrkB-T1 regulates the RhoA signaling and actin cytoskeleton in glioma cells. *Biochem Biophys Res Commun* 2006; 342: 867–874

Ohira K, Kumanogoh H, Sahara Y, Homma KJ, Hirai H, Nakamura S, Hayashi M. A Truncated Troponin-Myosin-Related Kinase B Receptor, T1, Regulates Glial Cell Morphology via Rho GDP Dissociation Inhibitor 1. *J Neurosci* 2005; 25: 1343–1353

Oliet SHR, Piet R, Poulain DA. Control of Glutamate Clearance and Synaptic Efficacy by Glial Coverage of Neurons. *Science* 2001; 292: 923–926

Ostroff LE, Manzur MK, Cain CK, Ledoux JE. Synapses lacking astrocyte appear in the amygdala during consolidation of pavlovian threat conditioning. *J Comp Neurol* 2014; 522: 2152–2163

Pan W, Zadina JE, Harlan RE, Weber JT, Banks WA, Kastin AJ. Tumor Necrosis Factor- $\alpha$ : a Neuromodulator in the CNS. *Neurosci Biobehav Rev* 1997; 21: 603–613

Panatier A, Vallée J, Haber M, Murai KK, Lacaille J-C, Robitaille R. Astrocytes Are Endogenous Regulators of Basal Transmission at Central Synapses. *Cell* 2011; 146: 785–798

Papadopoulos MC, Verkman AS. Aquaporin water channels in the nervous system. *Nat Rev Neurosci* 2013; 14: 265–277

Patel DC, Wallis G, Dahle EJ, McElroy PB, Thomson KE, Tesi RJ, Szymkowski DE, West PJ, Smeal RM, Patel M, Fujinami RS, White HS, Wilcox KS. Hippocampal TNF $\alpha$  Signaling Contributes to Seizure Generation in an Infection-Induced Mouse Model of Limbic Epilepsy. *eNeuro* 2017; 4: ENEURO.0105-17.2017

Pati S, Alexopoulos A v. Pharmacoresistant epilepsy: From pathogenesis to current and emerging therapies. *Cleve Clin J Med* 2010; 77: 457–467

Pekny M, Pekna M, Messing A, Steinhäuser C, Lee J-M, Parpura V, Hol EM, Sofroniew MV, Verkhratsky A. Astrocytes: a central element in neurological diseases. *Acta*

Neuropathol 2016; 131: 323–345

Peltola J, Palmio J, Korhonen L, Suhonen J, Miettinen A, Hurme M, Lindholm D, Keränen T. Interleukin-6 and Interleukin-1 receptor antagonist in cerebrospinal fluid from patients with recent tonic–clonic seizures. *Epilepsy Res* 2000; 41: 205–211

Perry VH, Gordon S. Macrophages and microglia in the nervous system. *Trends Neurosci* 1988; 11: 273–277

Peschon JJ, Torrance DS, Stocking KL, Glaccum MB, Otten C, Willis CR, Charrier K, Morrissey PJ, Ware CB, Mohler KM. TNF Receptor-Deficient Mice Reveal Divergent Roles for p55 and p75 in Several Models of Inflammation. *J Immunol* 1998; 160: 943–952  
Peterson AC, Li CR. Noradrenergic Dysfunction in Alzheimer's and Parkinson's Diseases—An Overview of Imaging Studies. *Front Aging Neurosci* 2018; 10: 127

Plata-Salamán CR, Ilyin SE, Turrin NP, Gayle D, Flynn MC, Romanovitch AE, Kelly ME, Bureau Y, Anisman H, McIntyre DC. Kindling modulates the IL-1 $\beta$  system, TNF- $\alpha$ , TGF- $\beta$ 1, and neuropeptide mRNAs in specific brain regions. *Brain Res Mol Brain Res* 2000; 75: 248–258

Pongratz G, Straub RH. The sympathetic nervous response in inflammation. *Arthritis Res Ther* 2014; 16: 504

Porter JT, McCarthy KD. Hippocampal Astrocytes In Situ Respond to Glutamate Released from Synaptic Terminals. *J Neurosci* 1996; 16: 5073–5081

Prince DA. Neurophysiology of epilepsy. *Annu Rev Neurosci* 1978; 1: 395–415

Procko C, Lu Y, Shaham S. Glia delimit shape changes of sensory neuron receptive endings in *C. elegans*. *Development* 2011; 138: 1371–1381

Qiu T, Guo J, Wang L, Shi L, Ai M, Xia Z, Peng Z, Kuang L. Dynamic microglial activation

is associated with LPS-induced depressive-like behavior in mice: An [18F] DPA-714 PET imaging study. *Bosn J Basic Med Sci* 2022; 22: 649–659

Ramakers GJA, Moolenaar WH. Regulation of Astrocyte Morphology by RhoA and Lysophosphatidic Acid. *Exp Cell Res* 1998; 245: 252–262

Ramón y Cajal S. *Histologie du système nerveux de l'homme & des vertébrés*. Paris : Maloine, 1909

Rath PC, Aggarwal BB. TNF-induced signaling in apoptosis. *J Clin Immunol* 1999; 19: 350–364

Ravizza T, Gagliardi B, Noé F, Boer K, Aronica E, Vezzani A. Innate and adaptive immunity during epileptogenesis and spontaneous seizures: Evidence from experimental models and human temporal lobe epilepsy. *Neurobiol Dis* 2008; 29: 142–160

Reichenbach A, Derouiche A, Kirchhoff F. Morphology and dynamics of perisynaptic glia. *Brain Res Rev* 2010; 63: 11–25

Renno T, Krakowski M, Piccirillo C, Lin JY, Owens T. TNF- $\alpha$  expression by resident microglia and infiltrating leukocytes in the central nervous system of mice with experimental allergic encephalomyelitis. Regulation by Th1 cytokines. *J Immunol* 1995; 154: 944–953

van Rheenen J, Condeelis J, Glogauer M. A common cofilin activity cycle in invasive tumor cells and inflammatory cells. *J Cell Sci* 2009; 122: 305–311

Risher WC, Andrew RD, Kirov SA. Real-time passive volume responses of astrocytes to acute osmotic and ischemic stress in cortical slices and in vivo revealed by two-photon microscopy. *Glia* 2009; 57: 207–221

Robel S. *Astroglial Scarring and Seizures: A Cell Biological Perspective on Epilepsy*.

Neuroscientist 2017; 23: 152–168

Robertson JM. Astrocyte domains and the three-dimensional and seamless expression of consciousness and explicit memories. *Med Hypotheses* 2013; 81: 1017–1024

Ruck A, Kendall DA, Hill SJ.  $\alpha$ - and  $\beta$ -adrenoceptor regulation of cyclic AMP accumulation in cultured rat astrocytes: A comparison of primary protoplasmic and mixed fibrous/protoplasmic astroglial cultures. *Biochem Pharmacol* 1991; 42: 59–69

Salm AK, McCarthy KD. The evidence for astrocytes as a target for central noradrenergic activity: Expression of adrenergic receptors. *Brain Res Bull* 1992; 29: 265–275

Sano F, Shigetomi E, Shinozaki Y, Tsuzukiya H, Saito K, Mikoshiba K, Horiuchi H, Cheung DL, Nabekura J, Sugita K, Aihara M, Koizumi S. Reactive astrocyte-driven epileptogenesis is induced by microglia initially activated following status epilepticus. *JCI Insight* 2021; 6: e135391

Santello M, Volterra A. TNF $\alpha$  in synaptic function: switching gears. *Trends Neurosci* 2012; 35: 638–647

Scheffer IE, Berkovic S, Capovilla G, Connolly MB, French J, Guilhoto L, Hirsch E, Jain S, Mathern GW, Moshé SL, Nordli DR, Perucca E, Tomson T, Wiebe S, Zhang Y, Zuberi SM. ILAE classification of the epilepsies: Position paper of the ILAE Commission for Classification and Terminology. *Epilepsia* 2017; 58: 512–521

Schiweck J, Eickholt BJ, Murk K. Important Shapeshifter: Mechanisms Allowing Astrocytes to Respond to the Changing Nervous System During Development, Injury and Disease. *Front Cell Neurosci* 2018; 12: 261

Schultz C, Engelhardt M. Anatomy of the Hippocampal Formation. In: Szabo K, Hennerici MG, eds. *The Hippocampus in Clinical Neuroscience*, vol. 34. Basel: S. Karger AG, 2014: 6–17

Schumann RR, Belka C, Reuter D, Lamping N, Kirschning CJ, Weber JR, Pfeil D. Lipopolysaccharide Activates Caspase-1 (Interleukin-1–Converting Enzyme) in Cultured Monocytic and Endothelial Cells. *Blood* 1998; 91: 577–584

Schwartzkroin PA. Hippocampal slices in experimental and human epilepsy. *Adv Neurol* 1986; 44: 991–1010

Shapiro LA, Wang L, Ribak CE. Rapid astrocyte and microglial activation following pilocarpine-induced seizures in rats. *Epilepsia* 2008; 49: 33–41

Sharma AK, Reams RY, Jordan WH, Miller MA, Thacker HL, Snyder PW. Mesial Temporal Lobe Epilepsy: Pathogenesis, Induced Rodent Models and Lesions. *Toxicol Pathol* 2007; 35: 984–999

Shelton DL, Sutherland J, Gripp J, Camerato T, Armanini MP, Phillips HS, Carroll K, Spencer SD, Levinson AD. Human trks: molecular cloning, tissue distribution, and expression of extracellular domain immunoadhesins. *J Neurosci* 1995; 15: 477–491

Sherpa AD, Xiao F, Joseph N, Aoki C, Hrabetova S. Activation of  $\beta$ -adrenergic receptors in rat visual cortex expands astrocytic processes and reduces extracellular space volume. *Synapse* 2016; 70: 307–316

Simon RP, Aminoff MJ, Benowitz NL. Changes in plasma catecholamines after tonic-clonic seizures. *Neurology* 1984; 34: 255–255

Simpson JE, Ince PG, Lacey G, Forster G, Shaw PJ, Matthews F, Savva G, Brayne C, Wharton SB. Astrocyte phenotype in relation to Alzheimer-type pathology in the ageing brain. *Neurobiol Aging* 2010; 31: 578–590

Sofroniew MV. Astrogliosis. *Cold Spring Harb Perspect Biol* 2015; 7: a020420

Sofroniew MV. Multiple Roles for Astrocytes as Effectors of Cytokines and Inflammatory

Mediators. *Neuroscientist* 2014; 20: 160–172

Sofroniew MV, Vinters HV. Astrocytes: biology and pathology. *Acta Neuropathol* 2010; 119: 7–35

Sollberger G, Strittmatter GE, Garstkiewicz M, Sand J, Beer H-D. Caspase-1: The inflammasome and beyond. *Innate Immun* 2014; 20: 115–125

Song Y, Buchwald P. TNF Superfamily Protein–Protein Interactions: Feasibility of Small-Molecule Modulation. *Curr Drug Targets* 2015; 16: 393–408

Soontornniyomkij V, Wang G, Pittman CA, Wiley CA, Achim CL. Expression of brain-derived neurotrophic factor protein in activated microglia of human immunodeficiency virus type 1 encephalitis. *Neuropathol Appl Neurobiol* 1998; 24: 453–460

Stafstrom CE. The Role of the Subiculum in Epilepsy and Epileptogenesis. *Epilepsy Curr* 2005; 5: 121–129

Stahl JL, Cook EB, Graziano FM, Barney NP. Differential and Cooperative Effects of TNF $\alpha$ , IL-1 $\beta$ , and IFN $\gamma$  on Human Conjunctival Epithelial Cell Receptor Expression and Chemokine Release. *Invest Ophthalmol Vis Sci* 2003; 44: 2010–2015

Steinhäuser C, Grunnet M, Carmignoto G. Crucial role of astrocytes in temporal lobe epilepsy. *Neuroscience* 2016; 323: 157–169

Steinhäuser C, Seifert G, Bedner P. Astrocyte dysfunction in temporal lobe epilepsy: K<sup>+</sup> channels and gap junction coupling. *Glia* 2012; 60: 1192–1202

Steinhauser HB, Hertting G. Lowering of the convulsive threshold by non-steroidal anti-inflammatory drugs. *Eur J of Pharmacol* 1981; 69: 199–203

Streit WJ, Kreutzberg GW. Lectin binding by resting and reactive microglia. *J Neurocytol*

1987; 16: 249–260

Sultana B, Panzini M-A, Carpentier AV, Comtois J, Rioux B, Gore G, Bauer PR, Kwon C-S, Jetté N, Josephson CB, Keezer MR. Incidence and Prevalence of Drug-Resistant Epilepsy: A Systematic Review and Meta-analysis. *Neurology* 2021; 96: 805–817

Suzuki S, Numakawa T, Shimazu K, Koshimizu H, Hara T, Hatanaka H, Mei L, Lu B, Kojima M. BDNF-induced recruitment of TrkB receptor into neuronal lipid rafts. *J Cell Biol* 2004; 167: 1205–1215

Szot P, Weinshenker D, White SS, Robbins CA, Rust NC, Schwartzkroin PA, Palmiter RD. Norepinephrine-Deficient Mice Have Increased Susceptibility to Seizure-Inducing Stimuli. *J Neurosci* 1999; 19: 10985–10992

Tada M, Diserens A-C, Desbaillets I, Tribolet N de. Analysis of cytokine receptor messenger RNA expression in human glioblastoma cells and normal astrocytes by reverse-transcription polymerase chain reaction. *J Neurosurg* 1994; 80: 1063–1073

Tatsumi K, Okuda H, Morita-Takemura S, Tanaka T, Isonishi A, Shinjo T, Terada Y, Wanaka A. Voluntary Exercise Induces Astrocytic Structural Plasticity in the Globus Pallidus. *Front Cell Neurosci* 2016; 10: 165

Theodosis DT. Oxytocin-Secreting Neurons: A Physiological Model of Morphological Neuronal and Glial Plasticity in the Adult Hypothalamus. *Front Neuroendocrinol* 2002; 23: 101–135

Theodosis DT, Piet R, Poulain DA, Oliet SHR. Neuronal, glial and synaptic remodeling in the adult hypothalamus: functional consequences and role of cell surface and extracellular matrix adhesion molecules. *Neurochem Int* 2004; 45: 491–501

Theodosis DT, Poulain DA, Oliet SHR. Activity-Dependent Structural and Functional Plasticity of Astrocyte-Neuron Interactions. *Physiol Rev* 2008; 88: 983–1008

Thom M. Review: Hippocampal sclerosis in epilepsy: a neuropathology review. *Neuropathol Appl Neurobiol* 2014; 40: 520–543

Thurman DJ, Beghi E, Begley CE, Berg AT, Buchhalter JR, Ding D, et al. Standards for epidemiologic studies and surveillance of epilepsy. *Epilepsia* 2011; 52: 2–26

Tsuda A, Ito M, Kishi K, Shiraishi H, Tsuda H, Mori C. Effect of penicillin on GABA-gated chloride ion influx. *Neurochem Res* 1994; 19: 1–4

Turrin NP, Rivest S. Innate immune reaction in response to seizures: implications for the neuropathology associated with epilepsy. *Neurobiol Dis* 2004; 16: 321–334

van Strien NM, Cappaert NLM, Witter MP. The anatomy of memory: an interactive overview of the parahippocampal–hippocampal network. *Nat Rev Neurosci* 2009; 10: 272–282

Vardjan N, Kreft M, Zorec R. Dynamics of  $\beta$ -adrenergic/cAMP signaling and morphological changes in cultured astrocytes. *Glia* 2014; 62: 566–579

Vargová L, Syková E. Astrocytes and extracellular matrix in extrasynaptic volume transmission. *Philos Trans R Soc Lond B Biol Sci* 2014; 369: 20130608

Ventura R, Harris KM. Three-dimensional relationships between hippocampal synapses and astrocytes. *J Neurosci* 1999; 19: 6897–6906

Verkhatsky A, Nedergaard M. Physiology of Astroglia. *Physiol Rev* 2018; 98: 239–389

Verkman AS. Aquaporins. *Curr Biol* 2013; 23: 52–55

Vezzani Annamaria, Conti M, De Luigi A, Ravizza T, Moneta D, Marchesi F, De Simoni MG. Interleukin-1 $\beta$  Immunoreactivity and Microglia Are Enhanced in the Rat Hippocampus

by Focal Kainate Application: Functional Evidence for Enhancement of Electrographic Seizures. *J Neurosci* 1999; 19: 5054–5065

Vezzani A, French J, Bartfai T, Baram TZ. The role of inflammation in epilepsy. *Nat Rev Neurol* 2011; 7: 31–40

Vezzani A, Granata T. Brain Inflammation in Epilepsy: Experimental and Clinical Evidence. *Epilepsia* 2005; 46: 1724–1743

Vezzani A., Ravizza T, Moneta D, Conti M, Borroni A, Rizzi M, Samanin R, Maj R. Brain-derived neurotrophic factor immunoreactivity in the limbic system of rats after acute seizures and during spontaneous convulsions: temporal evolution of changes as compared to neuropeptide Y. *Neuroscience* 1999; 90: 1445–1461

Volterra A, Meldolesi J. Astrocytes, from brain glue to communication elements: the revolution continues. *Nat Rev Neurosci* 2005; 6: 626–640

Waisman A, Liblau RS, Becher B. Innate and adaptive immune responses in the CNS. *Lancet Neurol* 2015; 14: 945–955

Wajant H, Pfizenmaier K, Scheurich P. Tumor necrosis factor signaling. *Cell Death Differ* 2003; 10: 45–65

Wajant H, Siegmund D. TNFR1 and TNFR2 in the Control of the Life and Death Balance of Macrophages. *Front Cell Dev Biol* 2019; 7: 91

Walther C. Hippocampal terminology: concepts, misconceptions, origins. *Endeavour* 2002; 26: 41–44

Walz W. Role of astrocytes in the clearance of excess extracellular potassium. *Neurochem Int* 2000; 36: 291–300

Wang N, Mi X, Gao B, Gu J, Wang W, Zhang Y, Wang X. Minocycline inhibits brain inflammation and attenuates spontaneous recurrent seizures following pilocarpine-induced status epilepticus. *Neuroscience* 2015; 287: 144–156

Weber A, Wasiliew P, Kracht M. Interleukin-1 (IL-1) Pathway. *Sci Signal* 2010; 3: cm1–cm1

Wilhelmsson U, Li L, Pekna M, Berthold C-H, Blom S, Eliasson C, Renner O, Bushong E, Ellisman M, Morgan TE, Pekny M. Absence of Glial Fibrillary Acidic Protein and Vimentin Prevents Hypertrophy of Astrocytic Processes and Improves Post-Traumatic Regeneration. *J Neurosci* 2004; 24: 5016–5021

Williams A, Piaton G, Lubetzki C. Astrocytes—Friends or foes in multiple sclerosis? *Glia* 2007; 55: 1300–1312

Wirrell E, Tinuper P, Perucca E, Moshé SL. Introduction to the epilepsy syndrome papers. *Epilepsia* 2022; 63: 1330–1332

Witcher MR, Kirov SA, Harris KM. Plasticity of perisynaptic astroglia during synaptogenesis in the mature rat hippocampus. *Glia* 2007; 55: 13–23

Witcher MR, Park YD, Lee MR, Sharma S, Harris KM, Kirov SA. Three-dimensional relationships between perisynaptic astroglia and human hippocampal synapses. *Glia* 2010; 58: 572–587

Wójciak-Stothard B, Entwistle A, Garg R, Ridley AJ. Regulation of TNF- $\alpha$ -induced reorganization of the actin cytoskeleton and cell-cell junctions by Rho, Rac, and Cdc42 in human endothelial cells. *J Cell Physiol* 1998; 176: 150–165

Xie P. TRAF molecules in cell signaling and in human diseases. *J Mol Signal* 2013; 8: 7

Yue B. Biology of the Extracellular Matrix: An Overview. *J Glaucoma* 2014: 20–23

Zhang W-P, Ouyang M, Thomas SA. Potency of catecholamines and other l-tyrosine derivatives at the cloned mouse adrenergic receptors. *Neuropharmacology* 2004; 47: 438–449

Zhang Y, Barres BA. Astrocyte heterogeneity: an underappreciated topic in neurobiology. *Curr Opin Neurobiol* 2010; 20: 588–594

Zhao H, Zhu C, Huang D. Microglial activation: an important process in the onset of epilepsy. *Am J Transl Res* 2018; 10: 2877–2889

Zhou B, Zuo Y-X, Jiang R-T. Astrocyte morphology: Diversity, plasticity, and role in neurological diseases. *CNS Neurosci Ther* 2019; 25: 665–673

Zidek W. Wasser- und Elektrolythaushalt. In: Blum HE, Müller-Wieland D, eds. *Klinische Pathophysiologie*. 11th ed. Stuttgart: Georg Thieme Verlag KG, 2020: 269-286

Zigmond SH. Signal transduction and actin filament organization. *Curr Opin Cell Biol* 1996; 8: 66–73

## 9. Acknowledgements

First, I would like to thank Prof. Dr. med. Christian Henneberger for giving me this unique opportunity to work on this topic. He was always there for me whenever I needed advice. His knowledge, as well as his unbiased perspective, always impressed me. Moreover, he particularly supported me in thinking logically and finding solutions on my own without ever leaving me alone. With his help, I was able to gain insights into this fascinating scientific field and further develop as a scientifically-minded person.

I would like to thank Dr. Gerald Seifert for supporting me not only through his interest in my project but also by taking care of the animal breeding and genotyping.

My heartfelt thanks go especially to Dr. Björn Breithausen, who not only taught me everything in the laboratory at the beginning of my project but also accompanied me through all the ups and downs of the project. Sometimes, I even had to laugh at his jokes. I would also like to thank Dr. Stefan Passlick. His knowledge and his willingness to help contributed to the completion of this work. I also shared a few laughs with him along the way. Dr. Kirsten Bohmbach was also a great help with her expertise and creativity whenever I ran out of ideas. I thank Dr. Daniel Minge and Dr. Petr Unichenko for their patience in explaining and demonstrating things to me, sometimes repeatedly. I also want to thank Dr. Alberto Pauletti, Catia Domingos, and Katharina Hill. Together, they made coming to the institute enjoyable, and I always felt well-supported both academically and personally.

A huge thank goes to all my friends who supported me through every mood along the way, especially Alex, who shared so much of the journey and was an even greater support than I could have ever imagined. Finally, I want to thank my parents and my siblings, who believed in me even though I often complained and then forgot to update them when things actually worked out. I guess things did work out after all.